Masters Thesis

엄빌리컬 케이블의 영향을 받는 UV의 운동에 관한 연구

A Study on the Motions of Underwater Vehicle (UV) with the Umbilical Cable Effect

Supervisor: Professor Hyeung-Sik Choi

July 2015

Graduate School of Korea Maritime and Ocean University
Division of Mechanical Engineering

Mai The Vu

본 논문을 Mai The Vu 의 공학석사 학위논문으로

인준함.

위원장 김 준 영 (인)

위 원 최 형 식 (인)

위 원 조 용 성 (인)

2015년 07월 10일

한국해양대학교 대학원

Acknowledgement

First of all, I would like to thank my supervisor, Professor Hyeung-Sik Choi, at the Department of Mechanical Engineering, Korea Maritime and Ocean University (KMOU), for his encouraging and introducing me this wonderful research. His trust and scientific excitement inpired me through my research and I am so lucky to work with him.

I am grateful to my co-supervisor, Professor Sam-sang You, major of Refrigeration, Air-conditioning and Energy System Engineering; Professor Joon-Young Kim, major of Marine Equipment Engineering, KMOU; Professor Yong-Seong Cho, major of Electronics Engineering, Dong-A University; for inviting me to research stay at KMOU. They always share their knowledge regarding the marine control systems and this helps me a lot in my research.

I would like to thank my colleagues at Intelligent Robot & Automation Lab (KIAL) and KMOU for their invaluable helps and supporting me in my research work. I want to thank you all for all your kindly help, support, interest and valuable hints.

I closely express my thanks to Korean and Vietnamese friends for their friendliness, sharing, and confidence.

I also want to thank my parents and brothers, who taught me the value of hard working by their own examples. They are always my strong support during the whole difficult time of my research. The acknowledgement would not be complete without the mention of my girlfriend who is always with me whenever I fell lonely far from home.

Korea Maritime and Ocean University, Pusan, Korea

July 23th 2015

Mai The Vu

A Study on the Motions of Underwater Vehicle (UV) with the Umbilical Cable Effect

Mai The Vu

Division of Mechanical Engineering

Graduate School of Korea Maritime and Ocean University

Abstract

This thesis presents a series of analyses on the behavior of the underwater vehicle (UV) including the umbilical cable (UC) effect. The mathematical model for hydrodynamics of UV including the coupled effect of the UC is proposed. The corresponding hydrodynamic coefficients on the UV are obtained from experiments or referring related papers. With relevant hydrodynamic coefficients, the 4th-order Runge–Kutta numerical method is used to analyze motion of the UV and the dynamic configuration of the UC. The modeling performed of the UC is using the two-end boundary-value problem and it is solved by using the multi-step shooting method. Simulations on the UV including forward moving, backward, ascending, descending, sideward moving and turning motions were performed for the UC and without UC effect. The developed hydrodynamic model may serve as a useful tool to improve the performance of the UV operated with the effects of UC. The effect of currents to the UC is also taken into consideration. The present results reveal that the UC significantly affects the motion of the UV and should not be neglected in the simulation.

Keywords: Remotely operated vehicle; Umbilical cable; Shooting method; unmanned marine vehicles; maneuvering.

Contents

Nomenclature

x, y, z	Axes of body fixed reference frame
X, Y, Z	Axes of earth fixed reference frame
$\dot{x}$	Linear velocity along the North-South axis (earth)
$\dot{y}$	Linear velocity along the East- West axis (earth)
$\dot{z}$	Linear velocity along the vertical axis (earth)
φ	Euler angle in North-South axis. Positive sense is clockwise as seen from back of the vehicle (earth)
θ	Euler angle in pitch plane. Positive sense is clockwise as seen from port of the vehicle (earth)
ψ	Euler angle in yaw plane. Positive sense is clockwise as seen from above (earth)
$\dot{\varphi}$	Roll Euler rate about North-South axis (earth)
$\dot{\theta}$	Pitch Euler rate about East-West axis (earth)
$\dot{\psi}$	Yaw Euler rate about North-South axis (earth)
u	Linear velocity along longitudinal axis (body)
v	Linear velocity along horizontal plane (body)
w	Linear velocity along depth (body)
p	Angular velocity component about body longitudinal axis
q	Angular velocity component about body lateral axis
r	Angular velocity component about body vertical axis
$\dot{u}$	Time rate of change of velocity along the body longitudinal axis
$\dot{v}$	Time rate of change of velocity along the body lateral axis
$\dot{w}$	Time rate of change of velocity along the body vertical axis
$\dot{p}$	Time rate of change of body roll angular velocity about the body longitudinal axis
$\dot{q}$	Time rate of change of body pitch angular velocity about the body lateral axis

$\dot{r}$	Time rate of change of body yaw angular velocity about the body vertical axis
W	Weight of the vehicle
B	Buoyancy of the vehicle
L	Length of the vehicle.
g	Acceleration due to gravity
ρ	Density of fluid
m	mass of the vehicle
I_{xx}	Mass Moment of Inertia about x-axis
I_{yy}	Mass Moment of Inertia about y-axis
I_{zz}	Mass Moment of Inertia about z-axis
I_{xy}	Cross Product of Inertia about xy-axes
I_{yz}	Cross Product of Inertia about yz-axes
I_{xz}	Cross Product of Inertia about xz-axes
CG	Center of gravity
x_G	x Coordinate of CG From Body Fixed Origin
y_G	y Coordinate of CG From Body Fixed Origin
z_G	z Coordinate of CG From Body Fixed Origin
CB	Center of buoyancy
x_B	x Coordinate of CB From Body Fixed Origin
y_B	y Coordinate of CB From Body Fixed Origin
z_B	z Coordinate of CB From Body Fixed Origin
W_c	The weight per length of the cable
D_c	Diameter of cable
L_c	Length of cable
E_c	Modulus of elasticity of cable

$X_{\dot{u}}$	Added mass in surge movement
$Y_{\dot{v}}$	Added mass in sway movement
$Z_{\dot{w}}$	Added mass in heave movement
$K_{\dot{p}}$	Added mass in roll movement
$M_{\dot{q}}$	Added mass in pitch movement
$N_{\dot{r}}$	Added mass in yaw movement
X_u	Linear damping in surge movement
Y_v	Linear damping in sway movement
Z_w	Linear damping in heave movement
K_p	Linear damping coefficient for roll movement
M_q	Linear damping coefficient for pitch movement
N_r	Linear damping coefficient for yaw movement
X_{uu}	Quadratic damping in surge movement
Y_{vv}	Quadratic damping in sway movement
Z_{ww}	Quadratic damping in heave movement
K_{pp}	Quadratic damping coefficient for roll movement
M_{qq}	Quadratic damping coefficient for pitch movement
N_{rr}	Quadratic damping coefficient for yaw movement

List of Tables

List of Figures

Chapter 1 Introduction

In this chapter, a brief information about underwater vehicles, their applications and importance and lastly our objectives of thesis are mentioned.

1.1 Underwater Vehicles

The ocean covers approximately 70% of the Earth's surface and contains numerous resources and life forms. Further, natural and mineral resources on land have steadily depleted, and hence, considerable attention has now focused on natural resources under seas, for example, oil, gas, and minerals under the seabed. However, it is not easy to explore and search vast underwater environments in traditional ways using manned systems and human divers. Therefore, underwater vehicles, especially unmanned systems that can perform difficult missions without risking human lives, are becoming popular. The underwater robots can help us better understand marine and other environmental issues, protect the ocean resources of the Earth from pollution, and efficiently utilize them for human welfare, in Fig. 1.1.

Fig.1.1: Application of underwater robots

Such unmanned underwater vehicles are often classified into two types-remotely operated vehicles (ROVs) and autonomous underwater vehicles (AUVs). Remotely

operated vehicles (ROVs) and autonomous underwater vehicles (AUVs) have been applied in a wide variety of areas. Recently, there has been a trend to use smaller autonomous underwater vehicles, both tethered and untethered, in rivers, lakes and oceans.

1.1.1 Autonomous Underwater Vehicles

Autonomous underwater vehicles tend to be very similar to the ROVs. However these vehicles are usually battery powered and carry its own computer. This onboard computer is the requirement for their autonomous behaviour. Autonomous Underwater Vehicles (AUVs) are usually torpedo shaped and as the name suggests not reliant on a connection to a surface vessel, and can operate for a prolonged period of time on their own. Therefore, their power capabilities and operating times are limited, and they cannot be tele-operated in real time. In particular, AUVs are designed to require little or no human supervision. They are much more focused on speed, energy conservation and hydrodynamic properties than the ROVs, and usually have only one main thruster. AUVs are generally used for data collection such as acoustic surveying of a seabed or monitoring of the ocean space in military operations.

Primarily oceanographic tools, AUVs carry sensors to navigate autonomously and map features of the ocean. Typical sensors include compasses, depth sensors, side-scan and other sonar's, magnetometers, thermistors and conductivity probes. Underwater robots require adequate guidance and control to perform useful tasks. Visual information is important to these tasks and visual servo control is one method by which guidance can be obtained. A connectionist learning approach can replace complex models and control schemes to coordinate and control thrusters. Autonomous Underwater Vehicles are a powerful tool for underwater data gathering. In military applications, AUVs are also known as Unmanned Undersea Vehicles (UUVs). They can operate in water as deep as 6000 meters and with recent advances in battery technology, these robotic submarines can travel tens of kilometres. The demand for advanced underwater robot technologies is growing

and will eventually lead to fully autonomous, specialized, reliable underwater robotic vehicles. A typical autonomous underwater vehicle is shown in Fig.1.2.

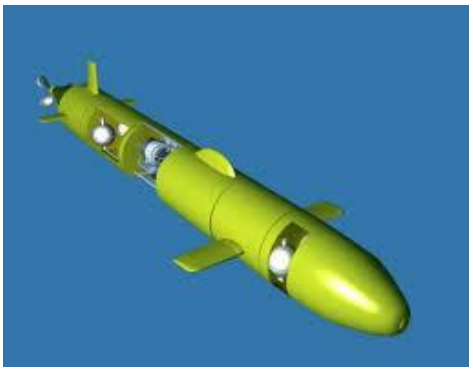

Fig.1.2: A typical Autonomous Underwater Vehicle

1.1.2 Remote Operated Underwater Vehicles

The use of Remotely Operated Vehicles (ROVs) has increased rapidly in the last decade due to widespread demand in the offshore oil and gas industries. They tend to be highly specialized for their specific task. Some are designed for scanning wide swaths of the ocean floor while others are designed for photography and recovery. A number of deep-sea animals and plants have been discovered or studied in their natural environment only through the use of ROVs.

An ROV typically has a low velocity, but is very maneuverable and well fit to solve complex tasks in deep water. ROVs are connected to, and controlled from, a surface vessel through an umbilical providing power and communications. Most ROV have a box-shaped frame, mostly because the slow operating speed and nearly unlimited power from the umbilical removes the need for hydrodynamic design and maneuverability and compactness is instead prioritized. Most ROVs will have thrusters in several directions to allow high precision control. ROVs are typically divided into several categories depending on their size, power and abilities. The smallest and weakest ROVs are in the micro and mini classes, and typically weights between 3 kg (micro) and 15 kg (mini). These ROVs usually have very little payload and are mostly used for exploration and surveying. The general classes ROVs are larger and can usually carry a small manipulator, have

less than 5 hp propulsion and can reach depths of 1000 meters. The two work classes are the most common in the subsea oil and gas industry and can carry two or more manipulators and usually have significant payload; the light work class typically has less than 50 hp propulsion and can dive to 2000 meters, while the heavy work class can have as much as 220 hp propulsion and a maximum depth of 3500 meters. A special class is the trenching/burial ROVs which are designed to carry a cable laying sledge and can operate down to 6000 meters with more than 200 hp propulsion. A typical remotely operated vehicle is shown as Fig.1.3.

Fig.1.3: A typical Remotely Operated Vehicle

1.2 Applications of Underwater Vehicles

With the development of Underwater Vehicles technology, its application areas have been expanding gradually. Its main applications include the following fields:

- Science: seafloor mapping; geological sampling; oceanographic monitoring;
- Environment: environmental remediation; inspection of underwater structures, including pipelines, dams, etc; long term monitoring (e.g., radiation, leakage, pollution)
- Oil and gas industry: ocean survey and resource assessment; construction and maintenance of undersea structures
- Military: shallow water mine search and disposal; submarine off-board sensors.

1.3 Motivation and Contributions of Thesis

Recently, the underwater vehicle (UV) is getting more and more important in exploration and exploitation of the underwater environment because it is a necessary underwater-technical system for observation and providing complex and technical works. There have been many researches about the design and development of the underwater vehicles in the world. Deam and Given (1983) summarized the researches of ROV and concluded five steps about developing ROV. Nomoto and Hattori (1986) made the detailed analysis on the designed performance for the deep ocean ROV, JAMSTEC DOPHIN 3 K, whose mission was to support the manned submersible, DEEP OCEAN 2000, to investigate the operation location under the water depth 3300 m. Their technical analyses were also extended to the JAMSTEC KAIKO with the maximum operation depth 11000 m. Stewart and Auster (1989) submitted a low-cost technology for developing ROV which is helpful to the related designers. Multiple AUVs, underwater docking, and obstacle avoidance are recent challenging issues in the field of AUV technologies.

Fig.1.4: A typical deep-sea-operated vehicle systems

Generally, the deep-sea-operated vehicle systems typically consist of a large supported vessel, a winch, umbilical cable and UV, as shown in Fig 1.4. However, most of researches on the numerical model of predicting the motion of the UV neglect the umbilical cable effect. The main reason is that including the umbilical cable effect will cause the numerical model to be very complicated and difficult to solve. Therefore, only few authors dealt with such kind of problem. Ablow and

Schechter (1983) proposed an implicit finite difference method to simulate an underwater cable that has been frequently referenced in the relevant literatures. However, their algorithm will become singular if the tension in the cable is lost. Burgess (1992) indicated the internal forces generated by the cable curvature could avoid the singular behavior of the implicit finite difference scheme, which was made by implementing three additional rotational equations of motion. Buckham et al. (2000) applied the finite-element method to calculate the tension and bending force on the slack tether attached to the ROV. Recently Feng and Allen (2004) extended the numerical scheme developed by Milinazzo et al. (1987) and presented a finite difference method to evaluate the effects of the umbilical cable on an underwater flight vehicle, which showed that the numerical scheme was effective and provided a means for developing a feed- forward controller to compensate for the cable effects. It means that the proposed numerical scheme can handle the dynamics of an underwater flight vehicle with cables of non-fixed length.

The hydrodynamic numerical model for simulating the UV maneuvering behavior is very important. A general non-linear model for the dynamics of UV can be derived either using a Newtonian or a Lagrangian method (Coute and Serranl, 1996; Fossen, 1994). In order to understand the behavior of the UV maneuvering in the ocean, the mathematical model with the umbilical cable effect based on the formulas with six degrees of freedom motions (Fossen, 1994) has been derived in the paper. The corresponding hydrodynamic coefficients about the maneuvering characteristics are obtained from experiments or referring related papers. The configuration simulation of the umbilical cable connecting to the UV is calculated by using the 4th Runge–Kutta method and the corresponding two-end boundary-value problem is solved by using the multi-step shooting method which is based on the search method developed by Hooke and Jeeves (1961) and Sagatun (2001). The 4th Runge–Kutta method is also applied to solve the six degrees of freedom motions of the UV with the umbilical cable effect. The compact hydrodynamic model with six degrees of freedom (DOF) motions and the numerical solution technique are described in the following section.

Chapter 2 Design Essentials Concepts and Assumption

In order to design any vehicle, it is essential to have background knowledge and fundamental concepts about the processes and physical laws governing the vehicle in its environment. With regard to an UV, factors such as buoyancy, stability, hydrodynamic damping and pressure have to be taken into consideration. This chapter introduces some of these fundamental concepts and ideas about underwater vehicles, and also examines the general design of these vehicles. The mechanical and electrical systems of past UV vehicles are also presented and examined closely to gain insight into different designs

2.1 UV Coordinate System

Analogous to flying vehicles, an UV has 6-DOF; three spatial coordinates, x, y and z; and three attitude defining Euler angles, roll, φ, pitch, θ, and yaw, ψ are shown in Fig.2.1.

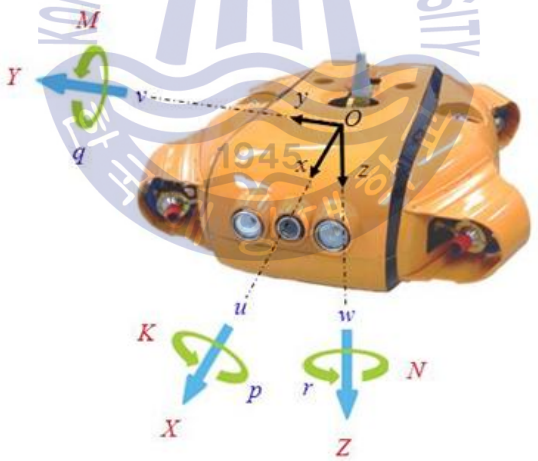

Fig.2.1: UV coordinate system.

The x axis points along the forward direction of the vehicle, defining the vehicle's longitudinal translation. The y axis points through the right hand or starboard side of the vehicle, defining the vehicle's lateral translation. The z axis defines the vehicle's vertical translation or depth. Note that the z axis is zero at the surface and points downwards; hence, it is positive for increasing depth. This is because the UV cannot travel further than the surface of the water.

The degree of freedom that an UV has allows it to be quite versatile. This high range of motion, however, can be problematic as it must be considered during the design process how each DOF will be controlled in order to keep the vehicle stable. Most UV are designed so as to be able to control as many DOF as possible.

2.2 Factors Affecting an Underwater Vehicle

Several forces act on an underwater vehicle that requires consideration for the design process. These include buoyancy, hydrodynamic damping, Coriolis and added mass. Buoyancy is one of the most important factors which significantly affects the vehicle's ability to submerge as well as its stability. Stability is also affected by external forces. Pressure is another significant factor for underwater vehicles that needs to be taken into consideration in the design process.

2.2.1 Buoyancy

The magnitude of the buoyant force, B, exerted on a body, floating or submerged, is equal to the weight of the volume of water displaced by that body [15]. The ability of an object to float depends on whether or not the magnitude of the weight of the body, W, is greater than the buoyant force. Clearly, if B > W, then the body will float, while if B < W it will sink (Figure 2.2). If B and W equate, then the body remains where it is.

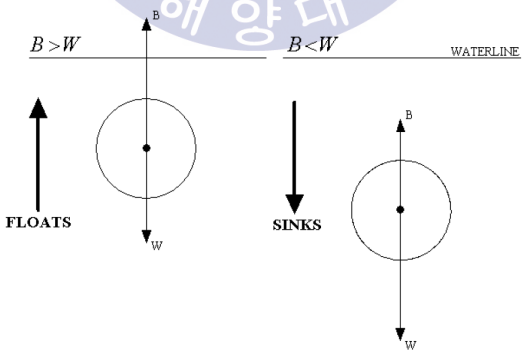

Fig.2.2: Effects of buoyancy and weight on an underwater body.

2.2.2 Hydrodynamic Damping

When a body is moving through the water, the main forces acting in the opposite direction to the motion of the body are hydrodynamic damping forces. These damping forces are mainly due to drag and lifting forces, as well as lineal skin

friction [1]. Damping forces have a significant effect on the dynamics of an underwater vehicle which leads to nonlinearity. Lineal skin friction can be considered negligible when compared to drag forces, and therefore, it is usually sufficient to only take into account the latter when calculating damping forces.

2.2.3 Stability

Assuming no water movement, the stability of a static body underwater is predominantly affected by the positions of the centres of mass, C_M , and buoyancy, C_B . The centre of buoyancy is the centroid of the volumetric displacement of the body [16]. If C_M and C_B are not aligned vertically with each other in either the longitudinal or lateral directions, then instability will exist due to the creation of a nonzero moment (Figure 2.3).

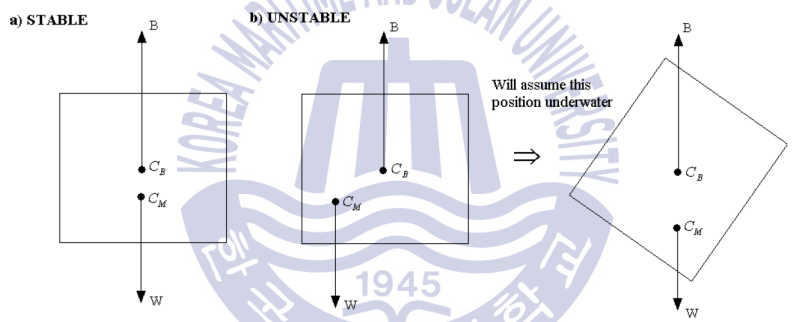

Fig.2.3: a) Stable configuration of underwater body. b) Instability of an underwater body through misalignment of centres of mass and buoyancy.

If C_M and C_B coincide in the same position in space, the vehicle will be very susceptible to perturbations. Ideally, the two centroids should be aligned vertically some distance apart from each other with C_M below C_B . This results in an ideal bottom-heavy configuration with innate stability.

As seen in Figure 2.4, this configuration produces a righting moment, RM, when the vehicle rolls or pitches that is directly proportional to the perpendicular distance between C_M and C_B , as well as to both B and W. This moment is conducive to the vehicle's stability, acting as a passive roll and pitch control system. The moment is given by,

$$RM = \frac{1}{2} d(B+W) \tag{2.1}$$

where d is the perpendicular distance between the acting forces B and W.

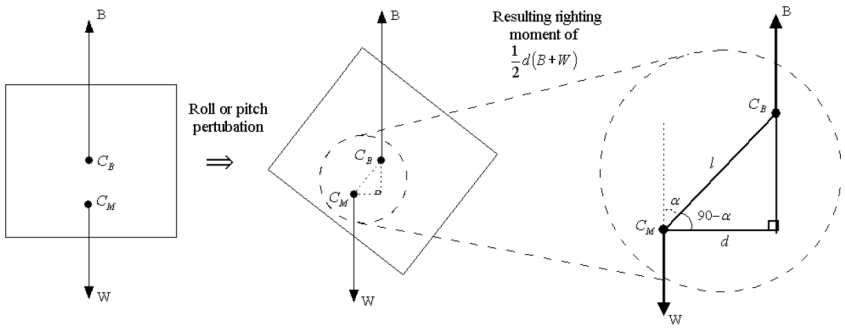

Fig.2.4: Righting moment caused by roll or pitch of vehicle.

The magnitude of RM varies sinusoidally with the angle α that the vehicle rolls or pitches. From Figure 2.4, equation 2.1 becomes

$$RM = \frac{1}{2} l(B+W)\sin\lambda \tag{2.2}$$

where l, B and W are constants for the vehicle; l being the distance between the centers of mass and buoyancy.

In the case of a dynamic underwater body, stability is affected not only by the centres of mass and buoyancy, but also by factors such as external forces and centres of drag. To increase dynamic stability, the centres of drag, determined by the centroids of the effective surface areas of the vehicle, should be aligned with the centres of the externally applied forces. In this manner, the vehicle will not tend to exhibit undesirable characteristics in its motion.

2.2.4 Coriolis

Coriolis is an inertial force that acts perpendicular to the direction of motion of a body. The force is proportional to both the velocity and rotation of the coordinate system. The effect of the Coriolis force then, is that the path of the body is deflected. In reality, however, the path of the body is not actually deflected, but only appears to be. This is due to the motion of the body's coordinate system [17]. Since the coordinate system of an UV rotates with respect to another reference frame, the

effect of the Coriolis force is usually taken into account and included in the equations of motion.

2.2.5 Added Mass

Another phenomenon that affects UV is added mass. When a body moves underwater, the immediate surrounding fluid is accelerated along with the body. This affects the dynamics of the vehicle in such a way that the force required to accelerate the water can be modeled as an added mass [18]. Added mass is a fairly significant effect and is related to the mass and inertial values of the vehicle.

2.2.6 Environmental Forces

Environmental disturbances can affect the motion and stability of a vehicle. This is particularly true for an UV where waves, currents and even wind can perturb the vehicle. When the vehicle is submerged, the effect of wind and waves can be largely ignored. The most significant disturbances then for UV are currents. In a controlled environment such as a pool, the effect of these environmental forces is minimal.

2.2.7 Pressure

As with air, underwater pressure is caused by the weight of the medium, in this case water, acting upon a surface. Pressure is usually measured as an absolute or ambient pressure; absolute denoting the total pressure and ambient being of a relativistic nature.

At sea level, pressure due to air is 14.7psi or 1atm. For every 10m of depth, pressure increases by about 1atm and hence, the absolute pressure at 10m underwater is 2atm. Although linear in nature, the increase in pressure as depth increases is significant and UV must be structurally capable of withstanding a relatively large amount of pressure if they are to survive.

2.3 General Design of an UV

There are several aspects in UV mechanical and electrical design that need to be looked at closely. International Submarine Engineering [19] identifies hull design, propulsion, submerging and electric power as major design aspects.

2.3.1 Hull Design

An UV must provide a pressure hull to house its components in a dry, watertight environment. The hull must allow components to be easily accessible and maintainable, as well as allowing for modularity in case of future changes or additions. As well as being light and strong, the hull should also be corrosion resistant as it will be subjected to a harsh saltwater environment.

Spherical hulls offer the best structural integrity, however, the shape inhibits the efficient use of the space available as most components and systems are rectangular in shape. Cylindrical hulls provide the best alternative, comprising high structural integrity and a shape conducive to the housing of electronic components.

2.3.2 Propulsion

Some sort of propulsion is required on all UV and is usually one of the main sources of power consumption. Most UV use motors for propulsion due to the scarcity and cost of alternative systems.

The location of the motors affects which DOF can be controlled. The positioning of the motors can also affect noise interference with onboard electronic components, as well as propeller-to-hull and propeller-to-propeller interactions. Propeller-to-hull and propeller-to-propeller interactions can have unwanted effects in the dynamics of an UV.

When travelling at a constant speed, the thrust produced by the motors is equal to the friction or drag of the vehicle, that is,

$$Thrust = Drag = \frac{1}{2}\rho s^2 Ac_D \tag{2.3}$$

Power consumption for the propulsion system increases dramatically as the speed of the vehicle increases. This is because the thrust power is equal to the product of the thrust and the speed, meaning thrust power is a function of speed cubed,

$$Thrustpower = Thrustxs = \frac{1}{2}\rho s^3 Ac_D \tag{2.4}$$

Therefore, because of an UV's limited energy supply, it must travel at a speed that does not draw too much power, but at the same time does not take too long to complete its mission. Obtaining the ideal speed becomes an optimisation problem.

2.3.3 Submerging

In the case of a submersible vehicle, since the volume of the vehicle remains constant, in order to dive deeper, it must increase the downward force acting upon it to counteract the buoyant force. It can accomplish this either by increasing its mass via the use of ballast tanks or by using external thrusters.

Ballasting is the more common approach for submerging. This method is mostly mechanical in nature and involves employing pumps and compressed air to take in and remove water. The alternative is to use thrusters that point downwards. This is a much simpler system, but is quite inefficient in terms of power consumption and not really suited at great depths.

To reduce the size of ballast tanks or the force required by thrusters for the process of submerging, UV are usually designed so as to have residual buoyancy. That is, the weight of the vehicle is made to be more or less equal to the buoyant force.

2.3.1 Electric Power

Electric power is commonly provided via sealed batteries. The ideal arrangement of batteries is to have them connected in parallel with diodes between each one to allow even discharge and to prevent current flow between batteries. Fuses or other protective devices should also be used to prevent excessive current flow in case of short circuits occurring or components malfunctioning.

The restrictive nature of power on UV influences the types of components and equipment that can be utilised. Components and equipment should be chosen so as to draw as little power as possible in order to allow the batteries to provide more than enough time for the vehicle to complete its mission.

Chapter 3 Mathematical Model of UV

In order to design controllers for dynamical systems, it is important to first model system dynamics using mathematical expressions. Hence, the vehicle is assumed to have port-starboard symmetry. The state-space representation of the vehicle's dynamics is presented and the hydrodynamic coefficients are estimated using the vehicle's basic parameters and dimensions. Determining the state vector representation and the modeling of their motion is the first step to control these vehicles.

3.1 General Structures and parameters of UV

The hull of the UV is streamlined for minimization of the effect of ocean currents. Four thrusters are symmetrically located at the corner of the hull for robust actuation of surge, sway movement, and yaw rotation. In addition to these, three vertical thrusters are deployed for heave, pitch movement, and roll rotation. The seven thrusters are deployed at a symmetric angle, suitable for six DOF motion control for dynamic positioning and attitude control in the UV mode, as shown in Fig.3.1.

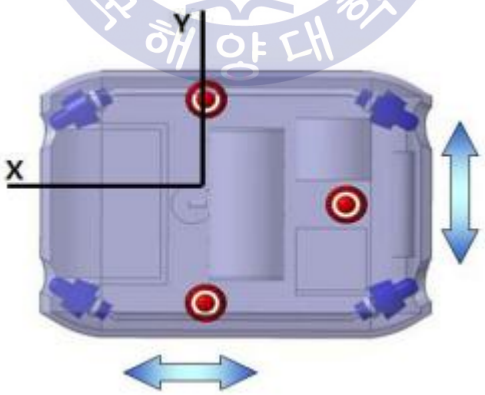

Fig.3.1: Actuator configuration for the 6 D.O.F

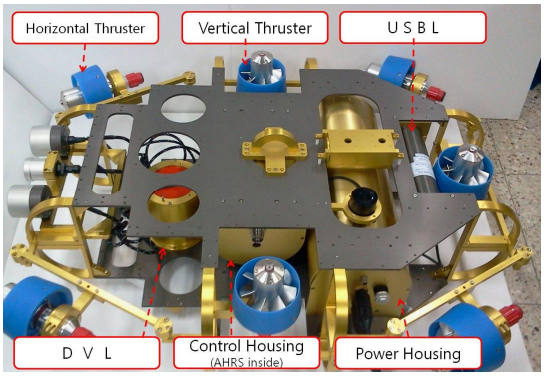

Fig.3.2: Internal view of the UV

The key components of the hull are largely composed of the body, control housing, power housing, battery housing, tether cable, manipulator, thrusters, sensors as in the doppler velocity logger (DVL), and ultimate short base line (USBL), as shown in Fig.3.2. The architecture of the UV is designed. Its size is designed to have a midium size and light weight as possible. The frame is made of an alluminum plate. Mechanism specification and parameters for simulation of the UV are given in Table 3.1 and Table 3.2. Hydrodynamic coefficients of UV system are shown as in Table 3.3.

Table 3.1: Mechanism specification of the UV

Classification	UV
Size	560×750×280 mm
Weight	80kgf
Max depth	200m
actuators	300W BLDC motor× 7
Degree of Freedom (D.O.F)	6
Battery housing	1
Power housing	1
Controller housing	1

Table 3.2: UV Parameters

Notation	Definition	Value	Unit
L_H	Length of UV	0.75	m
B_H	Width of UV	0.56	m
H_H	Height of UV	0.28	m
m_H	Mass of UV	80	kgf
g	Gravity Acceleration	9.81	m/s^2
ρ	Density of water	1025	kg/m^3
W_H	Weight of UV	784.8	N
B	Buoyancy force	784.8	N
CB	Center of buoyancy	$(0,0,-0.06)$	m
CG	Center of gravity	$(0,0,0)$	m
I_{xx}	Mass Moment of Inertia about x-axis	6.9	$kg.m^2$
I_{yy}	Mass Moment of Inertia about y-axis	26.1	$kg.m^2$
I_{zz}	Mass Moment of Inertia about z-axis	23.2	$kg.m^2$
I_{xy}	Cross Product of Inertia about xy-axes	0	$kg.m^2$
I_{yz}	Cross Product of Inertia about yz-axes	0	$kg.m^2$
I_{xz}	Cross Product of Inertia about xz-axes	0	$kg.m^2$

Table 3.3: Hydrodynamic coefficients of UV

Notation	Definition	Value	Unit
$X_{\dot{u}}$	Added mass in surge movement	-18.5	kg
$Y_{\dot{v}}$	Added mass in sway movement	-28.0	kg
$Z_{\dot{w}}$	Added mass in heave movement	-46.0	kg

$K_{\dot{p}}$	Added mass in roll movement	-1.3	$kg.m^2$
$M_{\dot{q}}$	Added mass in pitch movement	-6.8	$kg.m^2$
$N_{\dot{r}}$	Added mass in yaw movement	-5.9	$kg.m^2$
X_u	Linear damping in surge movement	-10	kg/sec
Y_v	Linear damping in sway movement	0	kg/sec
Z_w	Linear damping in heave movement	0	kg/sec
K_p	Linear damping coefficient for roll movement	-0.223	$Nm\,sec/rad$
M_q	Linear damping coefficient for pitch movement	-1.918	$Nm\,sec/rad$
N_r	Linear damping coefficient for yaw movement	-1.603	$Nm\,sec/rad$
X_{uu}	Quadratic damping in surge movement	-227.18	kg/m
Y_{vv}	Quadratic damping in sway movement	-405.41	kg/m
Z_{ww}	Quadratic damping in heave movement	-478.03	kg/m
K_{pp}	Quadratic damping coefficient for roll movement	-3.212	$Nm\,sec^2/rad$
M_{qq}	Quadratic damping coefficient for pitch movement	-14.002	$Nm\,sec^2/rad$
N_{rr}	Quadratic damping coefficient for yaw movement	-12.937	$Nm\,sec^2/rad$

3.2 Basic Assumptions

Generating mathematical model of UV is very challenging because of the nature of underwater dynamics mainly due to the non-linear and coupled character of plant equations. The challenge also dues to the lack of precise model of UV dynamics and parameters, as well as the appearance of environment disturbances. It is possible to simplify the number of parameter making the certain assumption related

with UV's construction. The following assertions were made for the dynamics of the UV in order to simplify the modeling. These assumptions are:

- UV is away from the free surface, walls and the bottom.
- The mass and distribution mass of the vehicle do not change during its operation.
- The UV travels at low speeds, that is, less than 2m/s.
- The UV is considered to be symmetrical about its three planes.
- Disturbances from the water environment on the UV such as currents and waves are negligible as it is fully submerged.
- The UV's degrees of freedom are decoupled.
- UV is a rigid body and is fully submerged once in water.
- Water is assumed to be ideal fluid that is incompressible, inviscid (frictionless) and irrotational.
- The earth-fixed frame of reference is inertial.
- The off-diagonal elements of the dynamic model matrices are much smaller than their counterparts.
- The hydrodynamic damping coupling is negligible at low speeds
- Hydrodynamic coefficients are not variable.
- The aligning moment ensures horizontal stability.
- The B-frame is positioned at the center of gravity, $r_G = [0 \quad 0 \quad 0]^T$

The above assertions not only have important ramifications for the modeling of the UV, but also for its control.

3.3 UV Kinematics

3.3.1 Coordinate Frames

To analyze the motion of the UV in 6 DOF, it is convenient to represent its coordinate into two frames, body-fixed and earth frame coordinate that depicted at Fig.3.3.

UV body axes X_0, Y_0, and Z_0 coincide with the axes with the principal axes of

inertia. Position and orientation of the UV are suggested to be described relative to inertial reference frame XYZ, while the linear and angular velocities to be expressed in the body-fixed coordinate system.

The UV motion in 6 DOF are described by vector

$$\eta = \left[\eta_1^T, \eta_2^T\right]^T \qquad \eta_1 = [x, y, z]^T \qquad \eta_2 = [\phi, \theta, \psi]^T$$
$$v = \left[v_1^T, v_2^T\right]^T \qquad v_1 = [u, v, w]^T \qquad v_2 = [p, q, r]^T \tag{3.1}$$
$$\tau = \left[\tau_1^T, \tau_2^T\right]^T \qquad \tau_1 = [X, Y, Z]^T \qquad \tau_2 = [K, M, N]^T$$

η denotes the position and orientation vector of UV with coordinates in the earth-fixed frame, while v denotes linear and angular velocity state vectors of the vehicle with coordinates in the body-fixed frame and τ is forces and moments acting to the vehicle in the body-fixed frame.

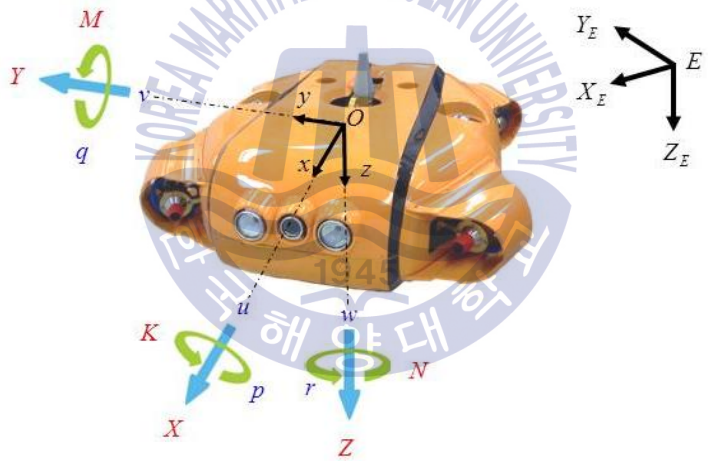

Fig.3.4: Body-fixed and earth-fixed reference frames.

Table 3.4. Notation used for UV

DOF	Motions & Rotations	Forces & Moments	Linear & Angular Velocities	Positions & Euler Angles
1	Motions in the x-direction (surge)	X	u	x
2	Motions in the y-direction (sway)	Y	v	y
3	Motions in the z-direction (heave)	Z	w	z
4	Rotation in the x-axis (roll)	K	p	ϕ
5	Rotation in the y-axis	M	q	θ

	(pitch)			
6	Rotation in the z-axis (yaw)	N	r	ψ

3.3.2 Attitude and Euler Angles

In marine and guidance and control systems, orientation is usually represented in Euler angle or quaternion. Euler angles define the rotation angle about the three Cartesian axes, x, y and z. There are many notations for Euler angles, however, the z-y-x form corresponding to rotation angles of yaw (ψ), pitch (θ), and roll (φ), respectively, is used here. The order of rotations is very important when converting from one coordinate system to another. When converting from body to world coordinates, it is conventional in robotics that the first rotation be ψ about the z axis, followed by θ about the intermediate y axis, and lastly φ about the second intermediate x axis. When converting from world to body coordinates, the reverse order is obviously used.

The rotation matrix of frame {B} relative to frame {W} which is the rotation matrix for converting from body-fixed to earth-fixed coordinates can be written as

$$ {}^{W}_{B}R(\eta_2) = R_z(\psi)R_y(\theta)R_x(\phi). \tag{3.2} $$

Where

$$ R_z(\psi) = \begin{bmatrix} \cos\psi & -\sin\psi & 0 \\ \sin\psi & \cos\psi & 0 \\ 0 & 0 & 1 \end{bmatrix} \tag{3.3} $$

$$ R_y(\theta) = \begin{bmatrix} \cos\theta & 0 & \sin\theta \\ 0 & 1 & 0 \\ -\sin\theta & 0 & \cos\theta \end{bmatrix} \tag{3.4} $$

$$ R_x(\phi) = \begin{bmatrix} 1 & 0 & 0 \\ 0 & \cos\phi & -\sin\phi \\ 0 & \sin\phi & \cos\phi \end{bmatrix} \tag{3.5} $$

By inserting (3.3-3.5) into (3.2), the rotation matrix can thus be expressed as

$$ {}^{W}_{B}R(\eta_2) = \begin{bmatrix} \cos\theta\cos\psi & \sin\phi\sin\theta\cos\psi - \cos\phi\sin\psi & \cos\phi\sin\theta\cos\psi + \sin\phi\sin\psi \\ \cos\theta\sin\psi & \sin\phi\sin\theta\sin\psi + \cos\phi\cos\psi & \cos\phi\sin\theta\sin\psi - \sin\phi\cos\psi \\ -\sin\phi & \sin\phi\cos\theta & \cos\phi\cos\theta \end{bmatrix} \tag{3.6} $$

Now that ${}^{W}_{B}R(\eta_2)$ has been established, it will be denoted simply as R for the remainder of this thesis for convenience. Note that the rotation matrix R is orthogonal thus its inverse will equal the transpose of the matrix, which is

$$ R^{-1} = R^{T} \tag{3.7} $$

This is useful for easily converting from earth-fixed to body-fixed coordinates. It is important to note that in using Euler angles, R is plagued by singularity problems at certain angles. This inhibits the conversion of world to body coordinates. However, because the control systems and bottom-heavy configuration of UV typically prevent the vehicle from attaining these angles, thus the use of Euler angles become sufficient and not resort to other mathematical techniques such as equivalent angle-axis representations. In general, an UV should be restricted to the following rotation angles,

$$ -\pi < \phi \le \pi, $$
$$ -\pi/2 < \phi < \pi/2, $$
$$ 0 \le \phi < 2\pi. $$

3.3.3 State Space Representation of the UV

A state space representation is defined to provide a compact way to model and analyze the UV. The vector notation includes the position vector v for the B and W-frame; the velocity vectors $\dot{\eta}$ for the B and W-frame, respectively

$$ v = \begin{bmatrix} \dot{x}_B & \dot{y}_B & \dot{z}_B & \dot{\phi}_B & \dot{\theta}_B & \dot{\psi}_B \end{bmatrix}^T = \begin{bmatrix} u & v & w & p & q & r \end{bmatrix}^T \tag{3.8} $$

And

$$ \dot{\eta} = \begin{bmatrix} \dot{x} & \dot{y} & \dot{z} & \dot{\phi} & \dot{\theta} & \dot{\psi} \end{bmatrix}^T \tag{3.9} $$

And the force/torque vector τ of the thruster input,

$$ \tau = \begin{bmatrix} \tau_x & \tau_y & \tau_z & \tau_\phi & \tau_\theta & \tau_\psi \end{bmatrix}^T \tag{3.10} $$

3.3.4 Velocity Transformation

The linear velocities of the UV in earth-fixed coordinate can be represented as,

$$\dot{\eta}_1 = {}^{W}_{B}R(\eta_2)v_1 = Rv_1. \tag{3.11}$$

This means

$$\left[\dot{x},\dot{y},\dot{z}\right]^T = R\left[u,v,w\right]^T. \tag{3.12}$$

And the inverse of the linear velocities transformation will be

$$v_1 = {}^{W}_{B}R\dot{\eta}_1 = R^T\dot{\eta}_1; \quad \left[u,v,w\right]^T = R^T\left[\dot{x},\dot{y},\dot{z}\right]^T; \tag{3.13}$$

The relation of body-fixed angular velocity vector $v_2 = \left[p,q,r\right]^T$ and the Euler angle rate vector $\dot{\eta}_2 = \left[\dot{\phi},\dot{\theta},\dot{\psi}\right]^T$ can be expressed as

$$\dot{\eta}_2 = {}^{W}_{B}Wv_2, \tag{3.14}$$

With

$${}^{B}_{W}W = W = \begin{bmatrix} 1 & \sin\phi\tan\theta & \cos\phi\tan\theta \\ 0 & \cos\phi & -\sin\phi \\ 0 & \sin\phi/\cos\theta & \cos\phi/\cos\theta \end{bmatrix}. \tag{3.15}$$

Since matrix W is not orthogonal, then the inverse transformation can not use its transpose value, thus the inverse transformation of the angular velocity from earth-fixed coordinate to body fixed written as

$$v_2 = {}^{W}_{B}W\dot{\eta}_2, \tag{3.16}$$

With

$${}^{B}_{W}W = W^{-1} = \begin{bmatrix} 1 & 0 & -\sin\theta \\ 0 & \cos\phi & \cos\theta\sin\phi \\ 0 & \sin\phi & \cos\theta\sin\phi \end{bmatrix} \tag{3.17}$$

By combining (3.11), (3.15) and (3.17), the velocity transformation from body-fixed to earth-fixed coordinate can be written as

$$\dot{\eta} = diag(R,W)v. \tag{3.18}$$

And the velocity transformation from earth-fixed to body-fixed coordinate can be written as

$$v = diag(R^T, W^{-1})\dot{\eta}. \tag{3.19}$$

3.4 UV Dynamic

The dynamic model presented in this section is based on the underwater robotic models proposed by Fossen (1994). UV dynamic model is derived from Newton-Euler motion equation given by

$$M\dot{v} + C(v)v + D(v)v + G(\eta_2) = \tau, \tag{3.20}$$

where

M = mass and inertia matrix including added mass,

C (v) = Coriolis and centripetal terms matrix including added mass,

D(v) = hydrodynamic damping matrix,

$G(\eta_2)$ = gravitational and buoyancy vector,

τ = external force and torque input vector,

v = velocity state vector.

3.4.1 Mass and Inertia Matrix

M consists of both a rigid body mass and inertia M_{RB} and a hydrodynamic added mass M_A, which can be written as

$$M = M_{RB} + M_A, \tag{3.21}$$

Assuming that frame {B} is located at the vehicle's center of gravity, $r_G = \begin{bmatrix} 0 & 0 & 0 \end{bmatrix}^T$, then M_{RB} can be written as

$$M_{RB} = \begin{bmatrix} m & 0 & 0 & 0 & 0 & 0 \\ 0 & m & 0 & 0 & 0 & 0 \\ 0 & 0 & m & 0 & 0 & 0 \\ 0 & 0 & 0 & I_x & -I_{xy} & -I_{xz} \\ 0 & 0 & 0 & -I_{yx} & I_y & -I_{yz} \\ 0 & 0 & 0 & -I_{zx} & -I_{zy} & I_z \end{bmatrix}. \tag{3.22}$$

With m is the mass of the UV and I terms represent the inertial tensors of the UV. The parameters of the added mass matrix are dependent on the shape of the UV. However they are constants when the vehicle is fully submerged. The parameters are usually in the vicinity of 10% to 100% of the corresponding parameters in the

rigid body mass matrix. The added mass matrix M_A, is denoted as

$$M_A = \begin{bmatrix} X_{\dot{u}} & X_{\dot{v}} & X_{\dot{w}} & X_{\dot{p}} & X_{\dot{q}} & X_{\dot{r}} \\ Y_{\dot{u}} & Y_{\dot{v}} & Y_{\dot{w}} & Y_{\dot{p}} & Y_{\dot{q}} & Y_{\dot{r}} \\ Z_{\dot{u}} & Z_{\dot{v}} & Z_{\dot{w}} & Z_{\dot{p}} & Z_{\dot{q}} & Z_{\dot{r}} \\ K_{\dot{u}} & K_{\dot{v}} & K_{\dot{w}} & K_{\dot{p}} & K_{\dot{q}} & K_{\dot{r}} \\ M_{\dot{u}} & M_{\dot{v}} & M_{\dot{w}} & M_{\dot{p}} & M_{\dot{q}} & M_{\dot{r}} \\ N_{\dot{u}} & N_{\dot{v}} & N_{\dot{w}} & N_{\dot{p}} & N_{\dot{q}} & N_{\dot{r}} \end{bmatrix}. \tag{3.23}$$

3.4.2 Coriolis and Centripetal Matrix

Similar with M matrix, $C(v)$ consists of both a rigid body Coriolis $M_{RB}(v)$ and an added mass Coriolis-like $C_A(v)$, which can be written as

$$C(v) = C_{RB}(v) + C_A(v). \tag{3.24}$$

The value of $C_{RB}(v)$ and $C_A(v)$ can always be parameterized such that $C_{RB}(v)$ and $C_A(v)$ are skew symmetrical. Using assumption that frame {B} is located at the vehicle's center of gravity, $r_G = \begin{bmatrix} 0 & 0 & 0 \end{bmatrix}^T$, then $C_{RB}(v)$ can be written as

$$C_{RB}(v)v = \begin{bmatrix} 0 & 0 & 0 & 0 & mw & -mv \\ 0 & 0 & 0 & -mw & 0 & mu \\ 0 & 0 & 0 & mv & -mu & 0 \\ 0 & mw & -mv & 0 & -I_{yz}q - I_{xz}p + I_z r & I_{yz}r + I_{xy}p - I_y q \\ -mw & 0 & mu & I_{yz}q + I_{xz}p - I_z r & 0 & -I_{xz}r - I_{xy}q + I_x p \\ mv & -mu & 0 & -I_{yz}r - I_{xy}p + I_y q & I_{xz}r + I_{xy}q - I_x p & 0 \end{bmatrix} \tag{3.25}$$

The Coriolis-like matrix induced by added mass $C_A(v)$ can be expressed as

$$C_A(v) = -\begin{bmatrix} 0 & 0 & 0 & 0 & -a_3 & a_2 \\ 0 & 0 & 0 & a_3 & 0 & -a_1 \\ 0 & 0 & 0 & -a_2 & a_1 & 0 \\ 0 & -a_3 & a_2 & 0 & -b_3 & b_2 \\ a_3 & 0 & -a_1 & b_3 & 0 & -b_1 \\ -a_2 & a_1 & 0 & -b_2 & b_1 & 0 \end{bmatrix} \tag{3.26}$$

Where

$$a_1 = X_{\dot{u}}u + X_{\dot{v}}v + X_{\dot{w}}w + X_{\dot{p}}p + X_{\dot{q}}q + X_{\dot{r}}r,$$

$$
\begin{aligned}
a_2 &= Y_{\dot{u}}u + Y_{\dot{v}}v + Y_{\dot{w}}w + Y_{\dot{p}}p + Y_{\dot{q}}q + Y_{\dot{r}}r, \\
a_3 &= Z_{\dot{u}}u + Z_{\dot{v}}v + Z_{\dot{w}}w + Z_{\dot{p}}p + Z_{\dot{q}}q + Z_{\dot{r}}r, \\
b_1 &= K_{\dot{u}}u + K_{\dot{v}}v + K_{\dot{w}}w + K_{\dot{p}}p + K_{\dot{q}}q + K_{\dot{r}}r, \\
b_2 &= M_{\dot{u}}u + M_{\dot{v}}v + M_{\dot{w}}w + M_{\dot{p}}p + M_{\dot{q}}q + M_{\dot{r}}r, \\
b_3 &= N_{\dot{u}}u + N_{\dot{v}}v + N_{\dot{w}}w + N_{\dot{p}}p + N_{\dot{q}}q + N_{\dot{r}}r,
\end{aligned}
\tag{3.27}
$$

For underwater vehicle that moves in low speed and has three planes of symmetry, the contribution of off-diagonal elements in the added mass M_A, can be neglected, thus $C_A(v)$ can be rewritten as

$$
C_A(v) = -\begin{bmatrix}
0 & 0 & 0 & 0 & -Z_{\dot{w}}w & Y_{\dot{v}}v \\
0 & 0 & 0 & Z_{\dot{w}}w & 0 & -X_{\dot{u}}u \\
0 & 0 & 0 & -Y_{\dot{v}}v & X_{\dot{u}}u & 0 \\
0 & -Z_{\dot{w}}w & Y_{\dot{v}}v & 0 & -N_{\dot{r}}r & M_{\dot{q}}q \\
Z_{\dot{w}}w & 0 & -X_{\dot{u}}u & N_{\dot{r}}r & 0 & -K_{\dot{p}}p \\
-Y_{\dot{v}}v & X_{\dot{u}}u & 0 & -M_{\dot{q}}q & K_{\dot{p}}p & 0
\end{bmatrix}
\tag{3.28}
$$

3.4.3 Hydrodynamic Damping Matrix

The hydrodynamic damping matrix $D(v)$ represents the drag and lift forces acting on a moving UV that will be highly nonlinear and coupled if vehicle moves at high speed. However, for a low-speed UV, the lift forces can be considered negligible when compared to the drag forces. These drag forces can be separated into two different terms consisting of a linear damping D_L and quadratic damping D_Q which can be written as,

$$
D(v) = D_L + D_Q|v|, \tag{3.29}
$$

Where

$$
D_L = diag\{X_u, Y_v, Z_w, K_p, M_q, N_r\}, \tag{3.30}
$$

$$
D_Q = diag\{X_{u|u|}, Y_{v|v|}, Z_{w|w|}, K_{p|p|}, M_{q|q|}, N_{r|r|}\}, \tag{3.31}
$$

$$D(v) = -\begin{bmatrix} X_u + X_{u|u|}|u| & 0 & 0 & 0 & 0 & 0 \\ 0 & Y_v + Y_{v|v|}|v| & 0 & 0 & 0 & 0 \\ 0 & 0 & Z_w + Z_{w|w|}|w| & 0 & 0 & 0 \\ 0 & 0 & 0 & K_p + K_{p|p|}|p| & 0 & 0 \\ 0 & 0 & 0 & 0 & M_q + M_{q|q|}|q| & 0 \\ 0 & 0 & 0 & 0 & 0 & N_r + N_{r|r|}|r| \end{bmatrix} \tag{3.32}$$

3.4.4 Gravitational and Buoyancy Vector

The gravitational and buoyancy vector, $G(\eta_2)$ is defined as

$$G(\eta_2) = -\begin{bmatrix} f_G(\eta_2) + f_B(\eta_2) \\ r_G \times f_G(\eta_2) + r_B \times f_B(\eta_2) \end{bmatrix}, \tag{3.33}$$

With

$$f_B(\eta_2) = -R^{-1}[0,0,B]^T, \tag{3.34}$$

And

$$f_G(\eta_2) = R^{-1}[W,0,0]^T, \tag{3.35}$$

where $f_B(\eta_2)$ is the buoyant force vector and $f_G(\eta_2)$ is the gravitational force vector. While $r_B = [x_B \quad y_B \quad z_B]^T$ and $r_G = [x_G \quad y_G \quad z_G]^T$ are center of the buoyancy and center of the gravity in frame {B} respectively. With center of the buoyancy positioned at $r_G = [0 \quad 0 \quad 0]^T$, then $G(\eta_2)$ can be re written as

$$G(\eta_2) = -\begin{bmatrix} f_G(\eta_2) + f_B(\eta_2) \\ r_B \times f_B(\eta_2) \end{bmatrix}, \tag{3.36}$$

By inserting (3.34) and (3.35) into (3.36), $G(\eta_2)$ will yields

$$G(\eta_2) = \begin{bmatrix} (W-B)\sin\theta \\ -(W-B)\cos\theta\sin\phi \\ -(W-B)\cos\theta\cos\phi \\ B\cos\theta(y_B\cos\phi - z_B\sin\phi) \\ -B(z_B\sin\theta + x_B\cos\theta\cos\phi) \\ B(x_B\cos\theta\sin\phi + y_B\sin\theta) \end{bmatrix} \tag{3.37}$$

3.4.5 Forces and Torque Vector

The external force and torque vector produced by the thrusters is defined as

$$\tau = \begin{bmatrix} X & Y & Z & K & M & N \end{bmatrix}^T = LU. \tag{3.38}$$

With

$$U = \begin{bmatrix} T_1 & T_2 & \dots & T_n \end{bmatrix}^T. \tag{3.39}$$

where L is a mapping matrix and U is a thrust vector. U is the vector of thrusts produced by the vehicle's thrusters. The number of thrust values in U depends on the number of thrusters on the vehicle. The mapping matrix L is essentially a 6 × n matrix that uses U to find the overall forces and moments acting on the vehicle.

3.4.6 Umbilical Cable Forces

Generally, the deep-sea-operated vehicle systems typically consist of a supported vessel umbilical cable (UC) and UV. However, most of researches on the numerical model of predicting the motion of the UV neglect the UC effect. The main reason is that including the UC effect will cause the numerical model to be very complicated and difficult to solve. Therefore, only few authors dealt with such kind of problem. UC is used for both power supply and communication to UV. The cable is treated as a long, thin, flexible circular cylinder. It is assumed that the dynamics of a cable are determined by gravity, hydrodynamic loading and inertial forces, no bending or torsional stiffness is taken into account in this study. The UC that connects the UV to the vessel can be affected by many parameters, including the motions of either the UV or the vessel, the current along the cable and the total length of the cable itself. The UC configuration can be optimized by numerical simulations. This is described in more detail in Chapter 4.

3.5 Simplification of UV Dynamic Model

The dynamic model presented in the previous section is quite complex and needs many parameters thus it will be very time consuming and difficult process. Therefore, simplification of the model was required. In order to simplify the UV dynamic, several assertions below are needed.

- The vehicle travels at low speeds (less than 2m/s).
- The vehicle is considered to be symmetrical about its three planes.
- Disturbances from the water environment on the vehicle such as currents and waves are negligible.
- The off-diagonal elements of the dynamic model matrices are much smaller than their counterparts,
- The hydrodynamic damping coupling is negligible when the vehicle travels at low speed.

If the decoupling is valid thus the Coriolis and centripetal terms matrices become negligible and consequently can be eliminated from the dynamic model. The dynamic model in (3.20) can be simplified as

$$M\dot{V} + D(V)V + G(\eta_2) = \tau, \tag{3.40}$$

3.5.1 Simplifying the Mass and Inertia Matrix

With the vehicle fixed-body frame is positioned at the center of gravity and since the vehicle is assumed fairly symmetrical about all axes, then UV rigid-body mass M_{RB} can be simplified to a good approximation to,

$$M_{RB} = \begin{bmatrix} m & 0 & 0 & 0 & 0 & 0 \\ 0 & m & 0 & 0 & 0 & 0 \\ 0 & 0 & m & 0 & 0 & 0 \\ 0 & 0 & 0 & I_x & 0 & 0 \\ 0 & 0 & 0 & 0 & I_y & 0 \\ 0 & 0 & 0 & 0 & 0 & I_z \end{bmatrix} \tag{3.41}$$

Or $M_{RB} = diag\{m, m, m, I_x, I_y, I_z\}$, (3.42)

with m is the mass of the UV, I_x , I_y I_y and I_z is the inertial force in x, y and z axis respectively.

Since the vehicle travels at low speed, thus added mass from (4.21) can be simplified as

$$M_A = \begin{bmatrix} X_{\dot{u}} & 0 & 0 & 0 & 0 & 0 \\ 0 & Y_{\dot{u}} & 0 & 0 & 0 & 0 \\ 0 & 0 & Z_{\dot{w}} & 0 & 0 & 0 \\ 0 & 0 & 0 & K_{\dot{p}} & 0 & 0 \\ 0 & 0 & 0 & 0 & M_{\dot{q}} & 0 \\ 0 & 0 & 0 & 0 & 0 & N_{\dot{r}} \end{bmatrix} \tag{3.43}$$

Or $M_A = diag\left\{X_{\dot{u}}, Y_{\dot{u}}, Z_{\dot{v}}, K_{\dot{p}}, M_{\dot{q}}, N_{\dot{r}}\right\}$, (3.44)

with $X_{\dot{u}}$, $Y_{\dot{u}}$, $Z_{\dot{w}}$, $K_{\dot{p}}$, $M_{\dot{q}}$ and $N_{\dot{r}}$ are added mass in the surge, sway, heave, roll, pitch and yaw movement respectively.

3.5.2 Simplifying the Hydrodynamic Damping Matrix

The matrix $D(v)$ is the hydrodynamic damping matrix consisting of both linear and quadratic terms. This hydrodynamic damping is caused by potential damping due to skin friction (linear damping) drag and vortex shedding (quadratic damping). The sum of these individual components gives the overall hydrodynamic damping effect on the UV. The hydrodynamic damping matrix can be simplified by using the following assumptions.

- As the UV is operating at around linear speed of 0.2 m/s (or angular speed of 0.2 rad/s), it is well within the linear damping region of maximum 2m/s. Hence, the linear hydrodynamic damping is used.
- The off-diagonal elements in $D(v)$ on an underwater vehicle are small compared to the diagonal elements.

Hence the hydrodynamic damping $D(v)$ from (3.29) also can be simplified as

$$D(v) = -\begin{bmatrix} X_u & 0 & 0 & 0 & 0 & 0 \\ 0 & Y_v & 0 & 0 & 0 & 0 \\ 0 & 0 & Z_w & 0 & 0 & 0 \\ 0 & 0 & 0 & K_p & 0 & 0 \\ 0 & 0 & 0 & 0 & M_q & 0 \\ 0 & 0 & 0 & 0 & 0 & N_r \end{bmatrix} \tag{3.45}$$

or

$$D(v) = -diag\left\{X_u, Y_v, Z_w, K_p, M_q, N_r\right\}, \tag{3.46}$$

3.5.3 Simplifying the Gravitational and Buoyancy Vector

In designing UV, it is desirable to make the UV neutrally buoyant or slightly positive buoyant by adding additional float or balancing mass. With that, the UV becomes neutrally buoyant, W = B. The center of gravity is located at $r_G = \begin{bmatrix} 0 & 0 & 0 \end{bmatrix}^T$, while the center of buoyancy r_B was found to be $r_B = \begin{bmatrix} 0 & 0 & z_B \end{bmatrix}^T$ for a good approximation, since z_B is not aligned to the center of the gravity in z axis. So, the gravitational force from (3.37) that can be simplified as

$$g(\eta) = \begin{bmatrix} 0 \\ 0 \\ 0 \\ -z_B W \cos\theta \sin\phi \\ -z_B W \sin\theta \\ 0 \end{bmatrix} \tag{3.47}$$

3.6 Thruster Modeling

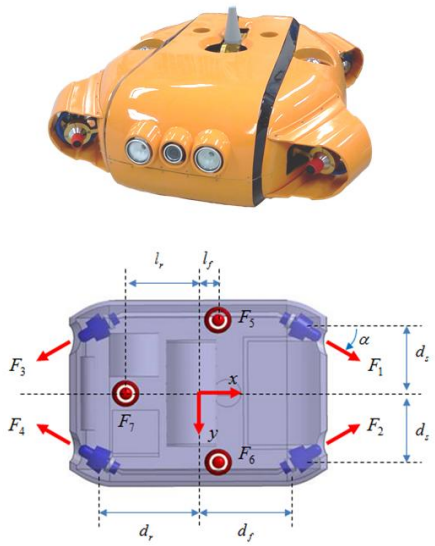

Fig.3.4: UV frame reference and torque vector.

The UV model considered in the present study is equipped with seven thrusters as shown in Figs.3.4; that is, four horizontal thrusters T_1, T_2, T_3 and T_4 which are installed at the bow and the stern part with inclined angle θ_T, are operated to control the surge, sway, and yaw motions. While three vertical thrusters T_5, T_6 and T_7 enable the AUV to have 3-DOF behaviors of the heave, roll, and pitch motions. Assume $(x_{ci}, y_{ci}, z_{ci})_{i=1,2,3,4}$ is the center of the i-th thruster, where θ_T is set to be 30^0 in the present study.

The center of the 1^{st} thruster T_1 is $x_{c1} = 0.3m$, $y_{c1} = -0.2m$, $z_{c1} = 0m$ and the moment induced by thruster T_1 can be obtained by

$$\vec{r}_1 \times \vec{F}_1 = \begin{bmatrix} x_{c1} \\ y_{c1} \\ z_{c1} \end{bmatrix} \times \begin{bmatrix} F_1 \cos\theta \\ F_1 \sin\theta \\ 0 \end{bmatrix} = \begin{bmatrix} x_{c1} \\ y_{c1} \\ 0 \end{bmatrix} \times \begin{bmatrix} F_1 \cos\theta \\ F_1 \sin\theta \\ 0 \end{bmatrix} = (x_{c1}F_1 \sin\theta - y_{c1}F_1 \cos\theta)\vec{k} \qquad (3.48)$$

The center of the 2^{nd} thruster T_2 is $x_{c2} = 0.3m$, $y_{c2} = 0.2m$, $z_{c2} = 0m$ and the moment induced by thruster T_2 can be obtained by

$$\vec{r}_2 \times \vec{F}_2 = \begin{bmatrix} x_{c2} \\ y_{c2} \\ z_{c2} \end{bmatrix} \times \begin{bmatrix} F_2 \cos\theta \\ -F_2 \sin\theta \\ 0 \end{bmatrix} = \begin{bmatrix} x_{c2} \\ y_{c2} \\ 0 \end{bmatrix} \times \begin{bmatrix} F_2 \cos\theta \\ -F_2 \sin\theta \\ 0 \end{bmatrix} = (-x_{c2}F_2 \sin\theta - y_{c2}F_2 \cos\theta)\vec{k}$$

(3.49)

The center of the 3^{rd} thruster T_3 is $x_{c3} = -0.3m$, $y_{c3} = -0.2m$, $z_{c3} = 0m$ and the moment induced by thruster T_3 can be obtained by

$$\vec{r}_3 \times \vec{F}_3 = \begin{bmatrix} x_{c3} \\ y_{c3} \\ z_{c3} \end{bmatrix} \times \begin{bmatrix} -F_3 \cos\theta \\ F_3 \sin\theta \\ 0 \end{bmatrix} = \begin{bmatrix} x_{c3} \\ y_{c3} \\ 0 \end{bmatrix} \times \begin{bmatrix} -F_3 \cos\theta \\ F_3 \sin\theta \\ 0 \end{bmatrix} = (x_{c3}F_3 \sin\theta + y_{c3}F_3 \cos\theta)\vec{k}$$

(3.50)

The center of the 4-th thruster T_4 is $x_{c4} = -0.3m$, $y_{c4} = 0.2m$, $z_{c4} = 0m$ and the moment induced by thruster T_4 can be obtained by

$$\vec{r}_4 \times \vec{F}_4 = \begin{bmatrix} x_{c4} \\ y_{c4} \\ z_{c4} \end{bmatrix} \times \begin{bmatrix} -F_4 \cos\theta \\ -F_4 \sin\theta \\ 0 \end{bmatrix} = \begin{bmatrix} x_{c4} \\ y_{c4} \\ 0 \end{bmatrix} \times \begin{bmatrix} -F_4 \cos\theta \\ -F_4 \sin\theta \\ 0 \end{bmatrix} = (-x_{c4}F_4 \sin\theta + y_{c4}F_4 \cos\theta)\vec{k}$$

(3.51)

The center of the 5-th thruster T_5 is $x_{c5} = 0.1m$, $y_{c5} = -0.18m$, $z_{c5} = 0m$ and the moment induced by thruster T_5 can be obtained by

$$\vec{r}_5 \times \vec{F}_5 = \begin{bmatrix} x_{c5} \\ y_{c5} \\ z_{c5} \end{bmatrix} \times \begin{bmatrix} 0 \\ 0 \\ F_5 \end{bmatrix} = \begin{bmatrix} x_{c5} \\ y_{c5} \\ 0 \end{bmatrix} \times \begin{bmatrix} 0 \\ 0 \\ F_5 \end{bmatrix} = (y_{c5}F_5)\vec{i} - (x_{c5}F_5)\vec{j} \tag{3.52}$$

The center of the 6-th thruster T_6 is $x_{c6} = 0.1m$, $y_{c6} = 0.18m$, $z_{c6} = 0m$ and the moment induced by thruster T_6 can be obtained by

$$\vec{r}_6 \times \vec{F}_6 = \begin{bmatrix} x_{c6} \\ y_{c6} \\ z_{c6} \end{bmatrix} \times \begin{bmatrix} 0 \\ 0 \\ F_6 \end{bmatrix} = \begin{bmatrix} x_{c6} \\ y_{c6} \\ 0 \end{bmatrix} \times \begin{bmatrix} 0 \\ 0 \\ F_6 \end{bmatrix} = (y_{c6}F_6)\vec{i} - (x_{c6}F_6)\vec{j} \tag{3.53}$$

The center of the 7-th thruster T_7 is $x_{c7} = -0.25m$, $y_{c7} = 0m$, $z_{c7} = 0m$ and the moment induced by thruster T_7 can be obtained by

$$\vec{r}_7 \times \vec{F}_7 = \begin{bmatrix} x_{c7} \\ y_{c7} \\ z_{c7} \end{bmatrix} \times \begin{bmatrix} 0 \\ 0 \\ F_7 \end{bmatrix} = \begin{bmatrix} x_{c7} \\ y_{c7} \\ 0 \end{bmatrix} \times \begin{bmatrix} 0 \\ 0 \\ F_7 \end{bmatrix} = (y_{c7}F_7)\vec{i} - (x_{c7}F_7)\vec{j} \tag{3.54}$$

Finally, the corresponding resultant force and moment induced by each thruster can be obtained by

$$\begin{aligned} F_{thrust} &= F_{Tx}\vec{i} + F_{Ty}\vec{j} + F_{Tz}\vec{k} \\ &= (F_1 + F_2 - F_3 - F_4)\cos\theta\vec{i} + (F_1 - F_2 + F_3 - F_4)\sin\theta\vec{j} + (F_5 + F_6 + F_7)\vec{k} \end{aligned} \tag{3.55}$$

$$\begin{aligned} M_{thrust} &= M_{Tx}\vec{i} + M_{Ty}\vec{j} + M_{Tz}\vec{k} \\ &= (y_{c5}F_5 + y_{c6}F_6 + y_{c7}F_7)\vec{i} + (-x_{c5}F_5 - x_{c6}F_6 - x_{c7}F_7)\vec{j} + (x_{c1}F_1\sin\theta - y_{c1}F_1\cos\theta \\ &\quad -x_{c2}F_2\sin\theta - y_{c2}F_2\cos\theta + x_{c3}F_3\sin\theta + y_{c3}F_3\cos\theta - x_{c4}F_4\sin\theta + y_{c4}F_4\cos\theta)\vec{k} \end{aligned} \tag{3.56}$$

In other way, the thruster allocation can be defined as follows

$$\mathbf{U}_v = LU \tag{3.57}$$

$$\mathbf{U}_v = \begin{bmatrix} F_{Tx} & F_{Ty} & F_{Tz} & M_{Tx} & M_{Ty} & M_{Tz} \end{bmatrix}^T \tag{3.58}$$

$$U = \begin{bmatrix} F_1 & F_2 & F_3 & F_4 & F_5 & F_6 & F_7 \end{bmatrix}^T \tag{3.59}$$

$$\begin{aligned} L &= \begin{bmatrix} \mathrm{c}\theta & \mathrm{c}\theta & -\mathrm{c}\theta & -\mathrm{c}\theta & 0 & 0 & 0 \\ \mathrm{s}\theta & -\mathrm{s}\theta & \mathrm{s}\theta & -\mathrm{s}\theta & 0 & 0 & 0 \\ 0 & 0 & 0 & 0 & 1 & 1 & 1 \\ 0 & 0 & 0 & 0 & y_{c5} & y_{c6} & 0 \\ 0 & 0 & 0 & 0 & -x_{c5} & -x_{c6} & -x_{c7} \\ -y_{c1}\mathrm{c}\theta & -y_{c2}\mathrm{c}\theta & y_{c3}\mathrm{c}\theta & y_{c4}\mathrm{c}\theta & 0 & 0 & 0 \\ +x_{c1}\mathrm{s}\theta & -x_{c2}\mathrm{s}\theta & +x_{c3}\mathrm{s}\theta & -x_{c4}\mathrm{s}\theta & & & \end{bmatrix} \\ &= \begin{bmatrix} c\alpha & c\alpha & -c\alpha & -c\alpha & 0 & 0 & 0 \\ s\alpha & -s\alpha & s\alpha & -s\alpha & 0 & 0 & 0 \\ 0 & 0 & 0 & 0 & 1 & 1 & 1 \\ 0 & 0 & 0 & 0 & -l_s & l_s & 0 \\ 0 & 0 & 0 & 0 & -l_f & l_f & l_r \\ d_s c\alpha & -d_s c\alpha & -d_s c\alpha & d_s c\alpha & 0 & 0 & 0 \\ +d_f s\alpha & -d_f s\alpha & -d_r s\alpha & +d_r s\alpha & & & \end{bmatrix} \end{aligned} \tag{3.60}$$

where U_v is the control forces and moments vector acting on the vehicle due to seven thrusters and U is the thrust vector; L is the thruster configuration matrix and θ is the angle between the longitudinal axis and direction of the propeller thrust; l_f

$= x_{c5} = -x_{c6}$ and $l_r = -x_{c7}$ are the distance from the center of buoyancy to the vertical thruster at the bow and stern respectively and $l_s = -y_{c5} = y_{c6}$ is the distance from the center line to the vertical thrusters; $d_s = y_{c2} = y_{c4} = -y_{c1} = -y_{c3}$ is the distance from the center of buoyancy to the port and starboard thruster, $d_f = x_{c1} = x_{c2}$ and $d_r = -x_{c3} = -x_{c4}$ are the distance from the center of buoyancy to the horizontal thruster at the bow and stern respectively.

3.7. Equations of Motion

Now that we have defined the required transformations between the body-fixed and earth-fixed coordinate systems for the velocities, orientations, and positions, we can detail the equations of motion for this UV. These equations of motion are adopted from work done originally by Healey [13] to derive this 6-DOF model. The technique used to derive these equations and relationships is founded on the Newton-Euler approach.

The following equations fully describe a vehicle's motion with 6-DOF, which include three translational and three rotational all in the body-fixed coordinate frame.

Surge

$$(m - X_{\dot{u}})\dot{u} = (-m + Z_{\dot{w}})wq + (m - Y_{\dot{v}})vr + (X_u + X_{u|u|}|u|)u + F_{xthruster} + F_{xcable} \quad (3.61)$$

Or

$$\dot{u} = [(-m + Z_{\dot{w}})wq + (m - Y_{\dot{v}})vr + (X_u + X_{u|u|}|u|)u + F_{xthruster} + F_{xcable}]/(m - X_{\dot{u}}) \quad (3.62)$$

Sway

$$(m - Y_{\dot{v}})\dot{v} = wp(m - Z_{\dot{w}}) + (-m - X_{\dot{u}})ur + (Y_v + Y_{v|v|}|v|)v + F_{ythruster} + F_{ycable} \quad (3.63)$$

Or

$$\dot{v} = [pw(m - Z_{\dot{w}}) + (-m - X_{\dot{u}})ur + (Y_v + Y_{v|v|}|v|)v + F_{ythruster} + F_{ycable}]/(m - Y_{\dot{v}}) \quad (3.64)$$

Heave

$$(m - Z_{\dot{w}})\dot{w} = vp(-m + Y_{\dot{v}}) + qu(m - X_{\dot{u}}) + (Z_w + Z_{w|w|}|w|)w + F_{zthruster} + F_{zcable} \quad (3.65)$$

Or

$$\dot{w} = [pv(-m + Y_{\dot{v}}) + qu(m - X_{\dot{u}}) + (Z_w + Z_{w|w|}|w|)w + F_{zthruster} + F_{zcable}]/(m - Z_{\dot{w}}) \quad (3.66)$$

Roll

$$(I_x - K_{\dot{p}})\dot{p} = vw(Z_{\dot{w}} - Y_{\dot{v}}) + (N_{\dot{r}} - I_z + I_y - M_{\dot{q}})rq + (K_p + K_{p|p|}|p|)p + z_B B\cos\theta\sin\phi + M_{xthruster} + M_{xcable} \tag{3.67}$$

Or

$$\dot{p} = [vw(Z_{\dot{w}} - Y_{\dot{v}}) + (N_{\dot{r}} - I_z + I_y - M_{\dot{q}})rq + (K_p + K_{p|p|}|p|)p + z_B B\cos\theta\sin\phi + M_{xthruster} + M_{xcable}]/(I_x - K_{\dot{p}}) \tag{3.68}$$

Pitch

$$(I_y - M_{\dot{q}})\dot{q} = uw(X_{\dot{u}} - Z_{\dot{w}}) + (I_z - I_x + K_{\dot{p}} - N_{\dot{r}})rp + (M_q + M_{q|q|}|q|)q - z_B B\sin\theta + M_{ythruster} + M_{ycable} \tag{3.69}$$

Or

$$\dot{q} = [uw(X_{\dot{u}} - Z_{\dot{w}}) + (I_z - I_x + K_{\dot{p}} - N_{\dot{r}})rp + (M_q + M_{q|q|}|q|)q - z_B B\sin\theta + M_{ythruster} + M_{ycable}]/(I_y - M_{\dot{q}}) \tag{3.70}$$

Yaw

$$(I_z - N_{\dot{r}})\dot{r} = uv(Y_{\dot{v}} - X_{\dot{u}}) + (M_{\dot{q}} - I_y + I_x - K_{\dot{p}})qp + (N_r + N_{r|r|}|r|)r + M_{zthruster} + M_{zcable} \tag{3.71}$$

Or

$$\dot{r} = [uv(Y_{\dot{v}} - X_{\dot{u}}) + (M_{\dot{q}} - I_y + I_x - K_{\dot{p}})qp + (N_r + N_{r|r|}|r|)r + M_{zthruster} + M_{zcable}]/(I_z - N_{\dot{r}}) \tag{3.72}$$

Chapter 4 Mathematical Model of Umbilical Cable (UC)

In this chapter an overview of cable modeling approaches is first given, and it is shown why catenary equations are the preferred method for cable modeling. Then the theory of catenary equations is treated. In addition, a catenary model of cable system is performed based on existing equations in the literature. It is also shown how the solutions of the static catenary equations are converted to polynomials. Shooting method is used to compute the static equilibrium configuration of a composite single line with boundary conditions specified at both ends. Mathematically the problem is a two point boundary value problem. If all boundary conditions are specified at one end, the configuration is uniquely determined. This reduces the problem to an initial value problem and the static configuration can be found by catenary computations, element by element, starting at the end with all boundary conditions specified.

4.1 General Structure of Umbilical Cable

The UC plays an important role in offering the power supply and communication function between the UV and the support vessel (Fig.4.1). However, the management and attachment of the cable and the drag relative to the current cause some restrictions on maneuverability of the UV. Therefore, the estimation of the corresponding effect caused by the UC and the current will be helpful while we are doing the analysis on the UV's maneuvering behaviors.

Fig.4.1: Umbilical cable

Table 4.1: Umbilical cable's parameters

Notation	Definition	Value	Unit
EA	The axial stiffness of the cable	3×10^4	N
W_c	The weight per length of the cable	0.5	N/m
D_c	Diameter of cable	0.025	m
L_c	Cable length	100	m
E_c	Modulus of elasticity	200×10^9	N/m^2
r_c	Mesh frame of cable	0:0.1:L	m

4.2 Basic Assumptions

In the present study, for simplifying the problem, the following assumptions are made to solve the corresponding configuration and tension of the UC attached to the UV:

- The UC is inextensible
- The UC can only resist tension force, not for bending moment and compression force.
- The hydrodynamic force on the UC can be resolved into tangential component and normal component.
- The cable's a long homogeneous linear elastic circular cylinder were small diameter compared with its length.
- There are no twisting moments acting on the cable.
- The forces acting on the cable are the self-weight, buoyancy, tangential and normal drag forces.
- The cable has no bending stiffness and no torsional stiffness. This means that only axial stiffness will be considered, and this simplifies the analysis of cables considerable compared to for instance beams.
- The cross-sectional area of the cable, A, will not undergo significant changes due to the axial deformation of the cable

4.3 Cable Modeling Approaches

Several methods with different properties exist for this purpose: finite element methods (FEM), finite difference methods (FDM), catenary equations (CE), lump-mass-spring formulations (LMS) and finite segment approaches (FSA). All these

methods are based on a particular and generalized mathematical formulation of the problem. The basic formulation can then be extended to describe different configurations of cables and wires, amongst other mooring cables, towing lines and suspended cables.

FEM methods solve complex elasticity and structural problems. In its most basic form it is a numerical technique for finding approximate solutions of partial differential equations and integral equations. Software packages that solve cable equations using FEM methods exist, and the solutions are accurate. The computational load is however heavy and it is difficult to incorporate such packages into control system designs [20].

Catenary equations provide a static representation of cables [21]. It is easier to gain insight into the mechanisms that govern the solution of the catenary equations than to understand the FEM representation. In addition, they provide a simple representation of the forces acting on the supports where the cable is attached. The equations are solved faster than FEM equations and the result is exact. Catenary equations are normally solved for two dimensions, but three-dimensional approaches also exist [22]. A disadvantage of the catenary approach is that the static solution may become inaccurate for deep water applications, because of dynamic interactions between the vessel and the cable system. If an exact solution is desired for such conditions a FEM method must be utilized.

The LMS formulation has a clear physical interpretation and does not require a large amount of computing. Dynamic analyses of three-dimensional cables based on the LMS approach are discussed in [23]. The method provides a set of ordinary differential equations with boundary conditions that is solved using the FDM method. A general LMS formulation allowing static and dynamic analysis of a variety of slender structures is presented in [24]. The FSA for cable dynamics is discussed in [25]. The cable is modeled as a series of links connected to each other by ball-and-sockets joints. The resulting equations are then solved using standard integration techniques such as Runge-Kutta.

Catenary equations are selected for cable modeling in this thesis. The simple

representation of cable forces and tensions is attractive. The basic theory of catenaries is well established and the equations are more suited for implementation in a feedback system than FEM approaches.

4.4 Three coordinate systems

To analyse the motion of the cable as well as its effect on the vehicle, it is convenient to define three coordinate systems, i.e. the earth-fixed frame (X,Y,Z) and the two cable frames along the cable (t, n, b) and the towed body-fixed frame (x, y, z).

As shown in Fig.4.2 the earth-fixed frame (X, Y, Z) is selected with k pointing vertically downwards. The origins of system (X, Y, Z) and (t, n, b) are coincident. The orientation of the local frame is so chosen that t is tangent to the cable in the direction of increasing tow cable length coordinate s, b is in the plane of i and j, t and n line in a vertical plane. The towed body-fixed frame $(x \quad y \quad z)$ is located at the mass centre of the towed body, with x coinciding with the longitudinal axis, and y pointing to starboard.

The relationship between the vehicle-fixed frame and the earth-fixed frame can be expressed in terms of Euler angles (Fossen, 1994), i.e.

$$[x \quad y \quad z] = [X \quad Y \quad Z] R(\phi, \theta, \psi) \tag{4.1}$$

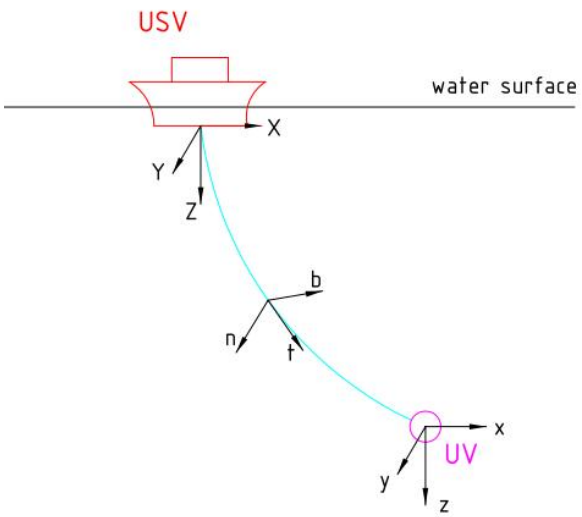

Fig.4.2: Three coordinates of the system

With

$$R(\phi,\theta,\psi)=\begin{bmatrix}\cos\theta\cos\psi & \sin\phi\sin\theta\cos\psi-\cos\phi\sin\psi & \cos\phi\sin\theta\cos\psi+\sin\phi\sin\psi\\ \cos\theta\sin\psi & \sin\phi\sin\theta\sin\psi+\cos\phi\cos\psi & \cos\phi\sin\theta\sin\psi-\sin\phi\cos\psi\\ -\sin\theta & \sin\phi\cos\theta & \cos\phi\cos\theta\end{bmatrix} \tag{4.2}$$

where $c.=\cos$, $s.=\sin$ and ϕ, θ, ψ are the roll, pitch and heading angle of the vehicle, respectively.

The relationship between the local frames and the earth-fixed frame can be expressed as follows [2], [3]:

$$\begin{bmatrix}t & n & b\end{bmatrix}=\begin{bmatrix}X & Y & Z\end{bmatrix}W(\vartheta,\varphi) \tag{4.3}$$

Where

$$W(\vartheta,\varphi)=\begin{bmatrix}\cos\vartheta\cos\varphi & -\cos\vartheta\sin\varphi & \sin\vartheta\\ -\sin\vartheta\cos\varphi & \sin\vartheta\sin\varphi & \cos\vartheta\\ -\sin\varphi & -\cos\varphi & 0\end{bmatrix} \tag{4.4}$$

Equation (4.4) represents a rotation through angle ϑ about the Z axis to bring X axis into the plane of t and n, rotation about the new X axis through $\pi/2$ to bring Z into coincidence with b, and rotation about b through φ to bring X and Y into coincidence with t and n. The relative position of two coordinate systems is shown in Fig. 4.3.

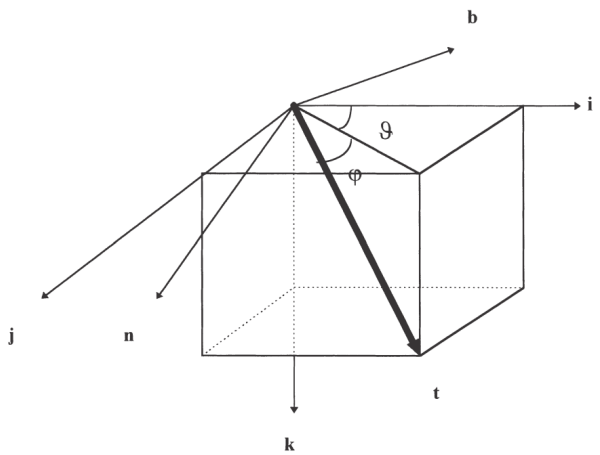

Fig.4.3: The relative position of two coordinate systems.

In terms of equation (4.1)-(44.), the relationship between the local frames and the vehicle-fixed frame can be written as:

$$\begin{bmatrix} t & n & b \end{bmatrix} = \begin{bmatrix} x & y & z \end{bmatrix} R^T(\phi,\theta,\psi) W(\vartheta,\varphi) \tag{4.5}$$

where the orthogonal property of R has been used.

4.5 Forces Acting on the Cable

The forces acting on the cable are (a) the tension, (b) its weight, (c) external forces. The external forces include fluid related forces such as hydrostatic forces and drag forces.

4.5.1 Weight and Buoyancy forces

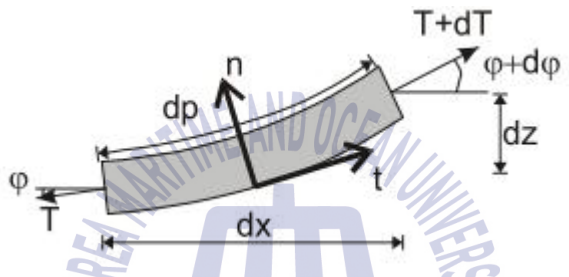

Fig.4.4: An infinite-small cable segment.

Consider Figure 4.4 which shows a cable segment. The cable's weight per unit length in air is denoted $w_a = mg$, where g is the earth's gravity and m is the mass per length unit. When the cable is submerged a hydrostatic force will appear according to

$$B = \rho_w g A \tag{4.6}$$

ρ_w is the density of water and A is the cross-sectional area.

This leads to the following definition of the stretched cable's weight in water, w_1:

$$w_1 = w_a - B \tag{4.7}$$

4.5.2 Fluid Hydrodynamic Forces

Consider the current acting on a small cable element dp in Figure 4.5.

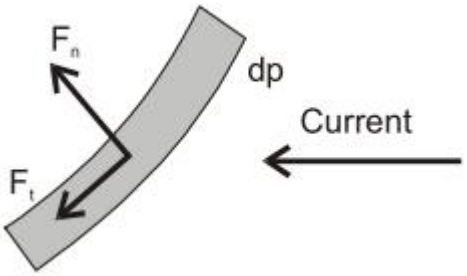

Fig.4.5: Static hydrodynamic forces acting on an infinite-small cable element.

The drag force has two components, namely, the tangential drag force and the normal drag force. From Morison's equation, the tangential drag force is proportional to the square of the tangential

$$df_{dt} = -\frac{1}{2} C_{DT} \rho_w d\,(dp) \left|v.t\right| (v.t)\, t = -\frac{1}{2} C_{DT} \rho_w d\,(dp) \left|v_t\right| v_t, \tag{4.8}$$

On the other hand, the normal drag force is proportional to the square of the normal component of the relative velocity and it is given by:

$$df_{dn} = -\frac{1}{2} C_{DN} \rho_w d\,(dp) \left|v - (v.t)t\right| \left(v - (v.t)t\right) = -\frac{1}{2} C_{DT} \rho_w d\,(dp) \left|v_n\right| v_n, \tag{4.9}$$

where ρ_w is the density of water, d is the cable's diameter, C_{DT} and C_{DN} are tangential and normal drag coefficients, t is tangential vector of the cable, v, v_t and v_n are velocity, normal velocity and tangential velocity on the cable on vectorial form. Notice that it is common to normalize to the projected area $d.(dp)$, in this kind of hydrodynamic forces. Some refer to f_{dn} as the normal friction force, but this is inaccurate. Friction forces are usually normalized to wet surface of the body. For a cable in the normal direction this leads to

$$df_{df} = -\frac{1}{2} C_{DF} \rho_w d\pi\,(dp) \left|v - (v.t)t\right| \left(v - (v.t)t\right) = -\frac{1}{2} C_{DF} \rho_w d\pi\,(dp) \left|v_n\right| v_n, \tag{4.10}$$

Where $C_{DF} = \frac{1}{\pi} C_{DN}$ (4.11)

Hydrodynamic forces may not be handled in the same way as gravity in the catenary equations. Gravity acts on each cable segment independently of its orientation. This means that the shape and tension may be solved explicitly.

Calculation of current forces requires information on the cable segment's orientation, and calculation of orientation requires knowledge of the current forces. Consequently, an iteration procedure is needed. The calculation of hydrodynamic forces (4.8), (4.9) and (4.10) assumes that the water's velocity is constant over the actual segment. For analytical solutions the hydrodynamic forces have to be constant over each segment.

4.5.3 Tension Force

The tension T acts along the tangent of the average cable configuration, where the average cable configuration is defined as the smoothest possible profile of the cable**.** The force on an element with un-stretched length can be written as:

$$\frac{d}{ds}(T_e\vec{t})ds = \left[\frac{\partial T_e}{\partial s}\vec{t} + T_e\frac{\vec{dt}}{ds}\right]ds$$
$$= \left[\frac{\partial T_e}{\partial s}\vec{t} + \frac{T_e}{\rho}\vec{n}\right]ds \qquad (4.12)$$

Given a cable tension, T_c Triantafyllou [26] shows that the effective tension, T may be written as

$$T_e = T_c + p_e A \qquad (4.13)$$

where p_e is the hydrostatic pressure at the specific point of the cable.

4.6 Dynamic equations of cable

4.6.1 Catenary Equations

The word catenary is derived from the latin word catena, referring to the shape of a chain or wire hanging between two points under its own weight. Catenary equations are widely used in mooring analysis of anchored bodies. The catenary equation theory is extensively covered in the literature. An overview of general catenary equations is given in [21]. In [26] the theory is extended to apply for submerged cables. Vertical and horizontal forces caused by the cable system will act on the UV at the terminal points. However, often only the horizontal forces are important for the UV response in the horizontal plane. Along the cable gravity and buoyancy forces are assumed to be most important. For this purpose a two-

dimensional approach is often considered to be sufficient. If varying current in space is considered, a three-dimensional approach may be needed.

4.6.2 Static Catenary Analysis

The coordinate system for analyzing the UC is shown in Fig.4.6. The x-axis is assumed to coincide with the X-axis. The origin O coincides with the end point of the UC. ϑ is the angle between xoz plane and the plane which includes the tangential line passing through the point A and perpendicular to xoy plane. φ is the angle between the tangential line passing through the point A and xoy plane. i_t, i_b, and i_n are the unit vector along the cable length s, ϑ and φ, respectively, and perpendicular to each other. Both i_t and i_n, are located on the vertical plane.

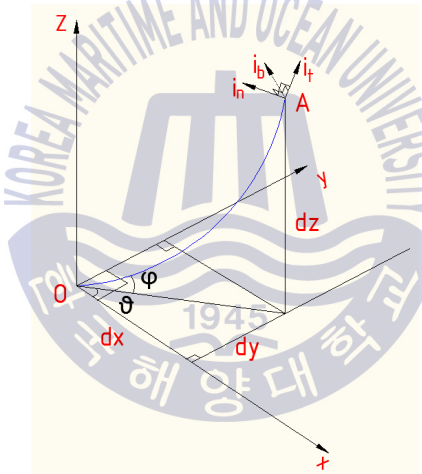

Fig.4.6: Coordinate for the UC

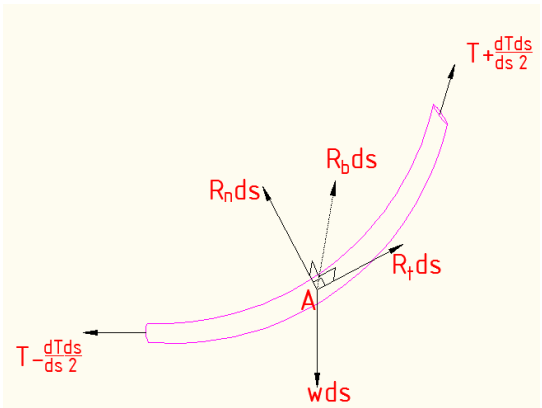

Fig.4.7: Forces acting on a segment of a cable profile

Considering the configuration of the UC as shown in Fig.4.6, we can obtain the following three linear differential equations.

$$dx = ds \times \cos\varphi \times \cos\vartheta \tag{4.14}$$

$$dy = ds \times \cos\varphi \times \sin\vartheta \tag{4.15}$$

$$dz = ds \times \sin\varphi \tag{4.16}$$

Considering the equilibrium state of the external force on the cable as shown in Fig.4.6 and Fig.4.7, we can obtain more three linear differential equations.

By balancing the forces of direction of i_t a cable segment, we have

$$\begin{aligned} &R_t ds - w\sin\varphi ds + (T + \frac{dT}{2})\cos(\frac{1}{2}\frac{d\varphi}{ds}ds)\cos(\frac{1}{2}\frac{d\vartheta}{ds}ds) \\ &-(T - \frac{dT}{2})\cos(\frac{1}{2}\frac{d\varphi}{ds}ds)\cos(\frac{1}{2}\frac{d\vartheta}{ds}ds) = 0 \end{aligned} \tag{4.17}$$

Or, the Eq. (4.17) becomes

$$dT = w\sin\varphi ds - R_t ds \tag{4.18}$$

By balancing the forces of direction of i_n a cable segment, we have

$$R_g ds + (T + \frac{dT}{2})\sin\frac{d\vartheta}{2}\cos(\varphi + \frac{d\varphi}{2}) + (T - \frac{dT}{2})\sin\frac{d\vartheta}{2}\cos(\varphi - \frac{d\varphi}{2}) = 0 \tag{4.19}$$

Assuming $\sin\frac{d\vartheta}{2} \approx \frac{d\vartheta}{2}$ and $\cos\frac{d\vartheta}{2} \approx 1$ the Eq. (4.19) can be rewritten as follows

$$d\vartheta = -\frac{R_g ds}{T\cos\varphi} \tag{4.20}$$

By balancing the forces of direction of i_b a cable segment, we have

$$d\varphi = \frac{(-R_\varphi ds + w\cos\varphi ds)}{T} \tag{4.21}$$

Finally, from Eq.(4.14), Eq.(4.15), Eq.(4.16), Eq.(4.18), Eq.(4.20) and Eq.(4.21), we can obtain the full linear differential equations of cable as follows

$$\frac{dx}{ds} = \cos\varphi \times \cos\vartheta \tag{4.22}$$

$$\frac{dy}{ds} = \cos\varphi \times \sin\vartheta \tag{4.23}$$

$$\frac{dz}{ds} = \sin\varphi \tag{4.24}$$

$$\frac{dT}{ds} = w\sin\varphi - R_t \tag{4.25}$$

$$\frac{d\vartheta}{ds} = -\frac{R_\vartheta}{T\cos\varphi} \tag{4.26}$$

$$\frac{d\varphi}{ds} = \frac{(-R_\varphi + w\cos\varphi)}{T} \tag{4.27}$$

where s is the arc length from the origin to the point A on the cable. T is the tension force along the cable. w is the cable weight per unit length in the water. R_t, R_ϑ and R_φ are the forces per unit length due to the current in i_t, i_n, and i_b directions, respectively.

4.7 Solution of the Catenary equation in the 3-D case

In this section, a detailed procedure for finding the general elastic catenary equations in 3-D is presented. This section is mainly based on Sagatun [22]. Consider a cable of length L with one end fixed in space and the other end free. The cable may have varying axial stiffness EA along its length. The symbol s represents the Lagrangian coordinate along the unstrained cable, whereas the symbol u will represent the corresponding point on the cable when it is strained. The force vector $f_0 = \begin{bmatrix} f_{0x} & f_{0y} & f_{0z} \end{bmatrix}^T$ represents the reaction forces from the cable on its termination point. The force vector $\overline{f}_i = \begin{bmatrix} \overline{f}_{ix} & \overline{f}_{iy} & \overline{f}_{iz} \end{bmatrix}^T$ represents a concentrated force acting on an arbitrary point i along the cable, and the distributed load vector $p_i = \begin{bmatrix} p_{ix} & p_{iy} & p_{iz} \end{bmatrix}^T$ force per unit length acts on the cable segment between points i and i-1. A force vector with all elements set to zero may be used to define a point along the cable on which a distributed load or the axial stiffness is altered. The proposed method is restricted to handle piecewise constant axial stiffness and distributed loads. However, continuously spatially varying stiffness or distributed load may be modeled with arbitrary accuracy by using a number of

cable segments. The result of the proposed method is an analytical piecewise continuous static solution of the form $r(s) = \begin{bmatrix} x(s) & y(s) & z(s) \end{bmatrix}^T$, where s varies from 0 to L. The discontinuities occur where a point load acts or where the axial stiffness or the distributed load change.

Remember the assumption of no significant reduction of the cable's cross-sectional area when it is stretched. Considering the cable with one-dimensional strain along the Lagrangian variable s, Hooke's law is

$$T = EA\left(\frac{dp}{ds} - 1\right) \tag{4.28}$$

Seeking a solution in Cartesian coordinates of the cable as a function of s, the identity $\frac{dr}{ds} = \frac{dr}{dp}\frac{dp}{ds}$ will be useful. $r = \begin{bmatrix} x & y & z \end{bmatrix}^T$ contains the Cartesian coordinates as a function of s or p. This leads to the relation

$$\frac{dr}{ds} = \frac{dr}{dp}\left(\frac{T}{EA} + 1\right) \tag{4.29}$$

Consider the first segment of a cable with distributed vertical force, w_z, a vertical concentrated force, $f_{1,z}$ and axial tension T in the end point. Inspection of Fig.4.8 gives

$$f_{oz} = T\left.\frac{dz}{dp}\right|_{s=s_1} + \overline{f}_{1,z} + w_z(s_1 - s_0) \tag{4.30}$$

for static equilibrium. s_i indicates the value of s in node i and $\overline{f}_{i,k}$ indicates the value of concentrated force in node i and Cartesian direction k

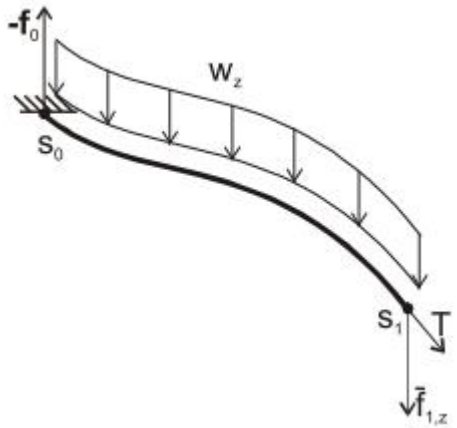

Fig.4.8: A cable segment with concentrated and distributed loads.

Assume that the cable is terminated in point 0, and that concentrated forces, $\overline{f}_i$ may act discrete points (cable nodes). Combination of this assumption and (4.30) written in vectorial form gives the following equation for the forces acting in the cable's terminating point:

$$f_o = T\frac{dr}{dp}\bigg|_{s=L} + \sum_{i=1}^{n}\overline{f}_i + \sum_{i=1}^{n} w_i(s_i - s_{i-1}) \tag{4.31}$$

where $\left\{s \in [0,L] \to \square, k \in [1,n] \to \square \,\middle|\, s \in [s_{k-1}, s_k]\right\}$. n is the number of cable segments and L is the cable's unstretched length. $w_i = \begin{bmatrix} w_{ix} & w_{iy} & w_{iz} \end{bmatrix}^T$ indicates the constant distributed force vector in segment i.

An investigation of Fig.4.9 may make it easier to keep the indexes of the variables right

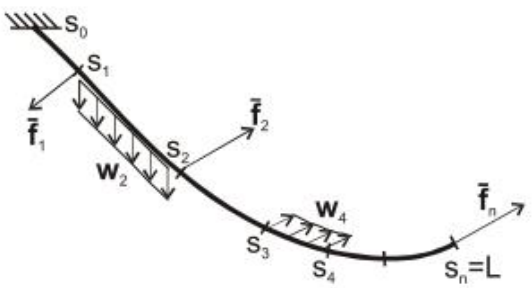

Fig.4.9: A cable of several segments with concentrated forces, $\overline{f}_i$ and distributed forces, w_i Notice the indexes.

A constant distributed force along the cable leads to a simplification of (4.31)

$$f_o = T\left.\frac{dr}{dp}\right|_{p(s=L)} + \sum_{i=1}^{n}\overline{f}_i + wL \tag{4.32}$$

where w is the constant distributed force along the cable.

Sagatun [22] gives the following derivation of a differential equation for the cable. It is assumed that (4.32) holds. Reordering of (4.32) leads to

$$T\left.\frac{dr}{dp}\right|_{p(s=L)} = f_o - \sum_{i=1}^{n}\overline{f}_i - wL \tag{4.33}$$

We want to find the tension vector as a function of s. Assume that $s(p)$ may be found from (4.29). Then the following relation must hold

$$T\frac{dr}{dp}(s) = f_o - \sum_{i=1}^{k}\overline{f}_i - ws \tag{4.34}$$

Where $\left\{s \in [0,L] \to \square, k \in [1,n] \to \square \,\middle|\, s \in [s_{k-1}, s_k]\right\}$. We define

$$T(p) = T\begin{bmatrix}\frac{dx}{dp}\\ \frac{dy}{dp}\\ \frac{dz}{dp}\end{bmatrix} = T\frac{dr}{dp} \tag{4.35}$$

$$T^T T = T^2 \frac{dr^T}{dp}\frac{dr}{dp} \tag{4.36}$$

Where $T \in \square^3$. The substitution

$$f_k = f_0 - \sum_{i=1}^{k}\overline{f_i} \tag{4.37}$$

Where $\left\{k \in [0,n] \to \square, s \in [1,L] \to \square \,\middle|\, s \in [s_{k-1}, s_k]\right\}$ gives

$$T_s = \sqrt{(f_k - ws)^T (f_k - ws)} \tag{4.38}$$

Combining (4.37) and (4.34) gives:

$$T\frac{dr}{dp}(s) = f_o - \sum_{i=1}^{k} \overline{f}_i - ws = f_k - ws, \tag{4.39}$$

Use of (4.29)

$$T\frac{dr}{dp}(s) = \left(\frac{1}{EA} + \frac{1}{T}\right)^{-1} \frac{dr}{ds} = f_k - ws, \tag{4.40}$$

Reordering leads to

$$\frac{dr}{ds} = (f_k - ws)\left(\frac{1}{EA} + \frac{1}{T}\right) \tag{4.41}$$

Remember that $T = f_k - ws$ represents the tension in vectorial form. Substituting (4.38) gives the final differential equation

$$\frac{dr}{ds} = (f_n - ps)\left(\frac{1}{\sqrt{(f_k - ps)^T (f_k - ps)}} + \frac{1}{EA}\right) \tag{4.42}$$

This is an ODE with s as the independent variable. This may be solved directly from the rewritten form

$$r_k = \int_{s_{k-1}}^{s_k} (f_n - ps)\left(\frac{1}{\sqrt{(f_k - ps)^T (f_k - ps)}} + \frac{1}{EA}\right) ds \tag{4.43}$$

where k is the actual cable segment. r_k is an expression for the local solution within segment k.

Numerical methods could have been utilized to solve the ODE/IVP, but Sagatun [22] gives the following solution to the integral

$$r_k(s) = \frac{\alpha(s)}{\beta^3}(f_k\beta^2 - f_k \otimes w \otimes w - f_k \otimes (P(f_k \otimes w))) - w\frac{1}{\beta^2}\sqrt{(f_k - ws)^T (f_k - ws)}$$
$$+\frac{1}{EA}\left(f_k s - \frac{1}{2}ws^2\right) + C_i \tag{4.44}$$

where $\otimes$ denotes component wise multiplication and

$$\beta = \sqrt{w^T w} = \|w\|_2 \tag{4.45}$$

$$\alpha = \ln\left(\left(\beta s - \frac{1}{\beta} f_k^T w\right) + \sqrt{\left(f_k - ws\right)^T \left(f_k - ws\right)}\right) \tag{4.46}$$

$$P = \begin{bmatrix} 0 & 1 & 1 \\ 1 & 0 & 1 \\ 1 & 1 & 0 \end{bmatrix} \tag{4.47}$$

Assume that we want segment no.1 of the global solution r(s) to start in the origin. We also want to ensure continuity between the segments. The following conditions should be fulfilled

$$r(0) = 0, \tag{4.48}$$

$$r(s_i)^- = r(s_i)^+, \left\{ i \in [1, n-1] \rightarrow \square \right\} \tag{4.49}$$

The integration constants, $C_i, i \in [0, n-1]$ may be calculated from

$$C_{k-1} = \begin{cases} -r_1(0), & for \quad k = 1 \\ r_{k-1}(s_{k-1}) - r_k(s_{k-1}), & for \quad k \in [2, n] \rightarrow \square, \quad for \quad n \geq 2 \end{cases} \tag{4.50}$$

If s belongs to a segment with index higher than 1, C_{k-1} must be calculated iteratively before the solution of r(s) can be found. The final global solution may now be calculated from

$$r(s) = \frac{\alpha(s)}{\beta^3}(f_k \beta^2 - f_k \otimes w \otimes w - f_k \otimes (P(f_k \otimes w))) - w\frac{1}{\beta^2}\sqrt{\left(f_k - ws\right)^T \left(f_k - ws\right)}$$
$$+ \frac{1}{EA}\left(f_k s - \frac{1}{2} w s^2\right) + C_{k-1} \tag{4.51}$$

Where $\left\{ s \in [0, L] \rightarrow \square, k \in [1, n] \rightarrow \square \mid s \in [s_{k-1}, s_k] \right\}$

4.8 Spatial variation in the distributed load

The solution given above is only valid for constant distributed load along the entire cable. However, an extension to different distributed loads for each segment may be found. Instead of using (4.32), we will assume that the distributed load is constant only within each segment. This means that f_0 must be calculated from (4.31). Eq. (4.39) must be rewritten to

$$T\frac{dr}{dp}(s) = f_o - \sum_{i=1}^{k}\overline{f}_i - \sum_{i=1}^{k-1} w_i\left(s_i - s_{i-1}\right) - w_k\left(s - s_{k-1}\right), \tag{4.52}$$

Where $\left\{s \in [0, L] \to \square, k \in [1, n] \to \square \,\middle|\, s \in \left[s_{k-1}, s_k\right]\right\}$. We modify (4.37) to

$$f_k = f_0 - \sum_{i=1}^{k}\overline{f}_i - \sum_{i=1}^{k-1} w_i(s_i - s_{i-1}) + w_k s_{k-1} \tag{4.53}$$

Now the derivation goes just like in the previous section, and we end up with

$$r_k = \int_{s_{k-1}}^{s_k} \left(f_n - w_k s\right)\left(\frac{1}{\sqrt{\left(f_n - w_k s\right)^T\left(f_n - w_k s\right)}} + \frac{1}{EA}\right) ds \tag{4.54}$$

Continuing on the boundary condition and claiming continuity between segments, the integration constants may be calculated as before. The new solution for spatially varying distributed loads with the assumptions made above, are given from

$$r(s) = \frac{\alpha(s)}{\beta^3}(f_k\beta^2 - f_k \otimes w_k \otimes w_k - f_k \otimes (P(f_k \otimes w_k))) - w_k\frac{1}{\beta^2}\sqrt{\left(f_k - w_k s\right)^T\left(f_k - w_k s\right)}$$
$$+\frac{1}{EA}\left(f_k s - \frac{1}{2}w_k s^2\right) + C_{k-1} \tag{4.55}$$

$$\beta = \sqrt{w_k{}^T w_k} = \left\|w_k\right\|_2 \tag{4.56}$$

$$\alpha = \ln\left(\left(\beta s - \frac{1}{\beta}f_k^T w_k\right) + \sqrt{\left(f_k - w_k s\right)^T\left(f_k - w_k s\right)}\right) \tag{4.57}$$

$$P = \begin{bmatrix} 0 & 1 & 1 \\ 1 & 0 & 1 \\ 1 & 1 & 0 \end{bmatrix} \tag{4.58}$$

4.9 Boundary Conditions

Boundary conditions must be given at both ends of the cable (upper end and lower end). Different types of boundary conditions may occur depending on the types of physical conditions at the two ends. As we assume that the vessel motion is fixed by using dynamic position control, the first boundary condition is given by fixing the position of the surface vessel. At the lower end, cable is connected to the

vehicle. So, the second boundary condition of lower end of the cable $X_0 = X_0(t)$ is given as a function of time. These two conditions can be expressed as follows,

$$x_0(0,t) = 0,\ y_0(0,t) = 0,\ z_0(0,t) = 0 \tag{4.59}$$

$$\text{And } x_L(L,t) = x_L,\ y_L(L,t) = y_L,\ z_L(L,t) = z_L \tag{4.60}$$

Where x_L y_L and z_L are position of UV during its motion.

4.10 Cable effect

The tension of the cable at the tow-point, i.e. $T(0,t)$, results in the additional forces and moments that affect the motion of the vehicle. The additional forces can be obtained by expressing the cable tension in the vehicle-fixed frame.

$$F_c(t) := \begin{bmatrix} F_{cX} \\ F_{cY} \\ F_{cZ} \end{bmatrix} = -R^T(\phi,\theta,\psi)W(\vartheta,\varphi)\begin{bmatrix} T(0,t) \\ 0 \\ 0 \end{bmatrix} \tag{4.61}$$

Where

$$F_{cX} = T(0,t)(c\psi c\theta c\vartheta c\varphi - s\psi c\theta s\vartheta c\varphi + s\theta s\varphi) \tag{4.62}$$

$$F_{cY} = T(0,t)(-c\theta s\phi s\varphi + s\phi c\psi s\theta c\vartheta c\varphi - s\phi s\psi s\theta s\vartheta c\varphi - c\psi c\phi s\vartheta c\varphi - s\psi c\phi c\vartheta c\varphi) \tag{4.63}$$

$$F_{cZ} = T(0,t)(-c\theta c\phi s\varphi + s\phi s\psi c\vartheta c\varphi + s\phi c\psi s\vartheta c\varphi + c\psi s\theta c\phi c\vartheta c\varphi - s\psi s\theta c\phi c\vartheta c\varphi) \tag{4.64}$$

In terms of the position of the tow-point in the vehicle-fixed frame, the cable induced moments are

$$M_c(t) := \begin{bmatrix} M_{cX} \\ M_{cY} \\ M_{cZ} \end{bmatrix} = r_c \times F_c(t) = \begin{bmatrix} x_c \\ y_c \\ z_c \end{bmatrix} \times \begin{bmatrix} F_{cX} \\ F_{cY} \\ F_{cZ} \end{bmatrix} = \begin{bmatrix} y_c F_{cZ} - z_c F_{cY} \\ z_c F_{cX} - x_c F_{cZ} \\ x_c F_{cY} - y_c F_{cX} \end{bmatrix} \tag{4.65}$$

where $\vec{r_c} = (x_c, y_c, z_c)$ is vector from the center of the gravity of UV to the connected point between the cable and UV.

4.11 Simulation results of umbilical cable

To this point we have considered catenaries as a cable with known properties and known loads. The goal has been to achieve a solution for the end point. Let us

revert this and try to find the force components when the two end points are known. The governing differential equations are still known, see (4.42). The problem has now changed from an ODE (Ordinary Differential Equations)/IVP (Initial Value Problems) to an ODE/BVP (Boundary Value Problems). An analytical solution to this problem could be found if f_k was solved from (4.42). Nobody has published such analytical solution, and we will have to deal with numerical solutions of the problem. The MATLAB's function bvp4c or e.g. a finite element solution will do if the cable's geometry is of particular interest.

Sometimes other problems arise when we are dealing with boundary value problems. We may for instance know the boundary coordinates, but want to find the end force to yield this solution. The ODE/BVP has now increased to include an estimation of the parameter $\overline{f_1}$. A shooting method based on the accurate analytical solution might be applied. Shooting method is used to compute the static equilibrium configuration of a composite single cable with boundary conditions specified at both ends. Mathematically the problem is a two point boundary value problem. If all boundary conditions are specified at one end, the configuration is uniquely determined. This reduces the problem to an initial value problem and the static configuration can be found by catenary computations, element by element, starting at the end with all boundary conditions specified.

We will now give an example where we use MATLAB's routine to estimate this force. A cable of length 100 meters is fastened in $\begin{bmatrix}0 & 0 & 0\end{bmatrix}$.The UC is divided into 100 equal length elements and the result from one element is propagated into next till it reaches the final end point at the UV. The initial guess for the forces in N is $\begin{bmatrix}4 & 5 & 180\end{bmatrix}^T$, cable's length is 100m, cable's weight is $W_c = -0.5N/m$, diameter $d_c = 0.025m$, modulus of elasticity $E_c = 200\times10^9 N/m^2$, axial stiffness $EA = 3\times10^4 N$ and density $\rho_c = 662.2kg/m^3$.The inertial reference frame (X, Y, Z) is defined at surface of waterline and the first cable's element is attached to the supported vessel. The UC forces in three-dimensional (3D) are computed by the

method in Sagatun [22] that uses Catenary equations with end forces estimates. MATLAB's routine bvp4c was applied to these parameters, and an estimate of the end force was found. The results are shown in Fig.4.11, Fig.4.12 and Fig.4.13. Even if the initial guess for the estimated force deviated from the correct value, the routine managed to find very good estimates. The results were dependent on the numerical option and the mesh in the variable s. The UC's parameters for simulation are shown in Table 4.1. Figure 4.10 shows profile of 3-D forces acting on the UC.

Table 4.2: UC's parameters for simulation

Cable parameters	
Length of cable (m)	L=100
3-D forces on cable (N/m)	$W = [3 \quad 3 \quad -5]$
Diameter of cable (m)	$d = 0.025$
Axial stiffness (N)	$EA = 3.10^4$
Position of end point (calculated from equation) (m)	$E_p = [86.4 \quad 0 \quad -45.42]$
Guess for end force (we know this guess is wrong) (N)	$F_g = [4 \quad 5 \quad 10]$

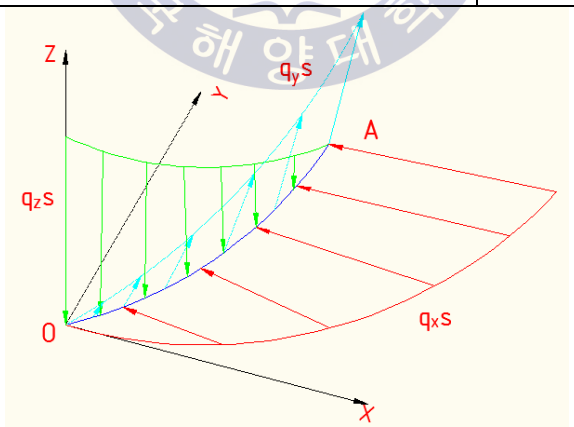

Fig.4.10: The all forces acting on the UC

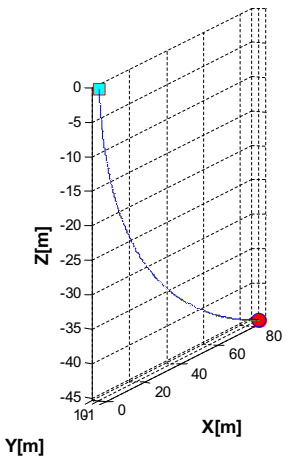

Fig.4.11: Static configuration of UC

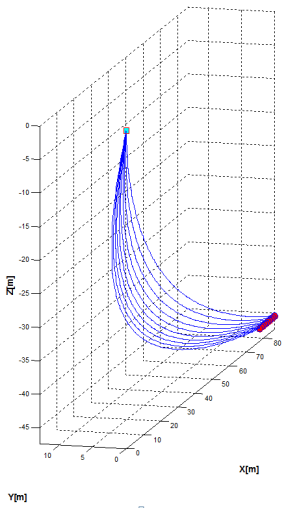

Fig.4.12: Dynamic configuration of UC

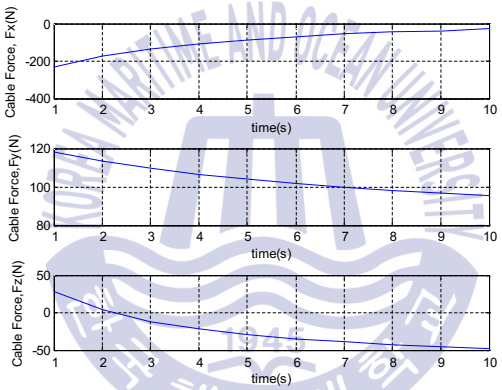

Fig.4.13: The end point forces of UC.

Figure 4.11 shows a cable of length L attached to a blue point and a red point. These points are defined as the cable supports and they are fixed in space. Here, as in the simulation, the top end or blue point is assumed to be fixed to the support ship, the bottom or red point is attached to the UV. Starting from support blue point and moving along the cable profile, each point on the cable is described by the Lagrangian coordinate s with respect to the origin. s is defined as the un-stretched Lagrangian coordinate. And the flow across the cable is determined by the relative velocity between UV and current. When the current is turned on, the cable is pushed to the left and during this motion, under the influence of the side current, and provided there is slack in the cable, the umbilical will form a curve. For

calculating the position of the red point, Eqs.4.51 was used to determine this point and calculated value is $E_p = \begin{bmatrix} 86.4 & 0 & -45.42 \end{bmatrix} m$. The Eqs.4.42 gives the end force equal $f_{end} = \begin{bmatrix} 230.55 & -117.94 & -27.97 \end{bmatrix}^T N$

The dynamic configuration of UC and the end point forces of cable are shown in Fig.4.12 and Fig.4.13, respectively. It is observed from Fig.4.12 that the trajectory of the red point move backward for about 10m in 10 seconds because the speed of red point is 1m/s. The end point forces in 3 dimensions of UC when the red point moves backward is shown in Fig.4.13. As we can see from this figure that the end point forces increases gradually with increasing in time in three components F_x, F_y, F_z.

Chapter 5 Simulation Results and Discussion

In this chapter, a series of analyses on the behavior of UV with the UC are analyzed. A simulator is implemented using a model of the underwater robot. For the vehilce, a MATLAB-Simulink model was used. The model used MATLAB three subsystems for the thruster modeling, cable modeling and underwater dynamic modeling. Fig.5.2 is shown block simulation program for UC. And Fig.5.1 illustrates the blocks used in the Matlab and Simulink, which thrusters are modeled by first subsystem. Other subsystems model dynamics and kinematics of the vehicle. The outputs of the Simulink model are position, orientation and velocity vectors in earth refernce frame and linear and angular velocity and acceleration vectors in body frame. As we can see in the Fig.5.1, the output of subsystems for UV dynamic modeling such as 3-D position x,y,z of UV are also input of subsystem for cable dynamic. It mean that to calculate the forces acting on the UV, we have to know the position of UV which attached with cable at termination point.

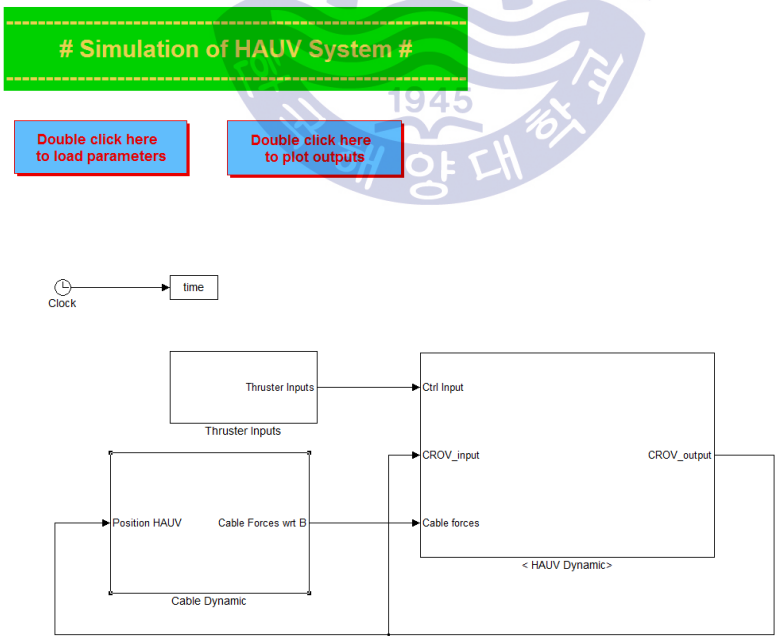

Fig.5.1: Simulation program for UV with UC

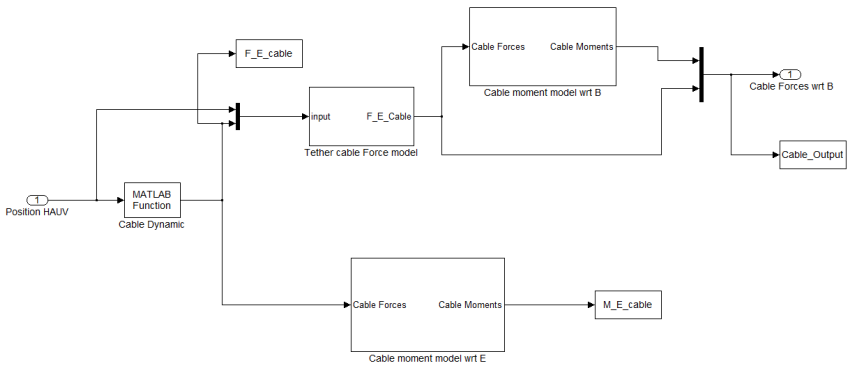

Fig.5.2: Block simulation program for UC

In the dynamical modeling, UV is regarded as a rigid body of constant mass moving in an ideal potential flow and the B-frame is positioned at the center of gravity. As well, UV is assumed to be neutrally buoyant. Let the vehicle's linear and angular velocities be defined in the vehicle-fixed referenced frame. The governing equations for describing the motion of UV in 6-DOF can be expressed as follows:

$$
\begin{cases}
\dot{u} = [(-m + Z_{\dot{w}})wq + (m - Y_{\dot{v}})vr + (X_u + X_{u|u|}|u|)u + F_{xthruster} + F_{xcable}]/(m - X_{\dot{u}}) \\
\dot{v} = [pw(m - Z_{\dot{w}}) + (-m - X_{\dot{u}})ur + (Y_v + Y_{v|v|}|v|)v + F_{ythruster} + F_{ycable}]/(m - Y_{\dot{v}}) \\
\dot{w} = [pv(-m + Y_{\dot{v}}) + qu(m - X_{\dot{u}}) + (Z_w + Z_{w|w|}|w|)w + F_{zthruster} + F_{zcable}]/(m - Z_{\dot{w}}) \\
\dot{p} = [vw(Z_{\dot{w}} - Y_{\dot{v}}) + (N_{\dot{r}} - I_z + I_y - M_{\dot{q}})rq + (K_p + K_{p|p|}|p|)p + z_B B\cos\theta\sin\phi + \\
M_{xthruster} + M_{xcable}]/(I_x - K_{\dot{p}}) \\
\dot{q} = [uw(X_{\dot{u}} - Z_{\dot{w}}) + (I_z - I_x + K_{\dot{p}} - N_{\dot{r}})rp + (M_q + M_{q|q|}|q|)q - z_B B\sin\theta + \\
M_{ythruster} + M_{ycable}]/(I_y - M_{\dot{q}}) \\
\dot{r} = [uv(Y_{\dot{v}} - X_{\dot{u}}) + (M_{\dot{q}} - I_y + I_x - K_{\dot{p}})qp + (N_r + N_{r|r|}|r|)r + M_{zthruster} + M_{zcable}]/(I_z - N_{\dot{r}})
\end{cases}
\tag{5.1}
$$

Note that these equations are written in the body-fixed coordinates. The Runge-Kutta method is used to solve these six nonlinear differential equations.

Consider the equations of motion in (5.1), in which eighteen parameters including added mass derivatives $X_{\dot{u}}\ Y_{\dot{v}}\ Z_{\dot{w}}\ K_{\dot{p}}\ M_{\dot{q}}\ N_{\dot{r}}$, linear damping $X_u\ Y_v\ Z_w\ M_q\ K_p\ N_r$ and quadratic drag coefficients $X_{u|u|}\ Y_{v|v|}\ Z_{w|w|}\ K_{p|p|}\ M_{q|q|}\ N_{r|r|}$ are involved.

In the present study a commercial UV is adopted as the numerical model for calculations. The principal dimension is 0.75 m (length) x 0.56 m (beam) x 0.28 m (depth) and all hydrodynamic coefficients about the maneuvering characteristics and related variables of the UV can be referred to related papers. The globe coordinates of initial position of the connected point to the UV and the other end point at the free surface near supported vessel are assumed to be (60, 0, 60)m and (0, 0, 0)m, respectively. The length of the UC is set to be 100 m, cable's weight is $W_c = -0.5N/m$, diameter $d_c = 0.025m$, modulus of elasticity $E_c = 200\times10^9 N/m^2$, axial stiffness $EA = 3\times10^4 N$ and density $\rho_c = 662.2kg/m^3$, are also assumed to meet the physically correct initial cable conditions which are obtained by using the multi-step shooting method once in advance.

The effects of the UC on the UV motions with different operations, i.e., forward, backward, ascending, descending, sideward and turning, are shown in Figs.5.3–5.50.

5.1 Forward Motion

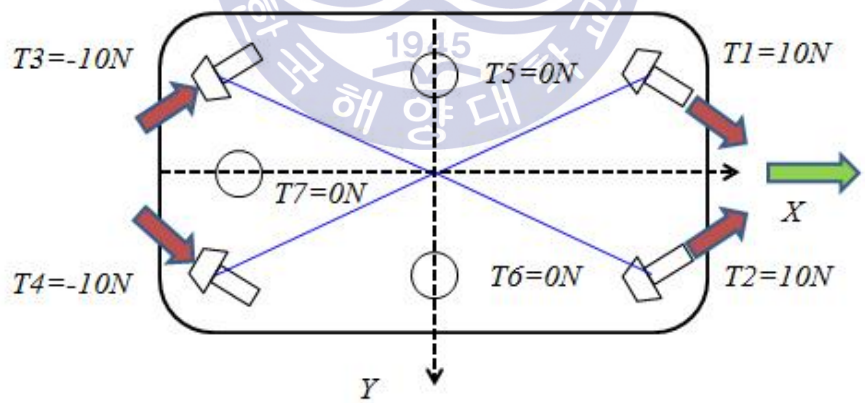

Fig.5.3: Thruster directions of UV in forward motion.

Fig.5.3 shows thruster directions of UV in forward motion. Let us consider the dynamic equation for each single-degree-of-freedom motion first. From (3.35) ~ (3.36) and (3.61) ~ (3.72), it follows that the dynamical equations of forward motion are simplified as:

$$\begin{cases} \dot{u} = [(X_u + X_{u|u|}|u|)u + F_{xthruster} + F_{xcable}]/(m - X_{\dot{u}}) \\ \dot{v} = F_{ycable}/(m - Y_{\dot{v}}) \\ \dot{w} = F_{zcable}/(m - Z_{\dot{w}}) \\ \dot{p} = M_{xcable}/(I_x - K_{\dot{p}}) \\ \dot{q} = M_{ycable}/(I_y - M_{\dot{q}}) \\ \dot{r} = M_{zcable}/(I_z - N_{\dot{r}}) \end{cases} \tag{5.2}$$

Fig.5.4 and 5.5 are the trajectory of the UV in both cases, attached with the UC and without UC doing the forward motion. If the UV is steered in surge to keep the vehicle moving forward, thus both thrusters T_1 and T_2 are set to be 10N ($T_1 = T_2 = 10N$) and both thrusters T_3 and T_4 are set to be -10N ($T_3 = T_4 = -10N$); that is, total thrust/weight = 0.44. All of thrusters T_5, T_6, T_7 are set to be 0N ($T_5 = T_6 = T_7 = 0N$) to make the pure forward motion and initial UV speed is 0m/s. Fig.5.6 is the force and moment of thruster system on the UV doing forward motion. It is observed from Fig.5.6 that for the forward motion, the force F_x keeps at constant value equal 34.6 N and other components equal zero, i.e, $F_y = F_z = M_x = M_y = M_z = 0N$.

The effect of the umbilical cable can be clearly seen by comparing Fig.5.7 with Fig.5.8. It is observed from Fig.5.7 that the UV moves forward for about 12 m in 30 sec with the velocity about 0.38 m/s. The results in Fig.5.8 show that the depth of the UV increases and UV will be move slightly leftward while the UV is moving forward. Besides, due to the attachment of the cable, the heave velocity appears to be oscillatory due to heave force F_{cz} of cable effect and so is the pitch motion. UV oscillates downward and the heave velocity w and the pitch angle θ also regularly oscillate. It means that the UV will move forward up and down with varied pitch angle. However, the roll and yaw motions are not affected by the cable in this case.

The force and moment of the UC including the current effect with respect to fixed body coordinate and Earth coordinate are shown in Fig.5.9 and Fig.5.10 for reference. The results show that the oscillatory heave force F_{cz} and pitch moment

M_{cy} cause the oscillatory heave and pitch motions, respectively. The results in Fig.5.9 also reveal that the sway force F_{cy} is negative, that is, leftward, and the heave force F_{cz} is positive leads to downward heave velocity; therefore, the UV has the tendency to descend and leftward while the UV is moving forward.

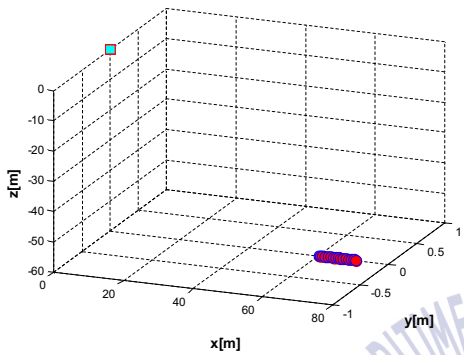

Fig.5.4: Trajectory of the forward motion without UC

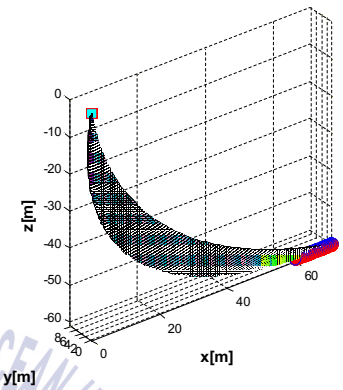

Fig.5.5: Trajectory of the forward motion with UC

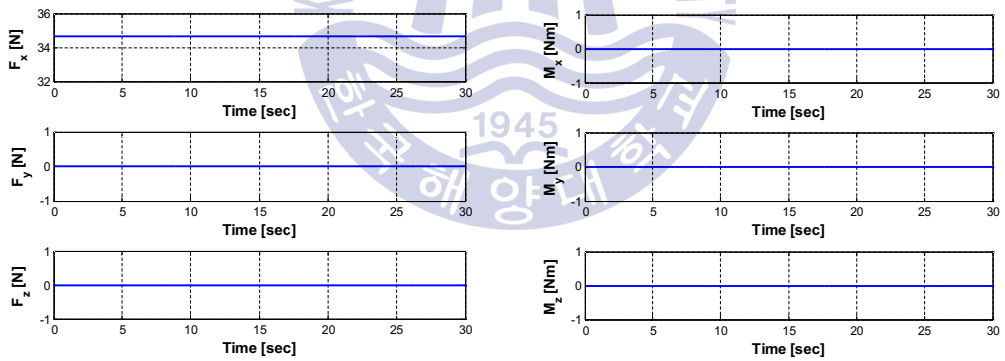

Fig.5.6: The force and moment of thruster system on the UV doing forward motion.

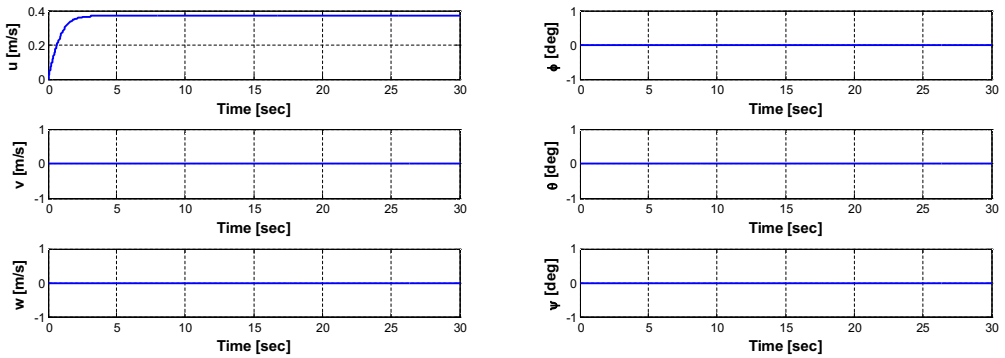

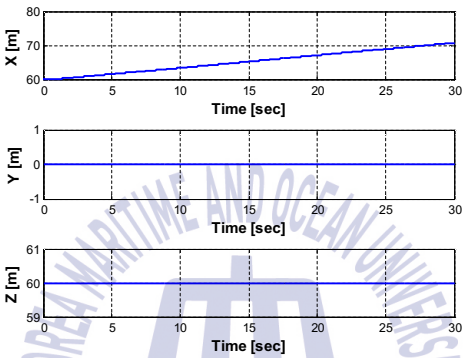

Fig.5.7: Simulation of the forward motion without UC.

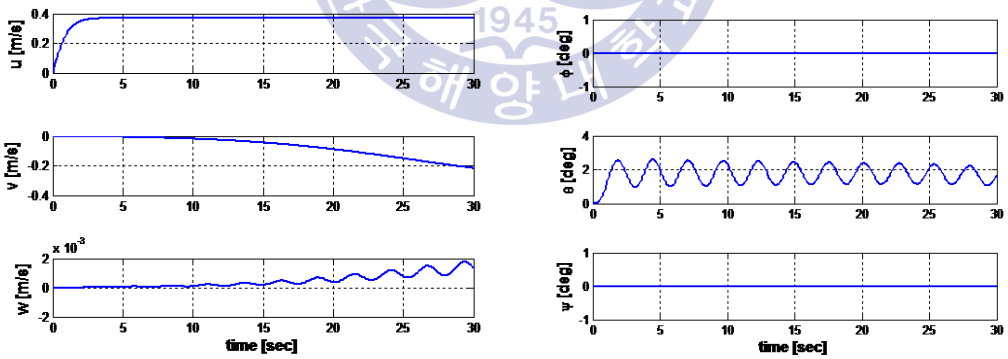

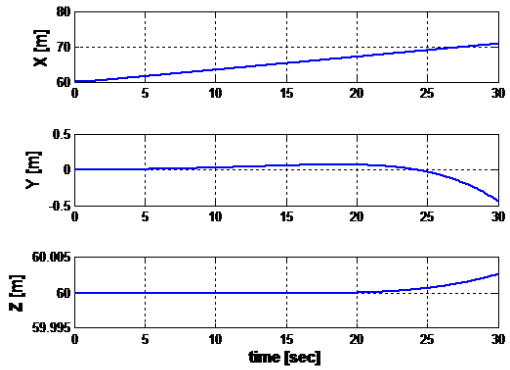

Fig.5.8: Simulation of the forward motion with UC.

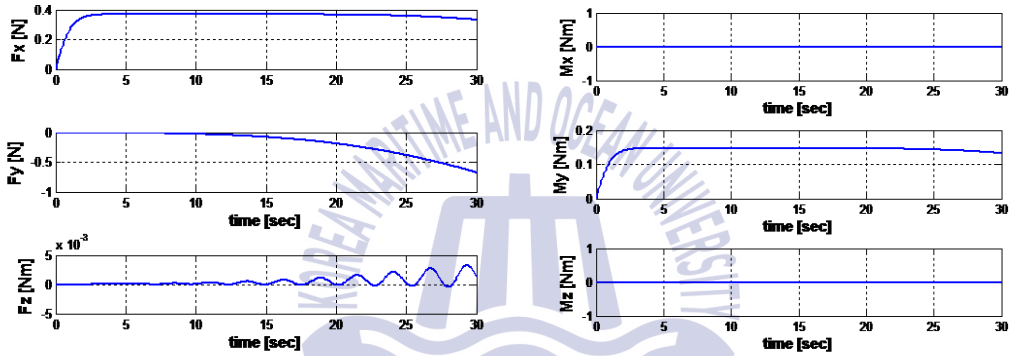

Fig.5.9: The force and moment of the cable on the UV doing forward motion w.r.t fixed body coordinate.

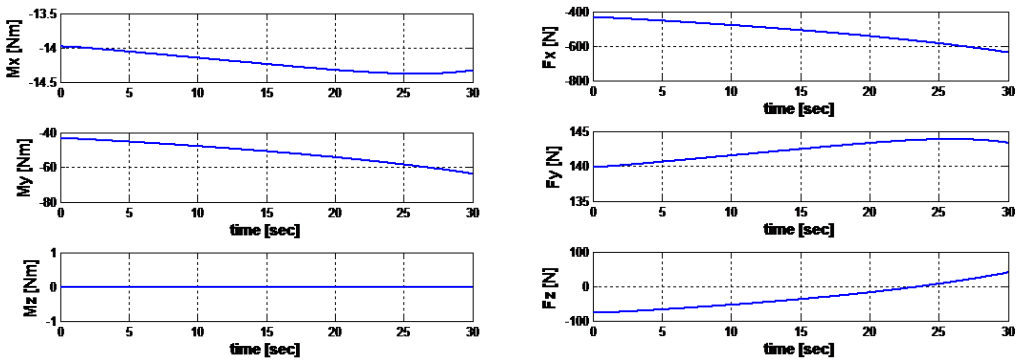

Fig.5.10: The force and moment of the cable on the UV doing forward motion w.r.t Earth coordinate.

5.2 Backward Motion

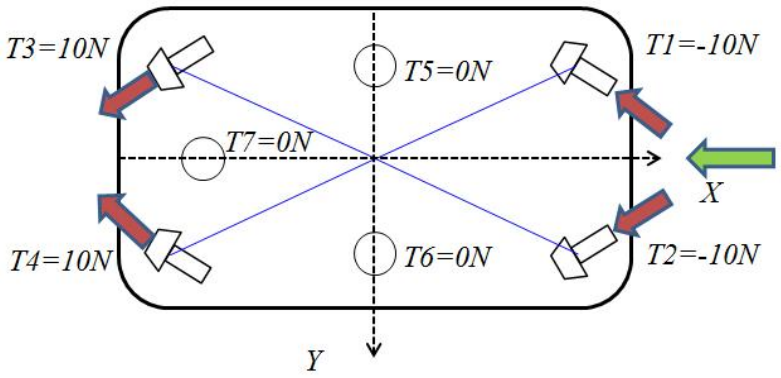

Fig.5.11: Thruster directions of UV in backward motion.

Let us consider the dynamic equation for each single-degree-of-freedom motion first. From (3.35) ~ (3.36) and (3.61) ~ (3.72), it follows that the dynamical equations of backward motion are simplified as:

$$\begin{cases} \dot{u} = [(X_u + X_{u|u|}|u|)u + F_{xthruster} + F_{xcable}]/(m - X_{\dot{u}}) \\ \dot{v} = F_{ycable}/(m - Y_{\dot{v}}) \\ \dot{w} = F_{zcable}/(m - Z_{\dot{w}}) \\ \dot{p} = M_{xcable}/(I_x - K_{\dot{p}}) \\ \dot{q} = M_{ycable}/(I_y - M_{\dot{q}}) \\ \dot{r} = M_{zcable}/(I_z - N_{\dot{r}}) \end{cases} \tag{5.3}$$

Fig.5.12 and 5.13 are the trajectory of the UV in both cases, attached with the UC and without UC doing the backward motion. If the UV is steered in surge to keep the vehicle moving backward as shown in Fig.5.11, thus both thrusters T_1 and T_2 are set to be -10N ($T_1 = T_2 = -10N$) and both thrusters T_3 and T_4 are set to be 10N ($T_3 = T_4 = 10N$); that is, total thrust/weight = 0.44. All of thrusters T_5, T_6, T_7 are set to be 0N ($T_5 = T_6 = T_7 = 0N$) to make the pure backward motion and initial UV speed is 0m/s. Fig.5.14 is the force and moment of thruster system on the UV doing backward motion. It is observed from Fig.5.14 that for the backward motion, the force F_x keeps at constant value equal -34.6 N and other components equal zero, i.e, $F_y = F_z = M_x = M_y = M_z = 0N$.

The force and moment of the UC including the current effect with respect to fixed body coordinate and Earth coordinate are shown in Fig.5.17 and Fig.5.18 for reference. The effect of the umbilical cable can be clearly seen by comparing Fig.5.15 with Fig.5.16. After comparing with the results in Figs.15 to 18, we can see that the effects are generally similar with forward motion case except the UV has the tendency to rightward.

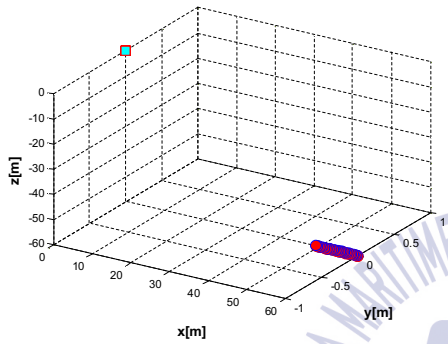

Fig.5.12: Trajectory of the backward motion without UC

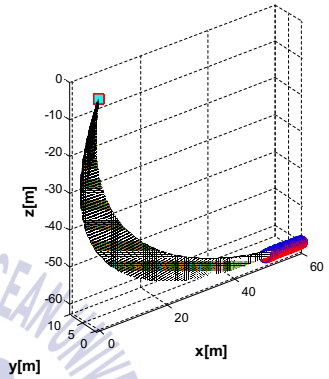

Fig.5.13: Trajectory of the backward motion with UC

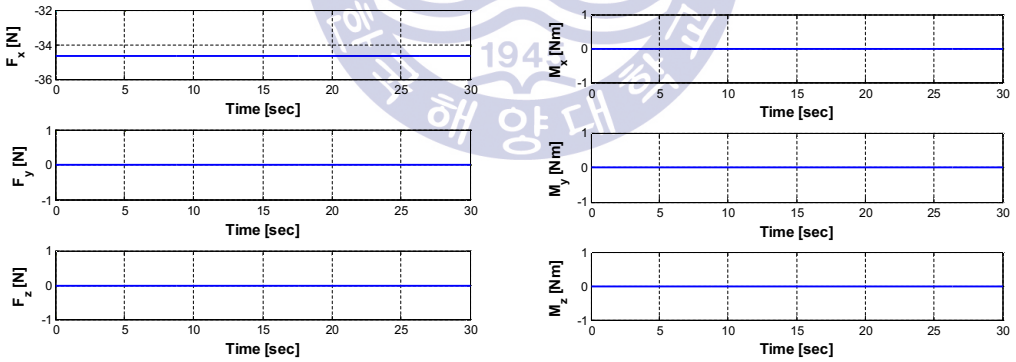

Fig.5.14: The force and moment of thruster system on the UV doing backward motion.

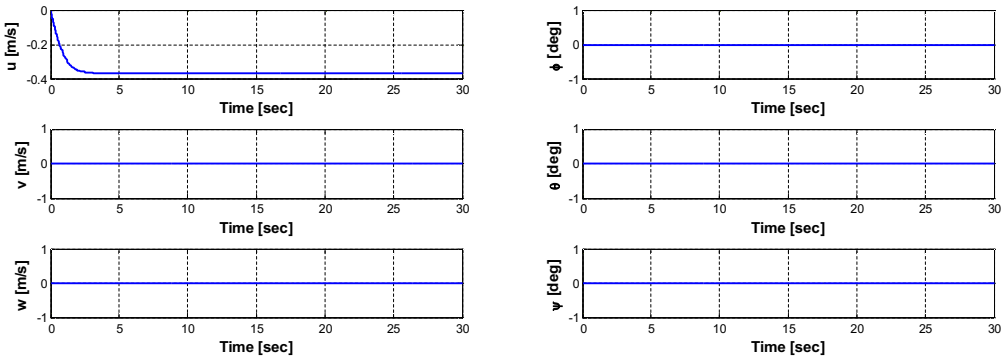

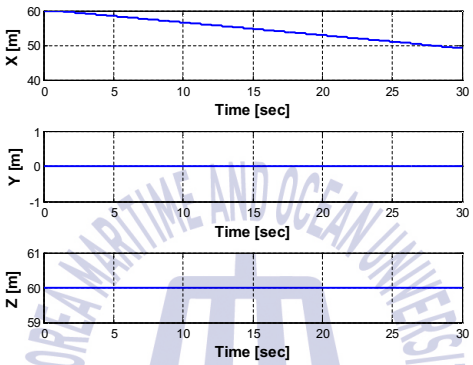

Fig.5.15: Simulation of the backward motion without UC.

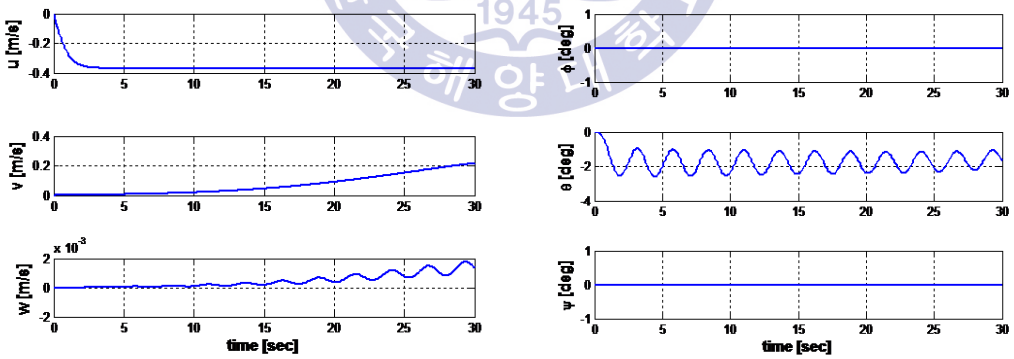

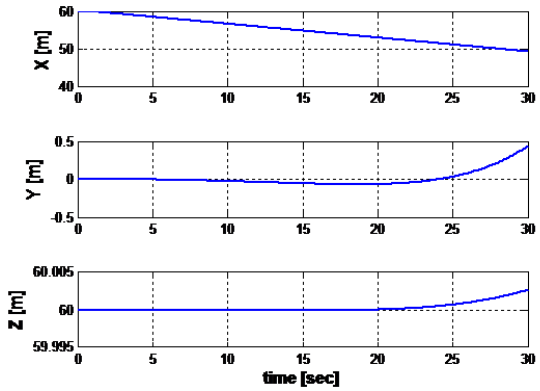

Fig.5.16: Simulation of the backward motion with UC.

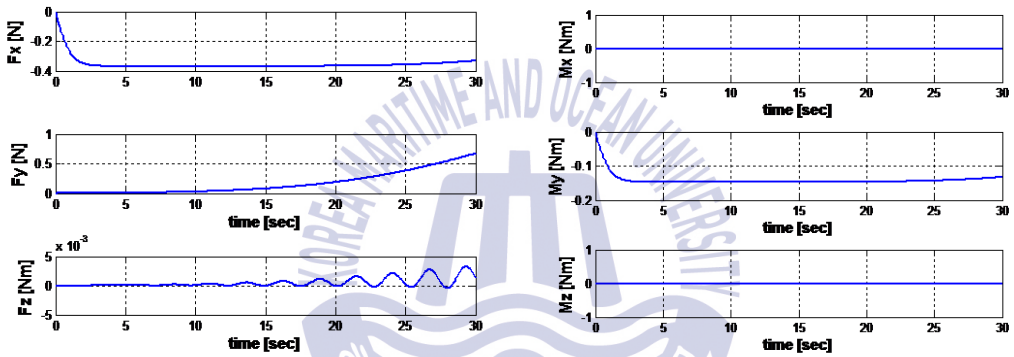

Fig.5.17: The force and moment of the cable on the UV doing backward motion w.r.t fixed body coordinate.

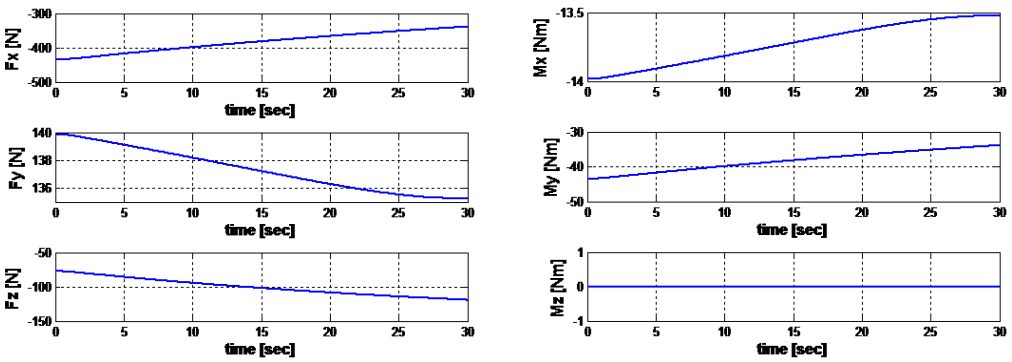

Fig.5.18: The force and moment of the cable on the UV doing backward motion w.r.t Earth coordinate.

5.3 Sideward Motion

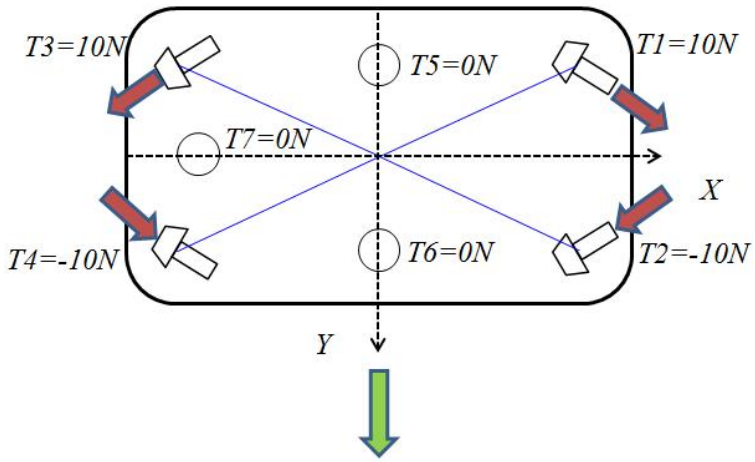

Fig.5.19: Thruster directions of UV in sideward motion.

Let us consider the dynamic equation for each single-degree-of-freedom motion first. From (3.35) ~ (3.36) and (3.61) ~ (3.72), it follows that the dynamical equations of sideward motion are simplified as:

$$\begin{cases} \dot{u} = F_{xcable}/(m - X_{\dot{u}}) \\ \dot{v} = [(Y_v + Y_{v|v|}|v|)v + F_{ythruster} + F_{xcable}]/(m - Y_{\dot{v}}) \\ \dot{w} = F_{zcable}/(m - Z_{\dot{w}}) \\ \dot{p} = M_{xcable}/(I_x - K_{\dot{p}}) \\ \dot{q} = M_{ycable}/(I_y - M_{\dot{q}}) \\ \dot{r} = M_{zcable}/(I_z - N_{\dot{r}}) \end{cases} \tag{5.4}$$

Fig.5.20 and 5.21 are the trajectory of the UV in both cases, attached with the UC and without UC doing the sideward motion. In order to make the UV operate the sideward motion as shown in Fig.5.19, both thrusters T_1 and T_3 are set to be 10N ($T_1 = T_3 = 10N$) and both thrusters T_2 and T_4 are set to be -10N ($T_2 = T_4 = -10N$); that is, total thrust/weight = 0.25. All of thrusters T_5, T_6, T_7 are set to be 0N ($T_5 = T_6 = T_7 = 0N$) to make the pure sideward motion and initial UV speed is 0m/s. Fig.5.22 is the force and moment of thruster system on the UV doing sideward motion. It is observed from Fig.5.22 that for the sideward motion, the force F_y keeps at constant value equal 20 N and other components equal zero,

i.e, $F_x = F_z = M_x = M_y = M_z = 0N$. The effect of the umbilical cable can be clearly seen by comparing Fig.5.23 with Fig.5.24. It is observed from Fig.5.23 that the UV moves rightward for about 6.5 m in 30 sec with the velocity about 0.23 m/s. The results in Fig.5.24 show that the depth of the UV decreases and UV will be move a little bit forward while the UV is moving sideward. Due to the attachment of the cable, the heave velocity appears to be oscillatory due to heave force F_{cz} of cable effect and so is the pitch motion. UV oscillates upward and the heave velocity w and the pitch angle θ also regularly oscillate. It means that the UV will move sideward up and down with varied pitch angle. Besides, we can see that the effect of the cable on the roll motion seems not quite significant. Finally, the yaw motion is not affected by the cable in this case.

The force and moment of the UC including the current effect with respect to fixed body coordinate and Earth coordinate are shown in Fig.5.25 and Fig.5.26 for reference. The results show that the oscillatory heave force F_{cz} and pitch moment M_{cy} cause the oscillatory heave and pitch motions, respectively. The results in Fig.5.25 also reveal that the sway force F_{cy} is positive, that is, rightward, and the heave force F_{cz} is negative leads to upward heave velocity; therefore, the UV has the tendency to ascend and rightward while the UV is moving sideward. Besides, the surge force F_{cx} is positive which decreases initially and then increases gradually, and pitch moment M_{cx} causes the roll motion.

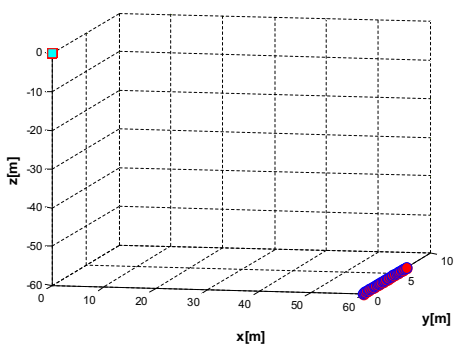

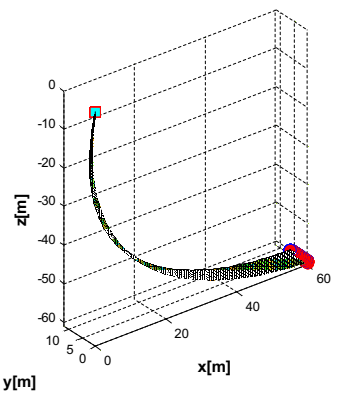

Fig.5.20: Trajectory of the sideward motion without UC

Fig.5.21: Trajectory of the sideward motion with UC

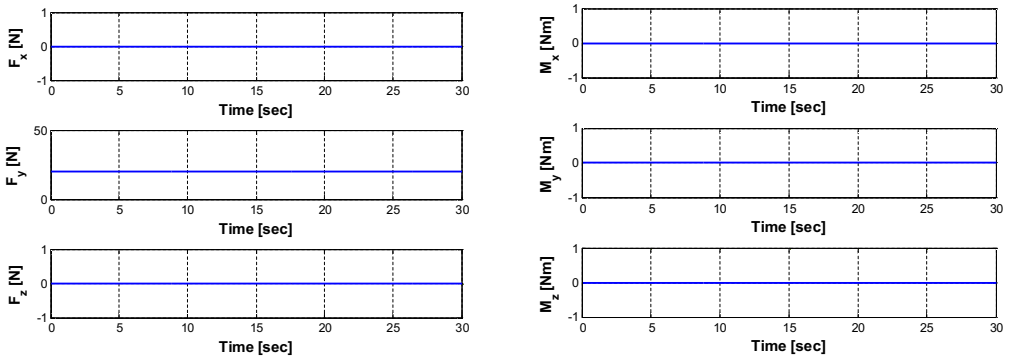

Fig.5.22: The force and moment of thruster system on the UV doing sideward motion.

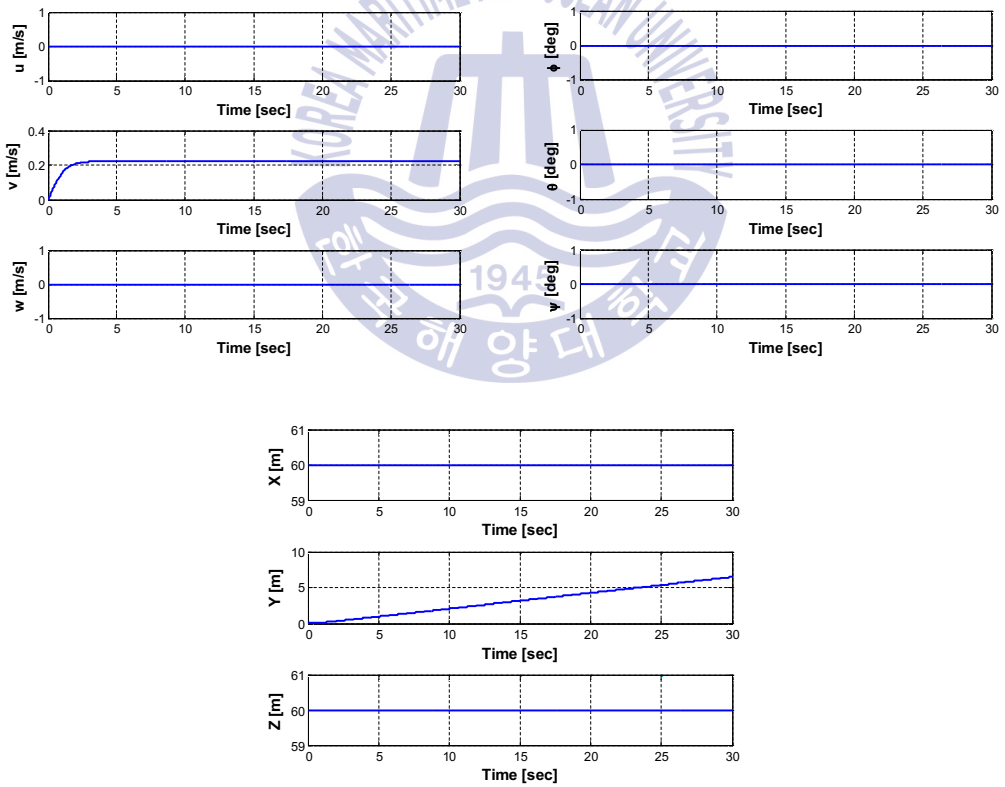

Fig.5.23: Simulation of the sideward motion without UC.

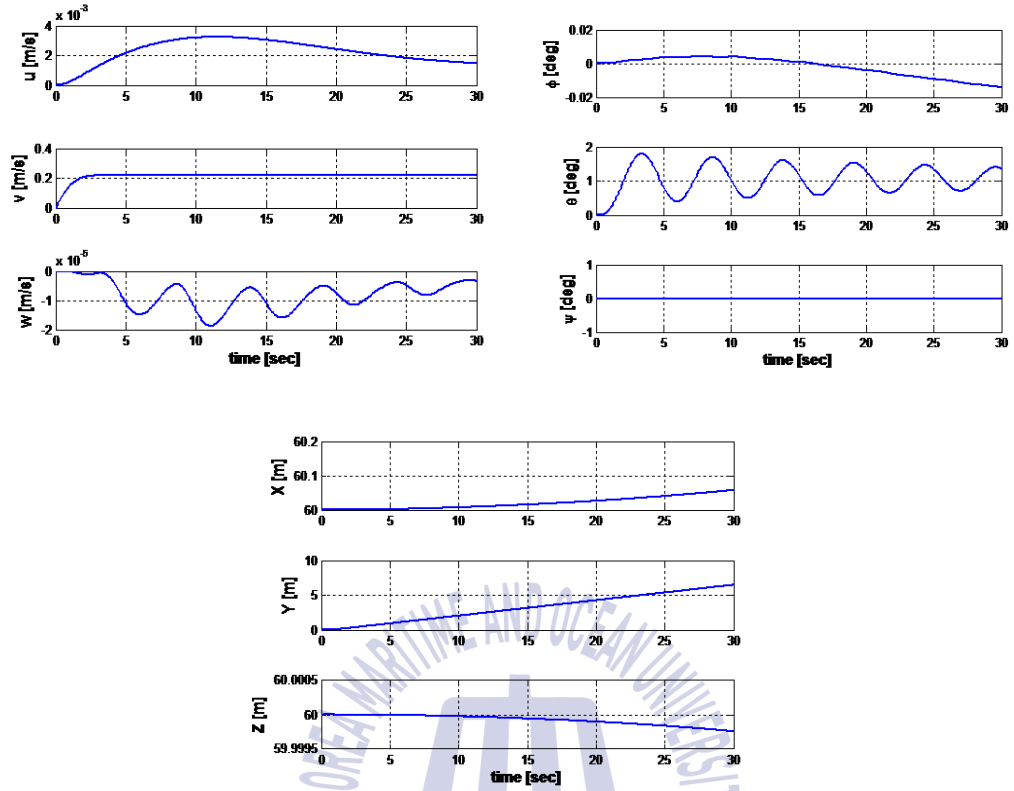

Fig.5.24: Simulation of the sideward motion with UC.

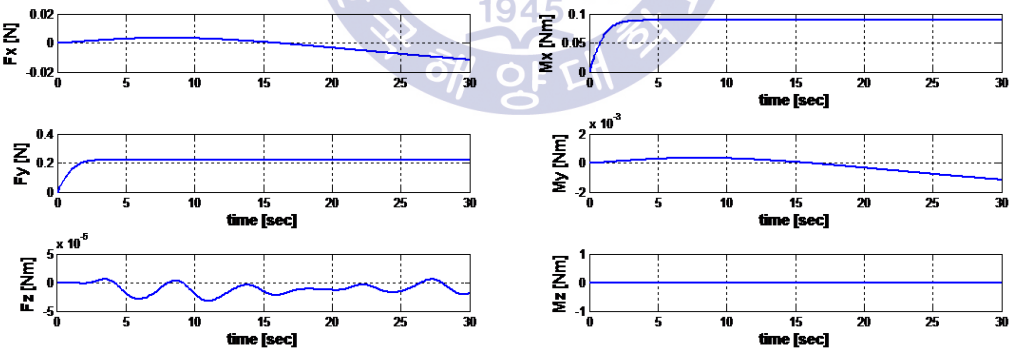

Fig.5.25: The force and moment of the cable on the UV doing sideward motion w.r.t fixed body coordinate.

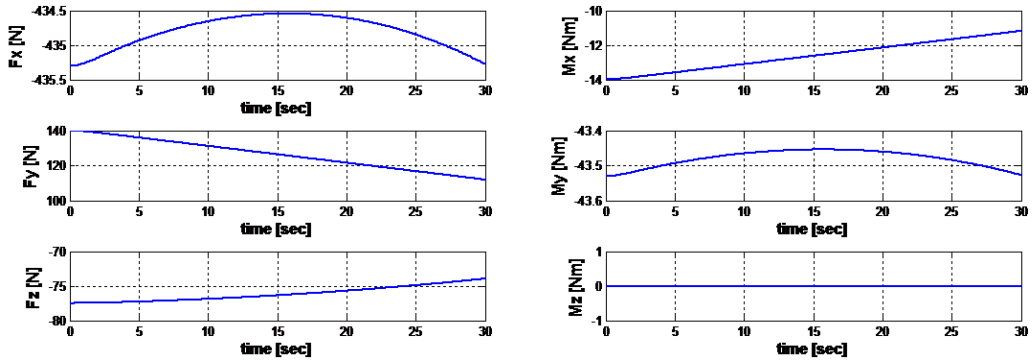

Fig.5.26: The force and moment of the cable on the UV doing sideward motion w.r.t Earth coordinate.

5.4 Ascending Motion

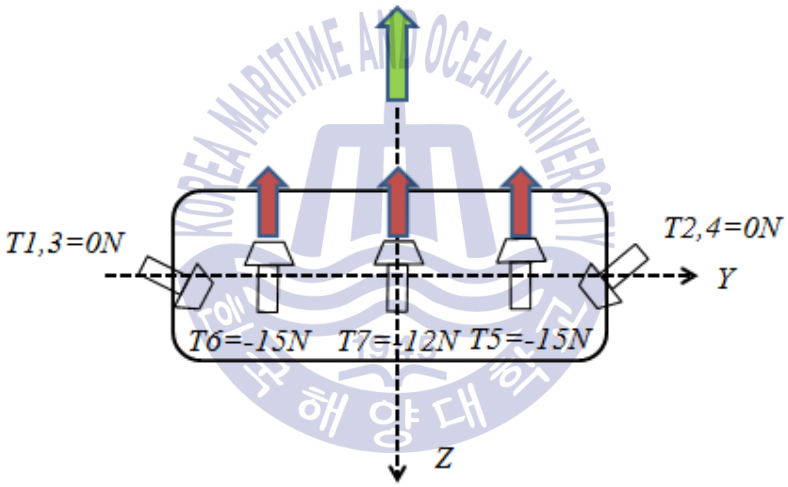

Fig.5.27: Thruster directions of UV in ascending motion.

Let us consider the dynamic equation for each single-degree-of-freedom motion first. From (3.35) ~ (3.36) and (3.61) ~ (3.72), it follows that the dynamical equations of ascending motion are simplified as:

$$\begin{cases} \dot{u} = F_{xcable}/(m - X_{\dot{u}}) \\ \dot{v} = F_{ycable}/(m - Y_{\dot{v}}) \\ \dot{w} = [(Z_w + Z_{w|w|}|w|)w + F_z + F_{zcable}]/(m - Z_{\dot{w}}) \\ \dot{p} = M_{xcable}/(I_x - K_{\dot{p}}) \\ \dot{q} = M_{ycable}/(I_y - M_{\dot{q}}) \\ \dot{r} = M_{zcable}/(I_z - N_{\dot{r}}) \end{cases} \tag{5.5}$$

Figs.5.28 and 5.29 are the trajectories of the UV doing the ascending motion, either with or without the umbilical cable, respectively. In order to make the UV operate the ascending motion as shown in Fig.5.27, both thrusters T_5 and T_6 are set to be -15N ($T_5 = T_6 = -15N$) and thruster T_7 is set to be -12N ($T_7 = -12N$); that is, total thrust/weight = 0.53. All of thrusters T_1, T_2, T_3 and T_4 are set to be 0N ($T_1 = T_2 = T_3 = T_4 = 0N$) to make the pure ascending motion and initial UV speed is 0m/s. Fig.5.30 is the force and moment of thruster system on the UV doing ascending motion. It is observed from Fig.5.30 that for the ascending motion, the force F_z keeps at constant value equal -42 N and other components equal zero, i.e, $F_x = F_y = M_x = M_y = M_z = 0N$. The effect of the umbilical cable can be clearly seen by comparing Fig.5.31 with Fig.5.32. It is observed from Fig.5.31 that the UV moves upward for about 9 m in 30 sec with the heave velocity about 0.3 m/s. While the umbilical cable is attached, we can see that the effect of the cable on the motions seems not significant except the heave velocity, Fig.5.32. The results show that the heave motion is slower due to the cable effect. The force and moment of the UC including the current effect with respect to fixed body coordinate and Earth coordinate are shown in Fig.5.33 and Fig.5.34 for reference. The results in Fig.5.34 also reveal that the heave force F_{cz} is negative leads to upward heave velocity; therefore, the UV has the tendency to upward.

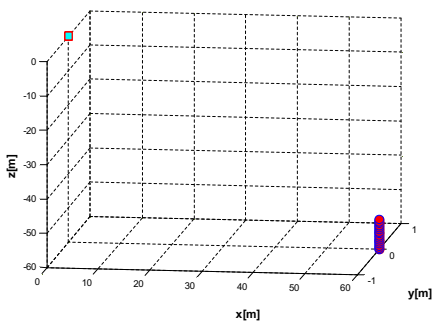

Fig.5.28: Trajectory of the ascending

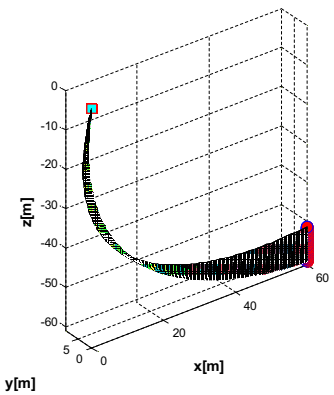

Fig.5.29: Trajectory of the ascending

motion without UC motion with UC

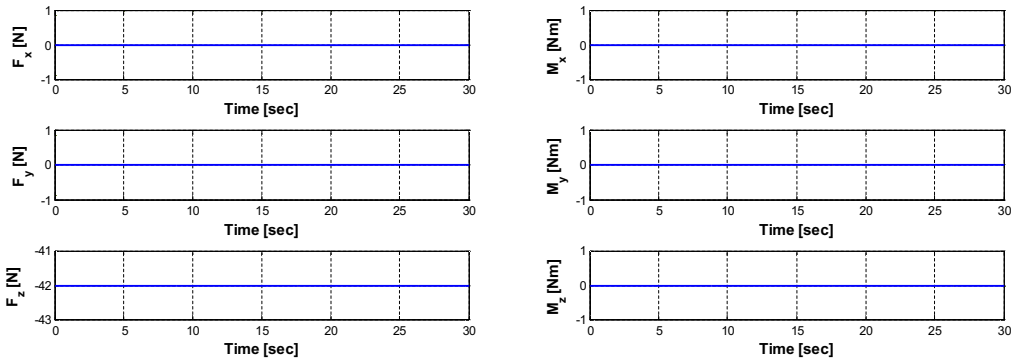

Fig.5.30: The force and moment of thruster system on the UV doing ascending motion.

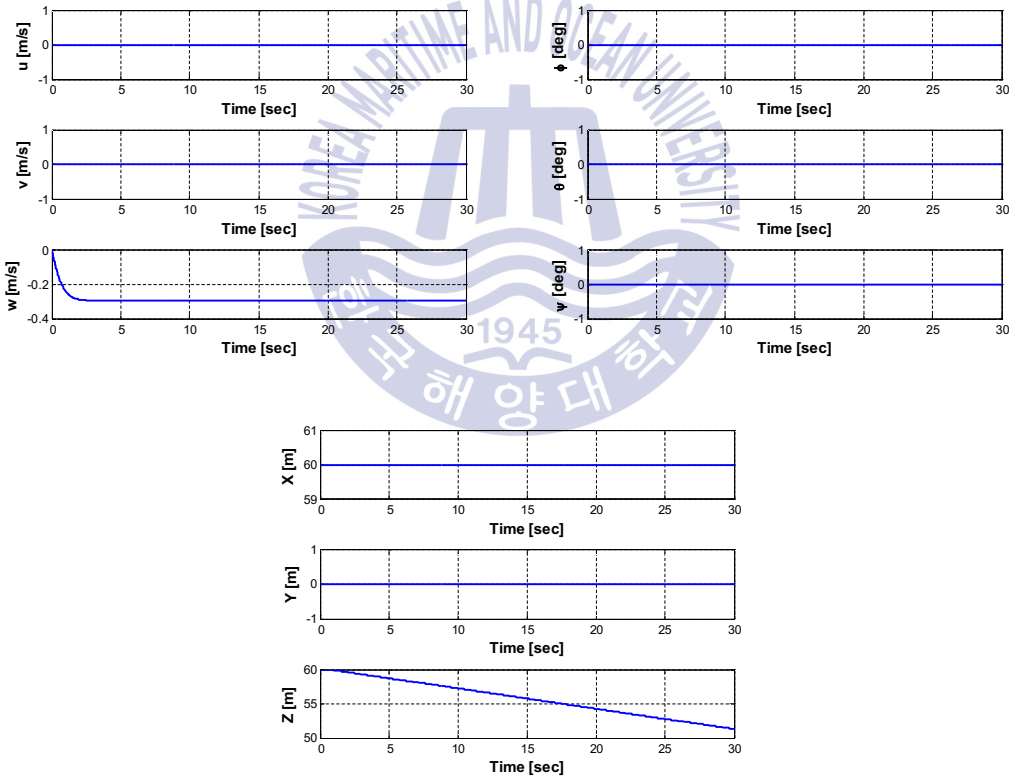

Fig.5.31: Simulation of the ascending motion without UC.

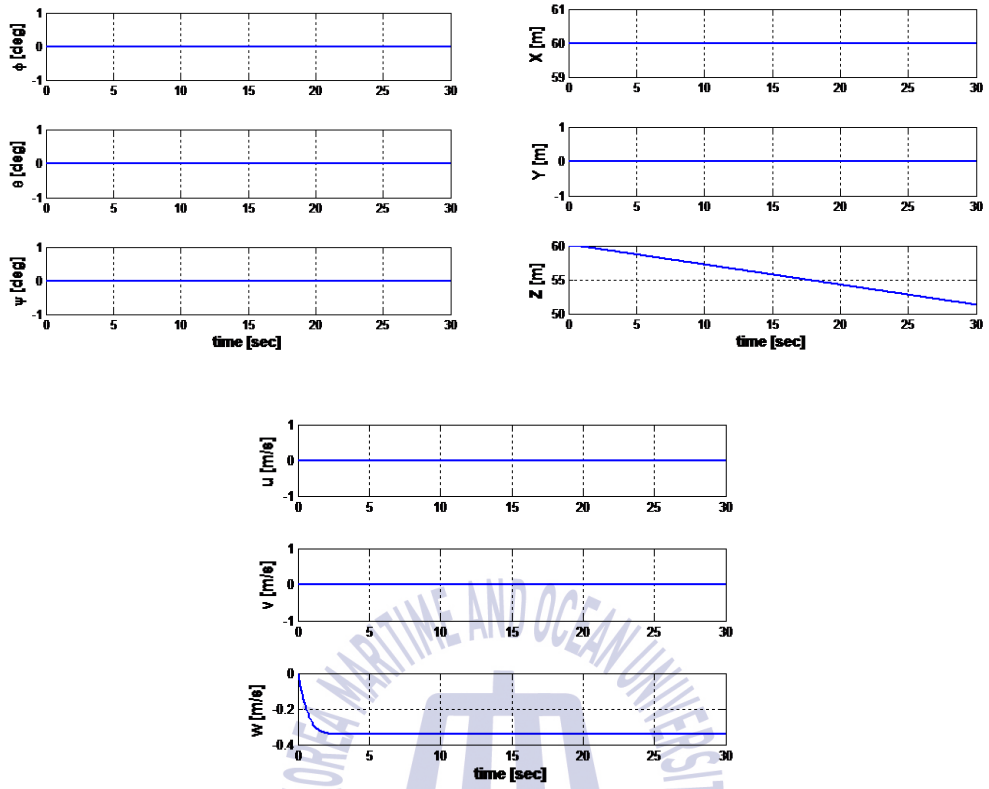

Fig.5.32: Simulation of the ascending motion with UC.

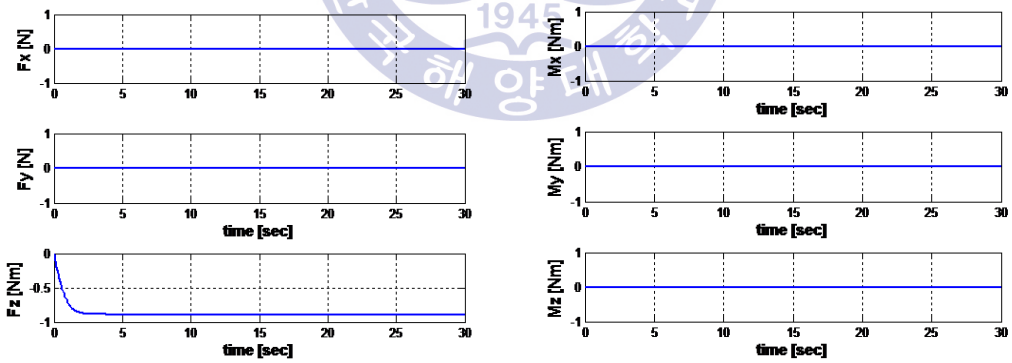

Fig.5.33: The force and moment of the cable on the UV doing ascending motion w.r.t fixed body coordinate.

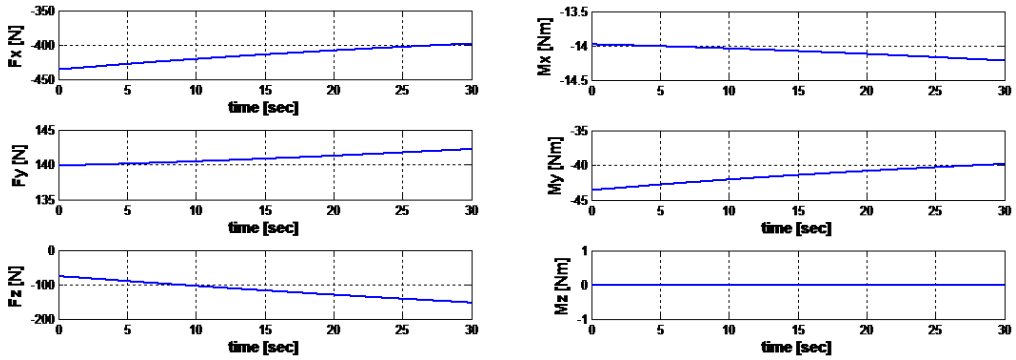

Fig.5.34: The force and moment of the cable on the UV doing ascending motion w.r.t Earth coordinate.

5.5 Descending Motion

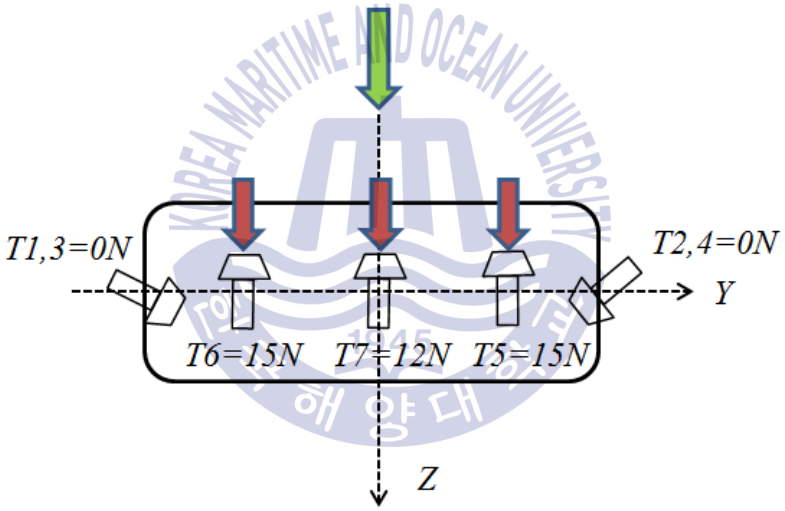

Fig.5.35: Thruster directions of UV in descending motion.

Let us consider the dynamic equation for each single-degree-of-freedom motion first. From (3.35) ~ (3.36) and (3.61) ~ (3.72), it follows that the dynamical equations of descending motion are simplified as:

$$\begin{cases} \dot{u} = F_{xcable}/(m - X_{\dot{u}}) \\ \dot{v} = F_{ycable}/(m - Y_{\dot{v}}) \\ \dot{w} = [(Z_w + Z_{w|w|}|w|)w + F_z + F_{zcable}]/(m - Z_{\dot{w}}) \\ \dot{p} = M_{xcable}/(I_x - K_{\dot{p}}) \\ \dot{q} = M_{ycable}/(I_y - M_{\dot{q}}) \\ \dot{r} = M_{zcable}/(I_z - N_{\dot{r}}) \end{cases} \tag{5.6}$$

Figs.5.36 and 5.37 are the trajectories of the UV doing the descending motion, either with or without the umbilical cable, respectively. In order to make the UV operate the descending motion as shown in Fig.5.35, both thrusters T_5 and T_6 are set to be 15N ($T_5 = T_6 = 15N$) and thruster T_7 is set to be 12N ($T_7 = 12N$); that is, total thrust/weight = 0.53. All of thrusters T_1, T_2, T_3 and T_4 are set to be 0N ($T_1 = T_2 = T_3 = T_4 = 0N$) to make the pure descending motion and initial UV speed is 0m/s. Fig.5.38 is the force and moment of thruster system on the UV doing descending motion. It is observed from Fig.5.38 that for the descending motion, the force F_z keeps at constant value equal 42N and other components equal zero, i.e, $F_x = F_y = M_x = M_y = M_z = 0N$. The effect of the umbilical cable can be clearly seen by comparing Fig.5.39 with Fig.5.40. The force and moment of the UC including the current effect with respect to fixed body coordinate and Earth coordinate are shown in Fig.5.41 and Fig.5.42 for reference. The results show that the similar conclusion with ascending motion can be applied to the case for descending motion except the heave force F_{cz} is positive.

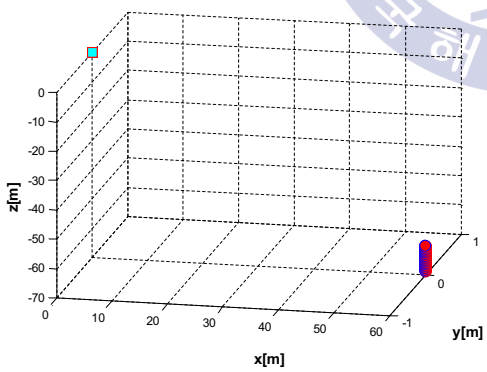

Fig.5.36: Trajectory of the descending motion without UC

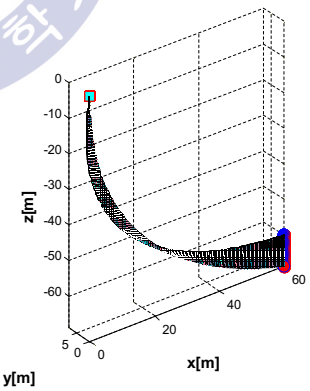

Fig.5.37: Trajectory of the descending motion with UC

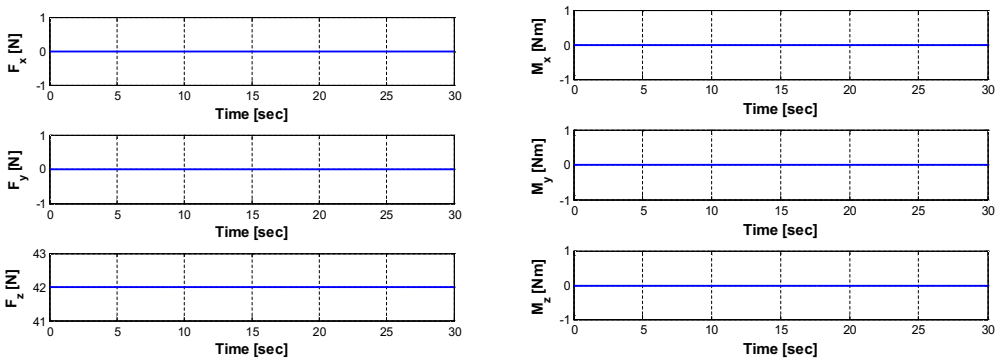

Fig.5.38: The force and moment of thruster system on the UV doing descending motion.

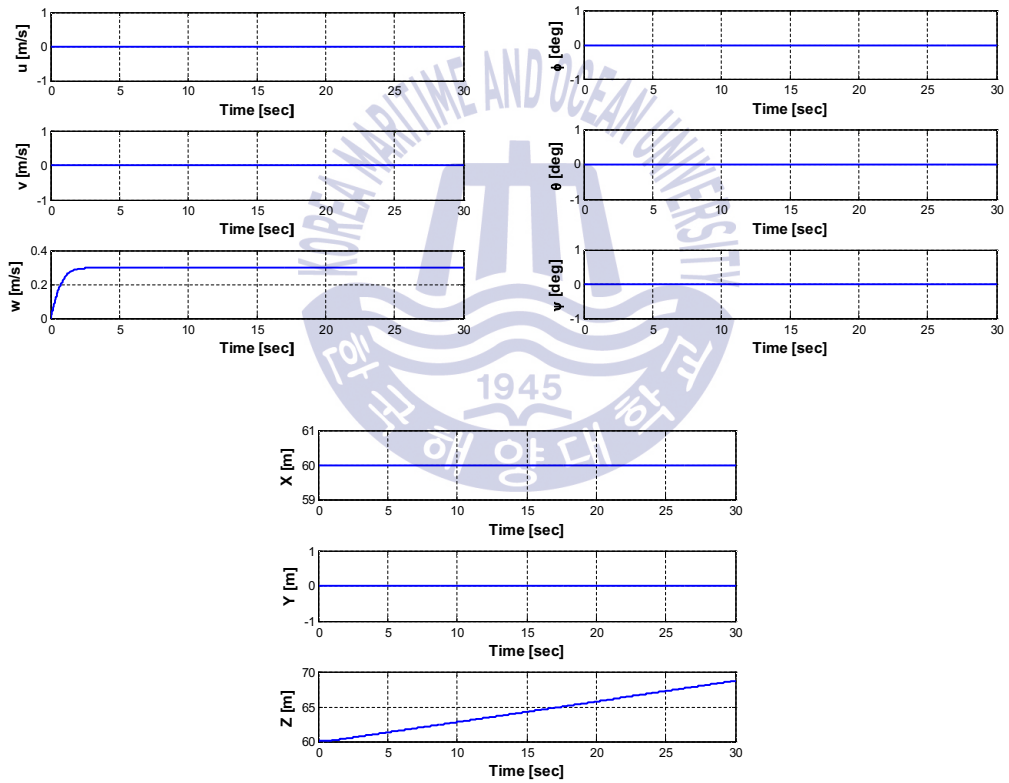

Fig.5.39: Simulation of the descending motion without UC.

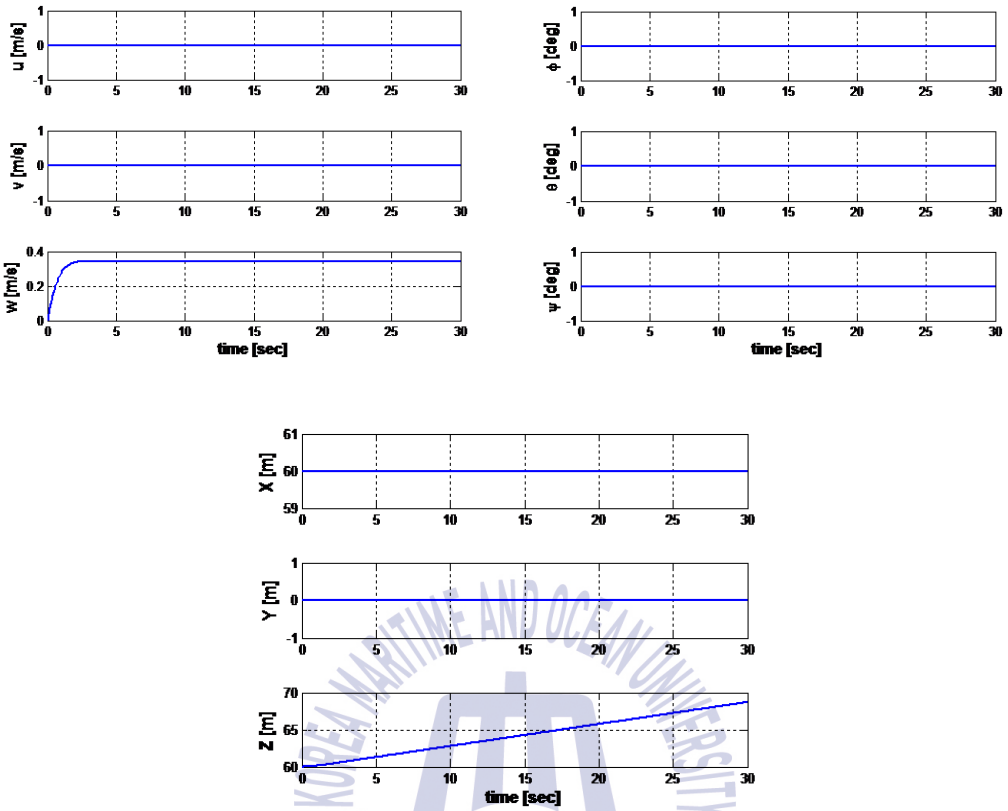

Fig.5.40: Simulation of the descending motion with UC.

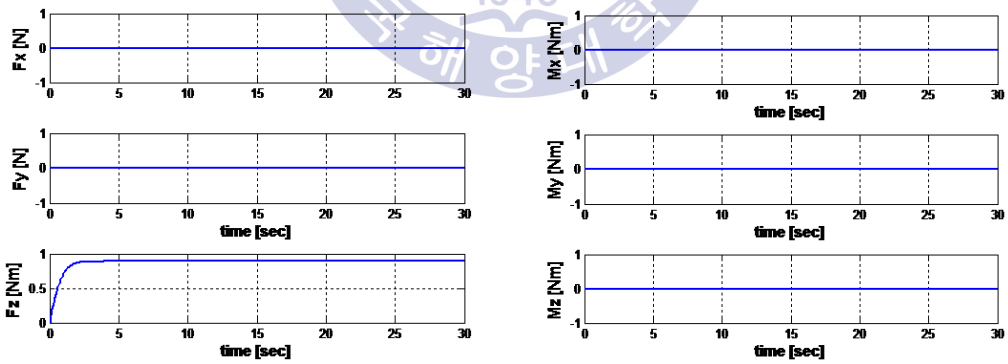

Fig.5.41: The force and moment of the cable on the UV doing descending motion w.r.t fixed body coordinate.

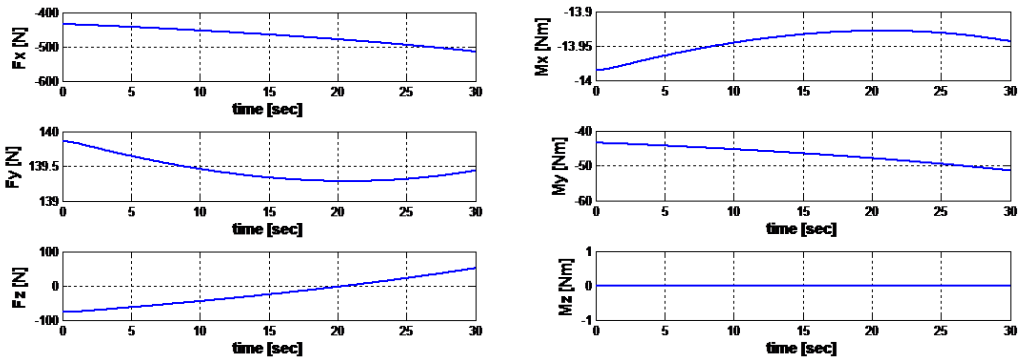

Fig.5.42: The force and moment of the cable on the UV doing descending motion w.r.t Earth coordinate.

5.6 Turning Motion

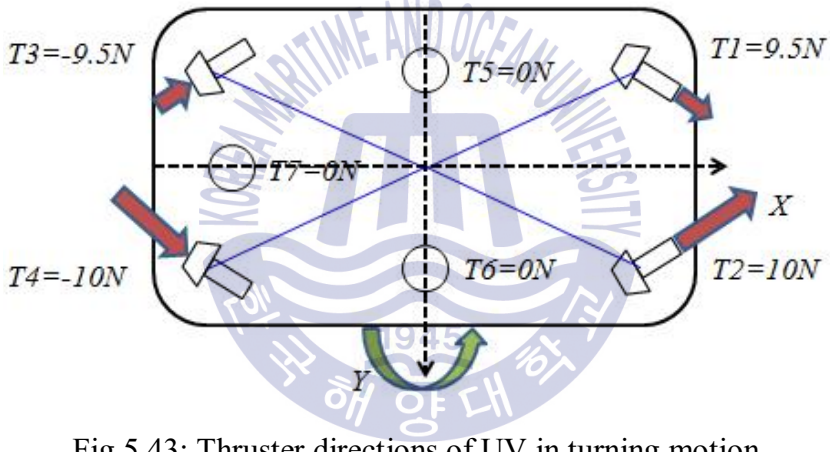

Fig.5.43: Thruster directions of UV in turning motion.

Fig.5.43 shows thruster directions of UV in turning motion. Let us consider the dynamic equation for each single-degree-of-freedom motion first. From (3.35) ~ (3.36) and (3.61) ~ (3.72), it follows that the dynamical equations of turning motion are simplified as:

$$\begin{cases} \dot{u} = [(m - Y_{\dot{v}})vr + (X_u + X_{u|u|}|u|)u + F_x + F_{xcable}]/(m - X_{\dot{u}}) \\ \dot{v} = [(-m - X_{\dot{u}})ur + (Y_v + Y_{v|v|}|v|)v + F_{ycable}]/(m - Y_{\dot{v}}) \\ \dot{w} = F_{zcable}/(m - Z_{\dot{w}}) \\ \dot{p} = M_{xcable}/(I_x - K_{\dot{p}}) \\ \dot{q} = M_{ycable}/(I_y - M_{\dot{q}}) \\ \dot{r} = [uv(Y_{\dot{v}} - X_{\dot{u}}) + (N_r + N_{r|r|}|r|)r + M_z + M_{zcable}]/(I_z - N_{\dot{r}}) \end{cases} \tag{5.7}$$

Figs.5.44 and 5.45 are the trajectory of the UV in both cases, attached with the UC and without UC doing the turning motion. In order to simulate the turning motion, the counterclockwise rotating forces 10 N and 9.5N are set for the thrusters T2 and T1, respectively and -10 N and -9.5N are set for the thrusters T4 and T3, respectively. All of thrusters T5, T6, T7 ($T_5 = T_6 = T_7 = 0N$) are set to be 0N to make the pure turning motion and initial UV surge speed is 0.3 m/s. Fig.5.46 is the force and moment of thruster system on the UV doing turning motion. It is observed from Fig.5.46 that for the turning motion, the surge force F_x and yaw moment M_z keep at constant value equal 33.8 N and -0.33Nm , respectively while other components equal zero, i.e, $F_y = F_z = M_x = M_y = 0N.$

The effect of the umbilical cable can be clearly seen by comparing Fig.5.47 with Fig.5.48. It is observed from Fig.5.47 that the UV initially moves forward, then moves rightward and finally moves backward. The results also reveal that the surge speed increases at the beginning and then decreases to a constant speed and the sway speed also increases from 0 m/s to a positive small constant speed. When the cable is considered in the turning motion, all motions are significantly affected as shown in Fig.5.48. With the cable effect, the depth, heave velocity, roll motion and pitch motion of the UV varies with time.

The depth of the UV decreases initially and then slightly increases to a steady value. Besides, due to the attachment of the cable, the heave velocity appears to be oscillatory due to heave force F_{cz} of cable effect and the roll angle θ also regularly oscillate. The surge and sway motions are also slightly different from those without umbilical cable. Besides, the pitch motion is also accompanied because of the umbilical cable. The cable makes the pitch motion initially increases positively and then decreases, even to the negative. However, yaw motion is not affected by the cable in this case.

The force and moment of the UC including the current effect with respect to fixed body coordinate and Earth coordinate are shown in Fig.5.49 and Fig.5.50 for

reference. The results show that the oscillatory heave force F_{cz} and roll moment M_{cx} cause the oscillatory heave velocity and roll motions, respectively. The results in Fig.5.49 also reveal that the surge force F_{cx} initially decreases positively and then increases. The sway force F_{cy} increases at the beginning and then decreases to negative value after about half time history.

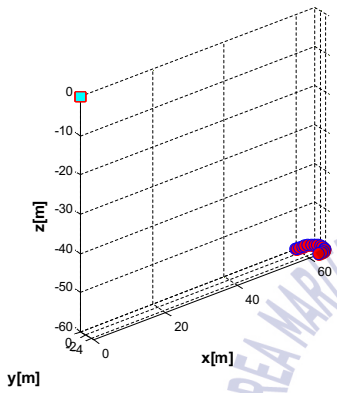

Fig.5.44: Trajectory of the turning motion without UC

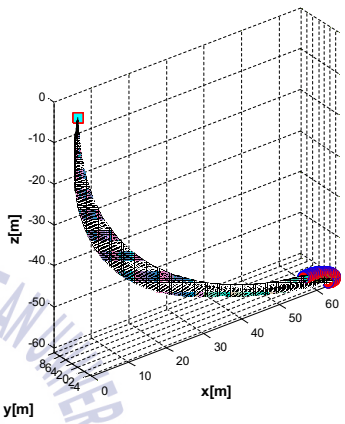

Fig.5.45: Trajectory of the turning motion with UC

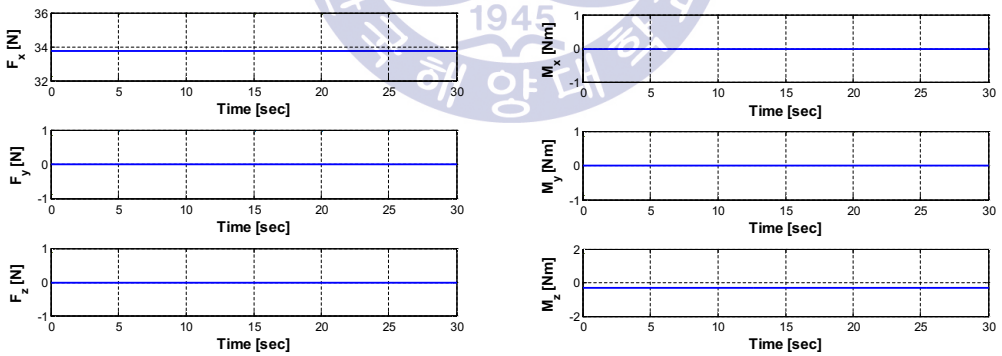

Fig.5.46: The force and moment of thruster system on the UV doing turning motion.

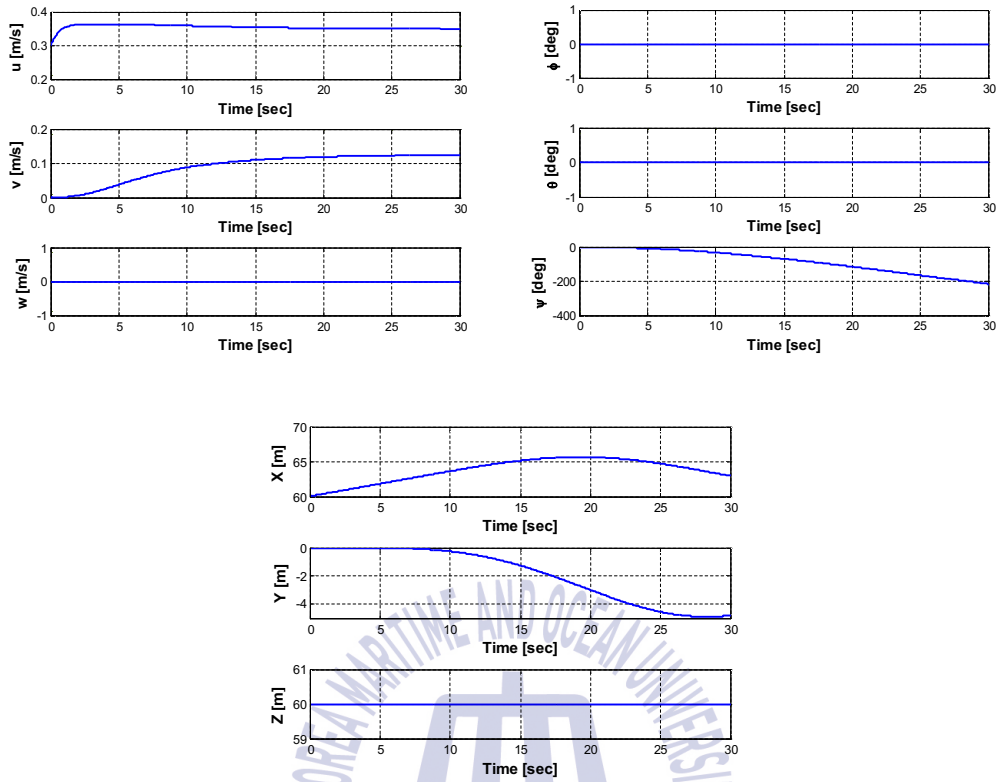

Fig.5.47: Simulation of the turning motion without UC.

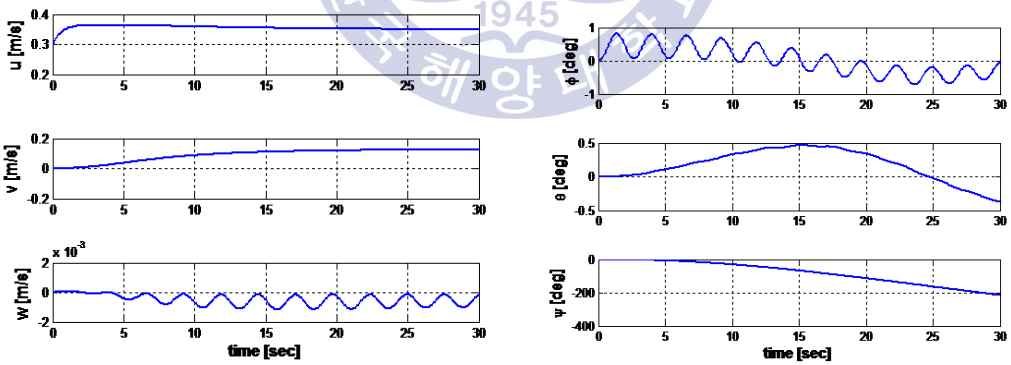

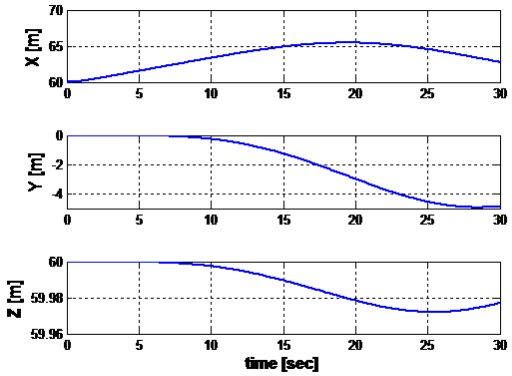

Fig.5.48: Simulation of the turning motion with UC.

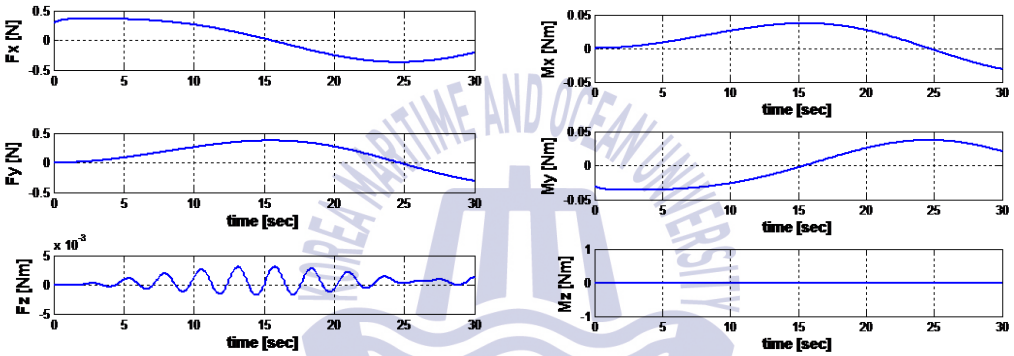

Fig.5.49: The force and moment of the cable on the UV doing turning motion w.r.t fixed body coordinate.

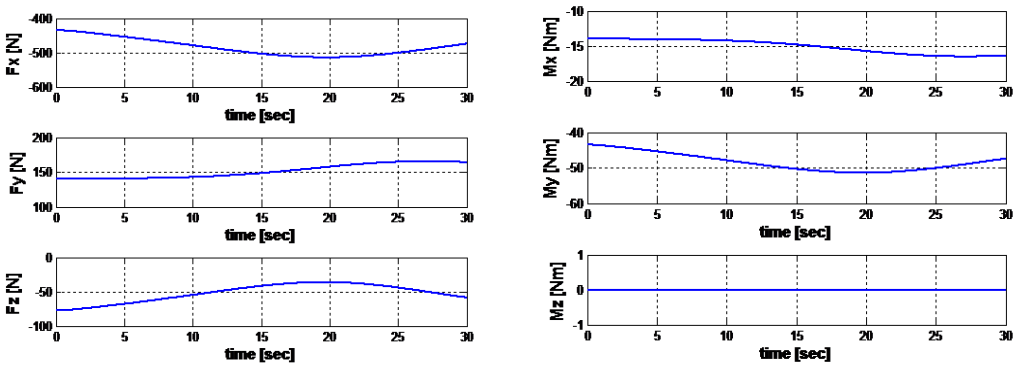

Fig.5.50: The force and moment of the cable on the UV doing turning motion w.r.t Earth coordinate.

Chapter 6 Conclusions

In this thesis, a series of analysis for the motion behavior of a UV with umbilical cable in the ocean has been done. The maneuvering behaviors of the UV including forward motion, backward motion, ascending motion, descending motion, sideward motion and turning motion have been studied and discussed. From the present overall results, the following conclusions can be drawn:

(1) The 4th Runge–Kutta method is also applied to solve the six degrees of freedom motions of the UV with the umbilical cable effect. The compact hydrodynamic model with six degrees of freedom motions and the numerical solution technique are described in the following section.

(2) The configuration simulation of the umbilical cable connecting to the UV is calculated by using the catenary equation and the corresponding two-end boundary-value problem is solved by using the multi-step shooting method which is based on the search method developed by Sagatun (2001).

(3) The effect of the current force on the umbilical cable will simultaneously affect UV motions because the umbilical cable is connected to the UV. Conclusively, the present results clearly reveal that the umbilical cable can affect significantly motions behaviors of the UV while it is operated in forward motion, backward motion, sideward motion and turning motion. Therefore, it must be carefully handled in these cases. Otherwise, when the UV is operated to do the ascending motion and descending motion in uniform current, we can see that the effect of the cable on the motions seems not significant except the heave velocity.

(4) Based on suitable assumptions, the numerical model developed in the thesis can numerically well simulate the motions of the UV with the umbilical cable in a uniform current at sea. Several comparisons have been made for discussion and some useful conclusions are drawn in this thesis. It believed that the results shown here can offer some important information about the

interaction effects between the UV and cable for the designers of the related field.

References

[1] Fossen, T.I., 1994. Guidance and Control of Ocean Vehicles. John Wiley & Sons, Chichester.

[2] Albow, C.M., Schechter, S., 1983. Numerical simulation of undersea cable dynamics. Ocean Engineering 10 (6), 443–457.

[3] Milinazzo, F., Wilkie, M., Latchman, S.A., 1987. An efficient algorithm for the dynamics of towed cable systems. Ocean Engineering 14 (6), 513–526.

[4] Ming-Chung Fang, Jeng-Horng Chen and Chang-Shang Hou, 2008. On the behavior of an underwater remotely operated vehicle in a uniform current. Marine techonology, Vol.45, N0.4, October 2008.

[5] Hooke, R., Jeeves, T.A., 1961. Direct search solution of numerical and statistical problems. Journal of the Association for Computing Machinery 8, 212–229.

[6] Deam, W., Given, D., 1983. ROV technology trends and forecast. OCEANS 15, 573–578.

[7] Nomoto, M., Hattori, M., 1986. A deep ROV DOPHIN 3K: designed performance analysis. IEEE Journal of Oceanic Engineering 11 (3), 373–391.

[8] Stewart, L.L., Auster, P.J., Low cost ROV's for science. In: Proceedings of OCEANS '89,Seattle, Washington DC, USA, 1989.

[9] Burgess, J.J., 1992. Equations of motion of a submerged cable with bending stiffness. Offshore Marine and Arctic Engineering 1-A, 283–289.

[10] Buckham, B., Nahon, M., Cote, G., 2000. Validation of a finite element model for slack ROV tethers. IEEE Journal of Oceanic Engineering, 1129–1136.

[11] Feng, Z., Allen, R., 2004. Evaluation of the effects of the communication cable on the dynamics of an underwater flight vehicle. Ocean Engineering 31, 1019–1035.

[12] Coute, G., Serranl, A.,1996. Molding and simulation of underwater vehicles. In: Proceedings of 4th IEEE CCA, Dearborn, MI, 1996.

[13] Chen, H.H., Chang, H.H., Chou, C.H., Tseng, P.H., 2007. Identification of hydrodynamic parameters for a remotely operated vehicle using projective mapping method. Symposium on Underwater Technology and Workshop on Scientific Use of Submarine Cables and Related Technologies.

[14] L.A.Gonzalez. Design, modeling and control of an autonomous underwater vehicle. PhD thesis, The university of Western Australia, 2004.

[15] Surface ships: Principles of stability. [online], 2004. Available: http://wrc.chinalake.navy.mil/warfighterenc/SHIPS/shipeng/stability/basics/basics.htm/.

[16] P. Brutzman. A Virtual World for an Autonomous Underwater Vehicle. PhD thesis, Naval Postgraduate School, 1994.

[17] Wikipedia.[online],2004.Available: http://en.wikipedia.org/wiki/Corioliseffect/

[18] D. Grosset et al. Quasi-rigid docking of auv for underwater manipulations. In Proceedings of the 4th International Workshop on Computer Science and Information Technologies, 2002.

[19] International submarine engineering web based auv designinfo. [online], 2000. Available: http://www.ise.bc.ca/WADEsysdesign.html/.

[20] Ole Morten Aamo and Thor Inge Fossen. Finite Element Modelling of Mooring Lines. Mathematics and Computers in Simulations, 53:415-422, 2000.

[21] Max Irvine. Cable Structures. Massachusetts Institute of Technology, 1981.

[22] Svein I. Sagatun. The Elastic Cable Under the Action of Consentrated and Distributed Forces. Journal of Offshore Mechanics and Arctic Engineering, 123:43-45,2001.

[23] Shan Huang. Dynamic Analysis of Three-Dimensional Marine Cables. Ocean Engineering, 21:587-605, 1994.

[24] Y. T. Chai and K. S. Varyani. Three Dimensional Lump Mass Formulation of a Catenary Riser with Bending, Torsion and Irregular Seabed Interaction Effect. Ocean Engineering, 29:1503-1525, 2002.

[25] J. M. Wingnet and R. L. Huston. Cable Dynamics - A Finite Segment Approach. Computers and Structures, 6:475-480, 1976.

[26] M. S. Triantafyllou. Cable Mechanics with Marine Applications. Department of Ocean Engineering, Massachusetts Institute of Technology, May 1990.

[27] M.A. Vaz , M.H. Patel. Three-dimensional behaviour of elastic marine cables in sheared currents. Applied Ocean Research 22 (2000) 45–53.

[28] N. Yang, D-S Jeng, and X. L. Zhou. Tension Analysis of Submarine Cables During Laying Operations. The Open Civil Engineering Journal, 2013, 7, 282-29.

[29] Ever Coarita and Leonardo Flores. Nonlinear Analysis of Structures Cable - Truss. International Journal of Engineering and Technology, Vol. 7, No. 3, June 2015.

[30] Marco D. Masciola, Meyer Nahon, and Frederick R. Driscoll. Static analysis of the lumped mass cable model using a shooting algorithm. ASCE Journal of Waterway, Port, Coastal, and Ocean Engineering, 2011.